DESIGNING RU CATALYSTS FOR SELECTIVE C-H BOND OXIDATION REACTIONS

A Dissertation
Submitted to the Graduate Faculty
of the
North Dakota State University
of Agriculture and Applied Science

By

Hashini Nuradha Kumari Herath

In Partial Fulfillment of the Requirements
for the Degree of
DOCTOR OF PHILOSOPHY

Major Department:
Chemistry and Biochemistry

October 2020

Fargo, North Dakota

North Dakota State University
Graduate School

Title

Designing Ru Catalysts for Selective C-H Bond Oxidation Reactions

By

Hashini Nuradha Kumari Herath

The Supervisory Committee certifies that this *disquisition* complies with North Dakota

State University's regulations and meets the accepted standards for the degree of

DOCTOR OF PHILOSOPHY

SUPERVISORY COMMITTEE:

Dr. Alexander Parent

Chair

Dr. Kenton Rodgers

Dr. Pinjing Zhao

Dr. Chad Ulven

Approved:

11/08/2020	Dr. Gregory Cook
Date	Department Chair

ABSTRACT

Oxidation reactions are fundamentally important reactions in organic synthesis. These reactions involve numerous chemical transformations and provide powerful synthetic methodology with synthetic values. One of the important areas of C-H bond oxidation is C-H bond hydroxylation. Hydroxy groups are extremely useful and can use as building blocks or intermediates to synthesize more valuable chemical compounds. However, selective C-H bond hydroxylation under mild conditions is a large challenge due to the relative ease of overoxidation and racemization. Therefore, development of catalysts for selective C-H bond hydroxylation utilizing environmentally benign oxidants, is highly demanding from practical viewpoint.

Typically, C-H bond oxidation proceeds via formation of high-valent metal oxo species. Attaining a high oxidation state of the metal complex is critical as it is the key step for many catalytic processes. Understanding ligand effects on structural and electronic changes of the metal complexes towards designing more robust catalysts is an effort of this dissertation. It will highlight initial attempts at developing novel ruthenium (Ru) catalysts and an analysis of their structural, electrochemical and spectroscopic properties. The catalytic behavior of the resulting complexes towards C-H bond hydroxylation reaction will also be shown.

Chapter I introduces the background of C-H bond activation and hydroxylation reactions by Ru catalysts. Also, this chapter details the study of C-H bond hydroxylation mechanisms, reaction intermediates, the importance of C-H bond hydroxylation, electronic effects of ligands, and the pioneering work in this field.

Chapter II describes development a of new Ru complex containing the pyridine alkoxide ligand, of general formula [Ru(tpy)(pyalk)Cl] (tpy = 2,2':6'2"-terpyridine, pyalk = 2-(2′-pyridyl)-2-propanol). This chapter outlines the detailed synthesis, structural, electrochemical

and spectroscopic properties of the complex by electrochemical techniques, UV Visible spectroscopy, NMR, mass spectrometry and X-ray crystallography.

In order to overcome some limitations on project 1, new ruthenium complexes [Ru(MepyPO$_3$H)(tpy)Cl] (**1**, tpy = 2,2':6'2"-terpyridine , MepyPO$_3$H = (pyridine-2-ylmethyl)phosphonic acid) and [Ru(bpyPO$_3$H)(bpy)Cl] (**2**, bpy(PO$_3$H$_2$) = 2,2-bipyridine-6-phosphonic acid, bpy = 2,2-bipyridine) bearing phosphonate ligands were prepared and fully characterized.   Catalytic properties of the complexes have been evaluated by testing their ability to catalyze C-H bond oxidation using a variety of sacrificial oxidants.

lab friendly and fun place to work. It is pleasure to thank my close and supportive circle of

friends all over the world for their care, love, encouragement and happy distractions to rest my

mind outside of my research.

Last not least, my deep and sincere gratitude to my family for their unconditional love,

support and encouragement to pursue my dreams of getting doctoral degree in Chemistry. A

special gratitude goes to my beloved parents, who have always being there for me and be a pillar

of strength in my life. Many thanks to my beloved sister for giving me the emotional support

whenever I needed and my brother for his warm and deep care. I would like to express my

sincere gratitude to my sister-in-law and brother-in-law for their continuous and unparalleled

love.   I thank my dear and beloved nieces for making my life so colorful and wonderful. This

journey would not have been possible without their support, and I dedicate this milestone to

them.

DEDICATION

This Dissertation is wholeheartedly dedicated to my beloved parents, who have been my

inspiration and continually provide their unconditional affection, love, and encouragement which

make me able to get success and honor.

Thank you for making this adventure through to the end!

TABLE OF CONTENTS

ix

LIST OF TABLES

LIST OF FIGURES

LIST OF SCHEMES

LIST OF ABBREVIATIONS

Å .... Angstrom

AgCl.. Silver chloride

Anal.. Analytical

Anhy... Anhydrous

$AgNO_3$ .... Silver nitrate

BDE .... Bond Dissociation Energy

Bpy 2,2-bipyridyl

Calcd .... Calculated

CAN .... Cerium (IV) ammonium nitrate

$CDCl_3$ .... Deuterated chloroform

CV .... Cyclic voltammetry

D_2O .... Deuterium oxide

DPV .... Differential Pulse Voltammetry

Equiv .... Equivalent

EtOAc .... Ethyl acetate

Et_2O .... Diethylether

EtOH .... Ethanol

Fc .... Ferrocene

GC .... Gas chromatography

HAT .... Hydrogen Atom Transfer

H_2O_2 .... Hydrogen peroxide

HRMS .... High resolution mass spectrometry

hr .... Hours

KCl .... Potassium Chloride

KIE... Kinetic Isotope Effect

M .... Metal

MeOH .... Methanol

μL .... Microliter

μmol .... Micromole

mL .... milliliter

mM .... Millimolar

mol .... Moles

Mol.Wt .... Molecular weight

$NaIO_4$ .... Sodium periodate

NHE .... Normal Hydrogen Electrode

NMR .... Nuclear magnetic resonance

PCET .... Proton Coupled Electron Transfer

P_i .... Phosphate Buffer

ppm .... Parts per million

Pt .... Platinum

RDS.. Rate Determining Step

Rt .... Room temperature

Ru .... Ruthenium

$RuCl_3 \cdot nH_2O$ .... Ruthenium trichloride hydrate

Temp .... Temperature

THF .... Tetrahydrofuran

TLC .... Thin layer chromatography

TMS .... (trimethylsilyl)propionic-2,2,3,3-d_4

TOF.. Turn Over Frequency

TON .... Turn Over Number

UV-Vis .... Ultraviolet Visible

CHAPTER 1. INTRODUCTION

1.1. C-H Bonds

The carbon-hydrogen bond (abbreviated to C-H bond hereafter) is the un-functionalized group[1] and an elementary building block, which is mainly found in alkanes or saturated hydrocarbons.[2] C-H bonds are the most ubiquitous[2,3] chemical linkage in nature. Alkanes constitute the cheapest and most abundant feedstock for organic chemicals[4] such as natural gas and petroleum. C-H bonds in alkanes are relatively inert towards conventional organic transformations, and breaking this bond is a thermodynamically demanding and kinetically slow process.[4] The strong localized C-H bond of these molecules could not readily participate in a chemical reaction due to the high bond dissociation energies[3] (typically 90-100 kcal/moles), low acidity (estimated $pK_a = 45–60$) and unreactive molecular orbitals.[2] Therefore, hydrocarbons are mainly used as fuels, and the energy of the bonds is released as heat.[4] Such reactions are not readily controllable and produce thermodynamically stable products such as carbon dioxide and water.[2] Consequently, selectively and efficiently converting C-H bonds into valuable functionalized organic compounds is an interesting alternative with a potentially huge economic impact.

1.2. C-H Bond Activation and Functionalization

Activation of C-H bond is highly sought after in organic chemistry because it introduces new functionality to inert aliphatic molecules.[5] As depicted in scheme 1, there are two processes involved in C-H activation. The first step involves cleavage of unreactive C-H bond in the presence of a catalyst,[6] referred to as C-H activation. This activation weakens the C-H bond, which increases the reactivity of the bond towards reagents.[7] The second step, C-H bond

functionalization introduces a variety of functional groups to the activated C-H bond leads to formation of new bonds such as C-C, C-O, C-N etc.[6,7]
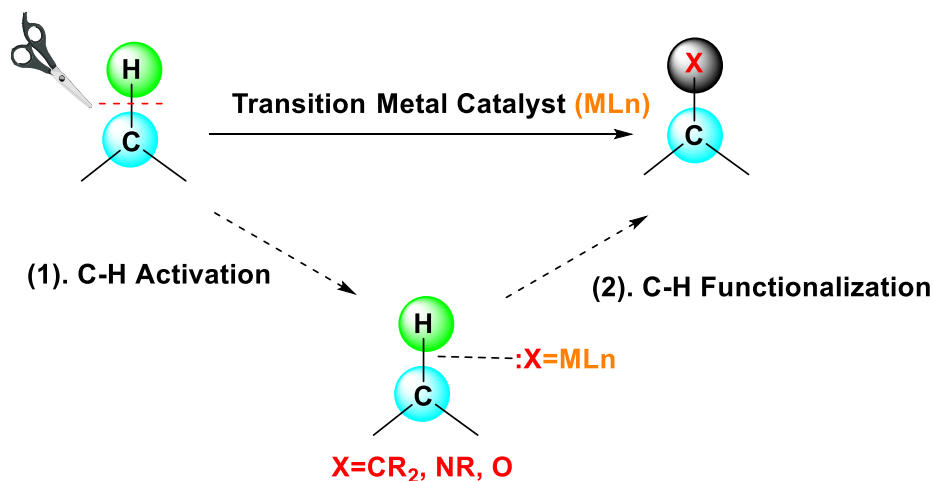
Scheme 1.1. C-H bond activation and functionalization

Activation of the relatively inert C-H bonds is one of the most difficult transformations,[8] and requiring extreme conditions,[9,10] as well as the use of organic reagents and oxidants in stoichiometric amounts.[10] Multiple methods have been employed for activation of C-H bonds, although transition metal catalysis is one of the most efficient ways to achieve both high activity and selectivity of C-H bonds.[4] The metal complexes can alter or enhance the reactivity of C-H bonds through associating in the relative energies of the orbitals or the polarity of C-H bonds.[2]

1.3. C-H Bond Oxidation/Hydroxylation

Among C-H activation reactions, C-H bond oxidation reactions to form C-O bond are one of the key areas in chemical synthesis.[11,12] In this context, focus has been devoted to C-H bond oxidation reactions, i.e. C-H bond hydroxylation by transition metal catalysts. Direct oxidation of C-H bonds to alcohol is one of the major synthetic targets and area of growing concern in catalysis research because it enables key steps in designing more complex molecules such as natural products and pharmaceuticals.[13,14]

These reactions are not only important for academic purposes but also significant for industrial purposes in relation to energy production.[15] One practically important application is conversion of methane to methanol.[15] Methane is the smallest hydrocarbon and the principle component of natural gas mostly found in regions that are not readily accessible.[2,15] Methane is not an economically viable source due to the difficulty of transporting this substance in the gaseous form. Therefore, it is more advantageous of converting methane gas to more readily transportable liquid methanol, which would significantly improve methane utilization. Another important application is conversion of linear alkanes into alcohols or carboxylic acids[15] and these molecules are more reactive than alkanes.

The hydroxylation of C-H bonds has been studied extensively, both to investigate the mechanism of enzymatic oxidation by cyctochrome P450 and to develop catalysts for synthetic applications to mimic biological oxidations.[10] In nature, hydroxylation of substrates are mediated by metalloenzymes such as cytochromes P450, which exhibits excellent selectivity under mild conditions and use only molecular oxygen as the terminal oxidant.[10,16] Inspired by the high catalytic activity of the biological system, a variety of transition metal catalysts including Mn, Pd, Fe, Pt and Ru have been developed and tested in selective C-H bond hydroxylation reactions.[17] Among synthetic metal complexes, ruthenium complexes have been intensively investigated due to the relative abundance of synthetically accessible complexes,[18] stability, high reactivity and relevance to iron complexes, which are involved in biological oxidation reactions.[19,20]

1.4. Mechanism of C-H Bond Hydroxylation Reactions

C-H bond oxidation mechanisms can be divided into two broad categories: inner and outer-sphere mechanisms. Inner-sphere mechanisms involve direct coordination between the

catalyst and substrate, which is typically followed by oxidative addition of the C-H bond to form an organometallic metal hydride species, followed by ligand exchange and reductive elimination of product.[6,15] In contrast, outer-sphere mechanisms typically involve electrophilic attack of the metal complex on the C-H bond to form the product, which may or may not be transiently coordinated to the metal center.[6] Typically, C-H bond activation in outer-sphere mechanism occurs via the formation of a high-valent metal complex containing activated ligand such as oxo-, oxyl species. All known cases of C-H bond hydroxylation follow outer-sphere reaction pathways.

1.4.1. High-Valent Metal-Oxo Species

High-valent metal-oxo (M=O) and oxyl (M-O·) species (Scheme 4) are the main reactive intermediates of C-H bond hydroxylation reactions,[21,22] and are formed by reaction of a transition metal catalyst with a sacrificial chemical oxidant. Metal-oxo complex consists of one σ bond and at least one π bond between metal and oxygen while oxyl species consist of a single σ bond between metal and the radical bearing oxyl ligand.[21] These two structures are electronically equivalent. Oxo species (O^{2-}) is a common ligand in high oxidation state metal complexes and interacts with a metal through π-donation of the strong donor lone pair in oxygen.[23] Among these high-valent oxo species, $Ru^{IV}=O$ complexes have been mostly investigated for catalytic oxidation reactions due to their high performance not only in organic substrates, but also in water.[21]

$$[M] \xrightarrow{\text{Oxidant}} \underset{M^{IV}}{\overset{O}{\|}} \text{ Or } M^{III}\!\!-\!\!O^{\cdot}$$

Scheme 1.2. Formation of high-valent oxo and oxyl species in the presence of metal complex and sacrificial oxidant

4

High-valent oxo species are typically formed in three ways including: Reductive activation of dioxygen as observed in Cytochrome P450 in biological oxidation reactions; oxo-transfer from active oxygen species such as iodosylbenzene (PhIO), m-chlorperbenzoic acid (m-CPBA), and hydroperoxides (H_2O_2 and ROOH); and proton-coupled electron transfer (PCET).[20,24] The reductive activation of dioxygen process is difficult to control in artificial experimental conditions[20] mainly due to the slow reaction kinetics of molecular oxygen. Organic peroxides provide low selectivity towards targeted species, which arises mainly from the inevitable production of undesirable radical intermediates.[25] Moreover, these peroxides generate hazardous waste which in turn reduces the overall sustainability of these reactions. Both of these methods to have an open site or labile ligand on the metal catalyst in-order to coordinate the desired oxidant for activation.[24]

Alternatively, PCET process is the most feasible way of forming high-valent oxo species as occurring in the oxygen evolving complex (OEC) in photosystem II in green plants.[20,25] PCET describes as transferring electrons and protons simultaneously or stepwise manner in any elementary step. Formation of high-valent oxo species via PCET involve two electron oxidation of a metal aqua complex in the presence of oxidant where two electron go to oxidant and two protons are accepted by water molecule as solvent .[24] It can generate targeted metal-oxo species selectively by controlling the redox potential and equivalent amount of oxidant used.[26] Additionally, this is most common reaction pathway to lower activation barrier in catalysis by preventing charge buildup on the complex.[27,28]
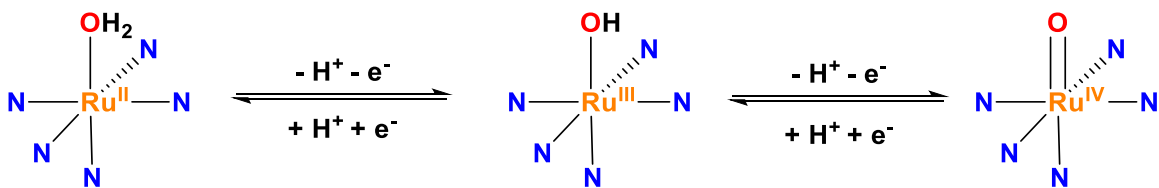
Scheme 1.3. Proton coupled electron transfer (PECT) process involving formation of high-valent Ru^{IV}-oxo species

The molecular orbital (MO) diagram of metal-oxo species shows the interaction between ruthenium d-orbitals (d_{xz}, d_{yz}) with oxygen p-orbitals (p_x, p_y). This coordination destabilizes both d_{xz} and d_{xy} which are degenerate highest occupied molecular orbitals (HOMO) to form π bond and $d_z{}^2$ to form a σ bond between ruthenium and oxygen.[29] As depicted in Fig 1, $Ru^{IV}=O$, the lone pair of oxygen is partially delocalized on the metal center, while the d_{xz} and d_{yz} orbitals are partially delocalized onto the oxygen.[29] This interaction leads to some electron transfer from ruthenium to oxygen.
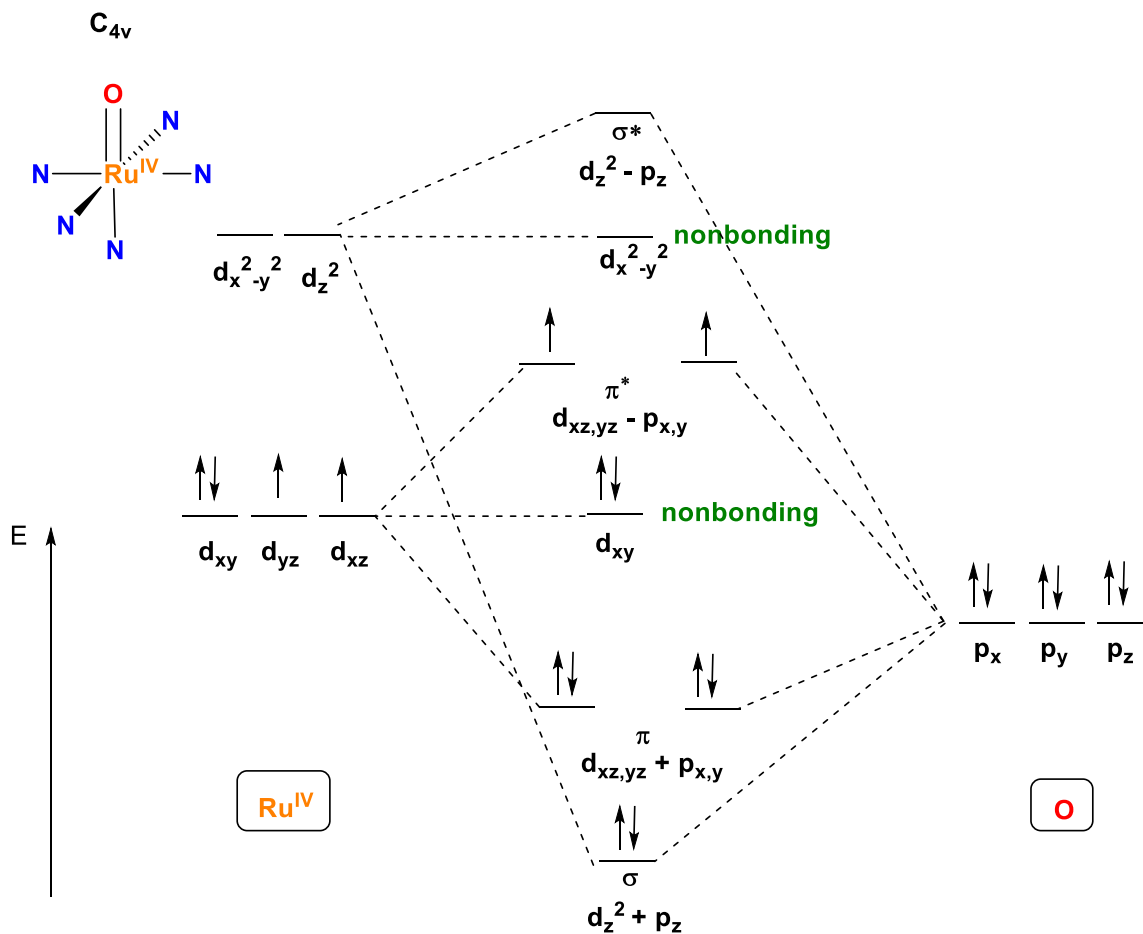
Figure 1.1. Schematic molecular orbital (MO) diagram for high-valent Ru^{IV}=O complex

Following formation of the ruthenium oxo or hydroxo species, C-H bond hydroxylation can proceed via two distinct pathways, radical rebound and oxene insertion. As the mechanism followed by an oxidation catalyst is the most important factor in determining its overall stereoselectivity, significant effort has been devoted to identifying which factors influence the pathway followed by different catalysts.

Radical Rebound

$[M]^{III}$—OH
+
R_2 R_1

$[M]^{II}$-OH$_2$ O ‖ M^{IV} Or M^{III}—O·   +   H R_1 R_2

Ox^n Ox^{n-2} + 2H$^+$

OH
R_1 R_2

$[M]^{IV}$=O R_2 R_1 H

Direct Insertion
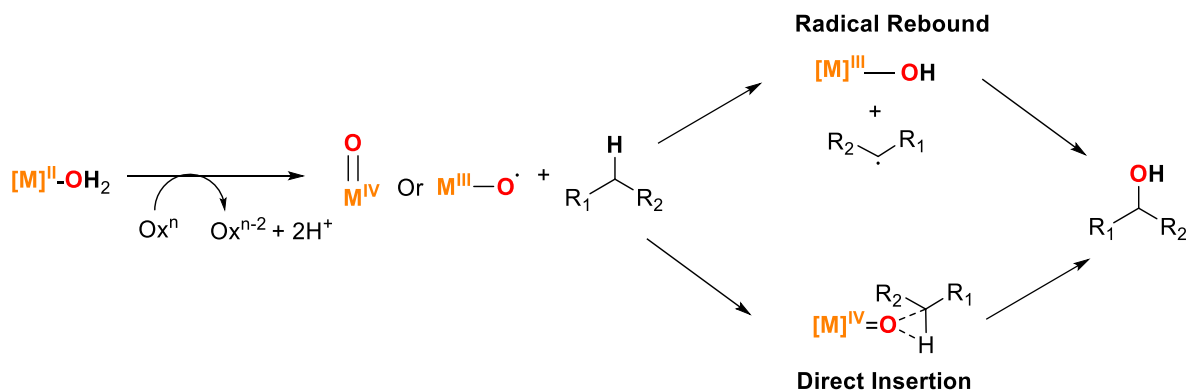
Scheme 1.4. General mechanisms of C-H bond hydroxylation by transition metal catalysts

1.4.2. Radical Rebound Mechanism

The most common mechanism of C-H bond hydroxylation is the radical rebound. Originally proposed by Groves,[30,31] the rebound mechanism involves initial H-atom abstraction from an aliphatic substrate by the high-valent metal oxo or hydroxo species (Scheme 4). The substrate radical species formed then further reacts with the Ru catalyst to form the C-O bond. Under this mechanism, the rate determining step (RDS) is typically H-atom abstraction by the high-valent Ru catalyst. As such, the overall rate of the reaction is directly controlled overall strength of the C-H bond dissociation energy (BDE), as well as the oxidizing potential of the catalyst. It is sufficient to say that, for any particular catalyst, the rate of the reaction follows that predicted by the Evans-Polanyi correlation,[32] i.e. the log of the rate constant (k) varies linearly with the BDE of the substrate C-H bond. Thus, the rebound mechanism selectively oxidizes weaker C-H bonds in preference to stronger C-H bonds, and greater selectivity is predicted for catalysts with lower oxidizing potentials. One of the prominent examples of radical rebound mechanisms involve Fenton's reagent, hydroxylation of alkanes by a mixture of hydrogen peroxide and ferrous salts.[33,34]

In the rebound mechanism, stereoselectivity is determined in the moments following H-atom abstraction. If the nascent substrate radical reacts quickly with the newly formed Ru-OH,

8

the original configuration of the C atom can be retained leading to a retention of stereochemistry. On the other hand, if there is even momentary delay in the rebound, the substrate radical has the opportunity to isomerize, resulting in a racemic product mixture. Further one electron H-atom abstraction is typically much faster in O-H than in C-H bond, resulted in formation of overoxidized product.

1.4.3. Direct Insertion Mechanism

Direct insertion mechanisms involve inserting an active ligand such as a carbene, nitrene, or oxene between the C-H bond without forming a metal-alkyl intermediate. While well established as a mechanism for the formation of C-C and C-N bonds,[35,36] relatively few examples of C-O bond formation via insertion have been reported. As originally proposed by Shaik for H_2 oxidation,[37] in the insertion mechanism the Ru=O or Ru-O$^•$ species reacts with the substrate in a single two-electron step to form a bound product alcohol in the RDS (Scheme 4). This bound product then exchanges for solvent and the Ru center can be re-oxidized to its high valent state by the oxidizing agent. Oxene insertion provides several advantages over radical rebound, the most important of which is that there is no opportunity of isomerization in the transition state, and therefore no racemization during the formation of the C-O bond and no formation of overoxidized products without presence of carbon radical intermediate (Scheme 5).
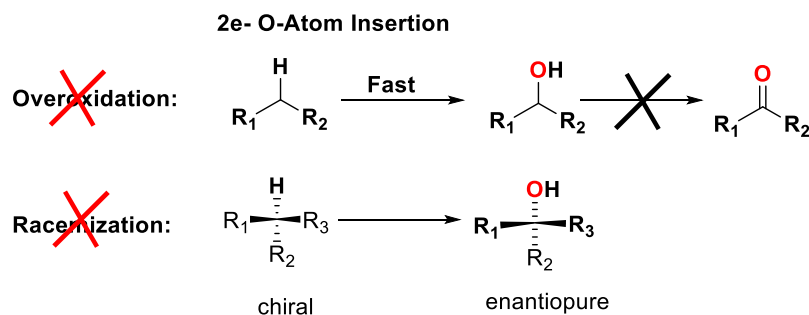
Scheme 1.5. Successful strategies to overcome overoxidation and racemization by inserting 2e⁻s to C-H bond

1.5. Electronic Properties of Ligands

Ligands often play crucial role in metal catalysts by promoting high oxidation state of the metal complex, that are often required to mediate oxidative transformations[28] such as water oxidation and other types of oxidations.[38,39] However, powerful oxidation catalysts can destroy the ligand set when achieving high oxidation states.[40] Thus, when designing the metal complexes, it is important to introduce more oxidatively robust chelate ligands to attain high oxidation states at a narrow potential window.[28,41] The redox potentials of metal complexes can be tuned through ligands by introducing electron donating and electron accepting ligands.[42] The negatively charge anionic ligands play a vital role in stabilizing high oxidation state of the metal complex with relatively low oxidation potential.[41] Therefore, introducing anionic ligands would be a promising approach to design catalysts for effective C-H bond oxidation.

1.5.1. Lever Electrochemical Parameter

Properties of the transition metal complexes can vary widely and mostly depend on the electronic and steric effects of the ligands.[43] One of the widely used parameter to measure electronic effects of the ligands is Lever parameter (E_L) which was introduced by Lever and Co-workers.[44] The Lever parameter is an empirical, ligand-based value determined by measuring the standard electrochemical potential (E_0) for the Ru(III)/(II) couple over a large variety of octahedral Ru complexes.[44] Data collected by this method is restricted to electrochemically reversible or at least quasi reversible redox couples at the metal ion.[44] The Lever parameters assigned to given ligands are used to determine the values of other ligands. When considering RuL_6 complex, E_L is defined as the one sixth of $\sum E_L$. The ligand parameters of over 200 different ligands collected in acetonitrile[44] are presented and the model is tested for wide range

of coordination and organometallic complexes. On the basis of ligand parameters of individual

ligands, the redox potential of Ru(III/II) is defined according to the following equation.

$$E_{1/2} = S_M[\Sigma a_i E_L(L_i)] + I_M$$

Where $E_L(L_i)$ is the Lever parameter of ligand L_i and a_i is the number of such ligands.

The quantities of S_M and I_M are constants which depend on the identity of the metal and solvent.

Linear correlation was observed between $E_{1/2}(Ru(III/II))$ value and sum of the Lever parameters

(ΣE_L) of ligands in a given complex (Figure 2). The standard parameters are independent of

supporting electrolytes and discrete solvent effects.[44] However, data collected in water may be

more scattered than those collected in common organic solvents due to the variation of

electrolytes and pH in water (Figure 2).
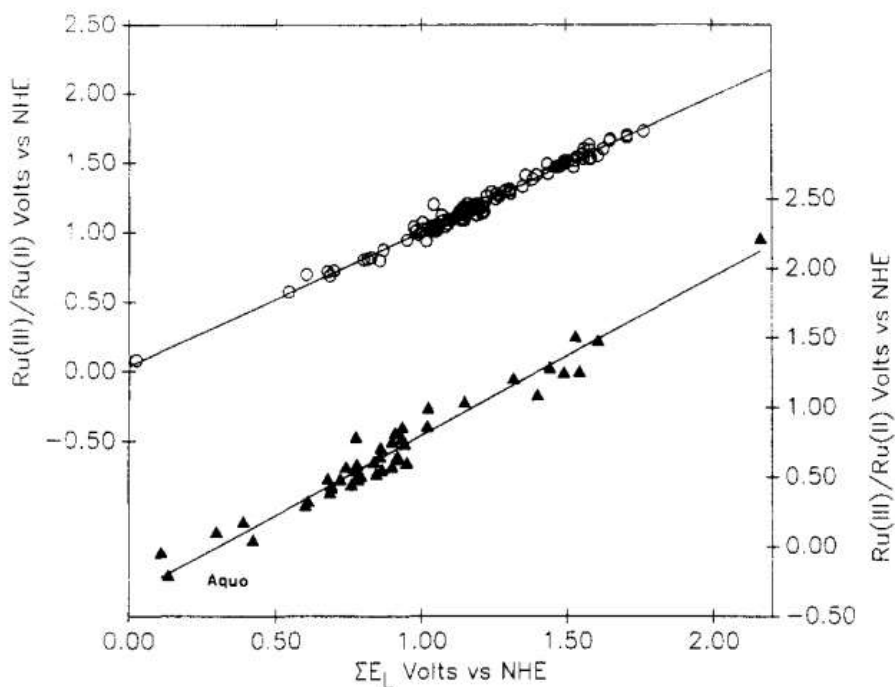
Figure 1.2. Plot of observed Ru(III)/(II) redox potentials of RuXxYyZz complexes against the sum of the Lever electrochemical parameter (ΣE_L) of substituted ligands. (top, open circles) measured in organic phase and referred to left hand y axis; (bottom, closed triangles) measured in water and referred to right hand y-axis. All the data are vs NHE[44]

11

Later Dovletoglou, Adeyemi, and Meyer's were published interesting results showing the relationship between variation of sum of the Lever electrochemical parameter (ΣE_L) on $\Delta E_{1/2}$ {$=E_{1/2}$ (Ru(IV/III)) – (Ru(III/II))} for series of ruthenium polypyridyl aqua complexes.[45] Lever parameter was derived for the series of related five ancillary ligands containing sigma σ and π acceptor ligands in Ru^{IV}=O/Ru^{III}-OH and Ru^{III}-OH/Ru^{II}-OH_2 couples. As depicted in Figure 3, the effect of ligand variation on $\Delta E_{1/2}$ values falls into two distinct regions. Ruthenium complexes containing σ-donor ligands show negative (-1.0) slope and increases $\Delta E_{1/2}$ value result in stabilization of Ru^{III} by electron donating effect whereas π acceptor ligands show positive (+1.2) slope and increases $\Delta E_{1/2}$ value result in stabilization Ru^{II} by back bonding effect. However, by extrapolation of these two lines, the intersection at E_L=1.06 V and $\Delta E_{1/2}$ = -0.11 V indicates a region where Ru^{III} is unstable with respect to disproportion. In such case, Ru^{IV} and Ru^{II} is relatively stable with respect to Ru^{III} and the complex behaves as a two electron oxidant (($E_{1/2}(Ru^{III}/Ru^{II})$>$E_{1/2}(Ru^{IV}/Ru^{III})$)). Ruthenium complexes with reduced $\Delta E_{1/2}$ value will disfavor HAT reaction and can undergo PCET process.
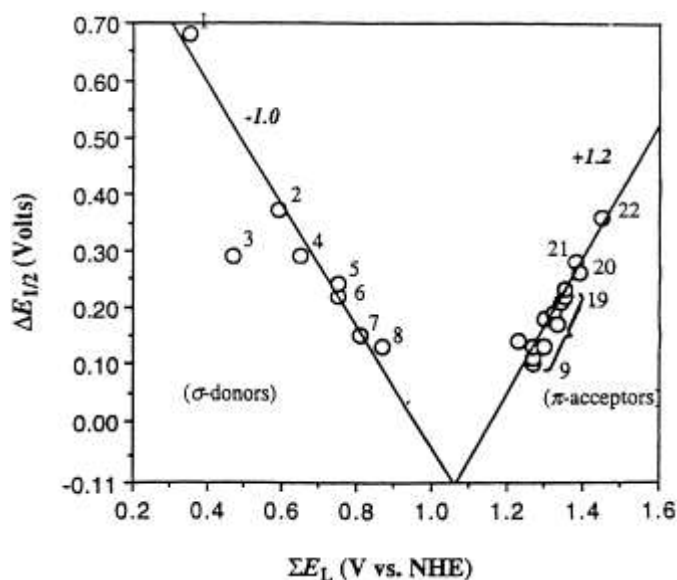
Figure 1.3. Plot of difference between Ru^{IV}/Ru^{III} and Ru^{III}/Ru^{II} potentials ($\Delta E_{1/2}$) as function of sum of Lever parameters (ΣE_L) of Ru^{III}/Ru^{II} couple[45]

1.5.2. Polypyridine Ligands
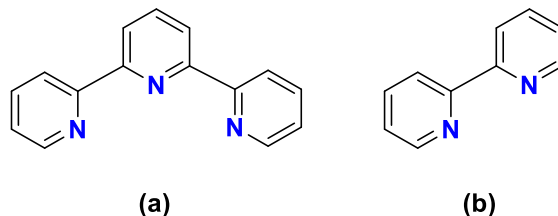
Figure 1.4. Structures of terpyridine (a), and bipyridine (b) ligands

Most ruthenium complexes consist of polypyridine ligands. Among these, 2,2':6',2"-terpyridine (tpy) and 2,2'-bipyridine (bpy) are very commonly used ligands in coordination chemistry. The major role of polypyridine ligands is to provide lone pair to the metal center through σ-donation to form a dative bond. Apart from the nitrogen lone pairs, delocalized π* orbitals in the ring can act as acceptors of metal electron density. Therefore, pyridine coordination provides large field stabilization energy and can thus be effective in forming low spin transition metal complexes.[29] Polypyridine ligands are also effective chelating ligands, enabling them to tolerate harsh oxidation and hydrolysis conditions.[29]

1.5.3. Pyridine Alkoxide Ligand
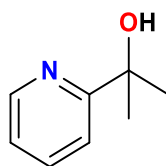
Figure 1.5. Structure of pyridine alkoxide ligand. Deprotonation occurs on binding to the metal center

Pyridine alkoxide (pyalkH) ligand is one of the best robust ligands for achieving high oxidation activity, due to its strong donor ability and oxidative resistance.[28] The ligand consists combination of pyridyl, alcohol and methyl groups which makes the ligand strong amphilic character. Therefore, it is soluble in wide range of aqueous and nonaqueous solvents.

13

Pyridine itself is a good donor and acts as an anchor to readily binds with metal to form a stable metal ligand bond, while the alkoxide group provides strong σ donation[44] and can stabilize high oxidation states of metals. Binding of alkoxide ligands with low oxidation metals become less stable, and ligand prone to protonation and dissociation during catalytic turnover.[28]

1.5.4. Phosphonic Acid Ligands

(a)   (b)
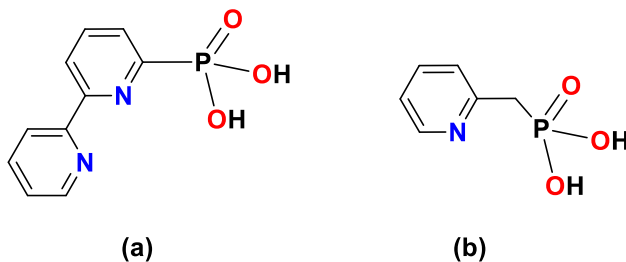
Figure 1.6. Structures of polypyridyl phosphonate ligands, bipyridine phosphonate (a), and methylpyridine phosphonate (b). Deprotonation occurs at one of the hydroxyl group (-OH) on binding to the metal center

Phosphonates are versatile ligands, however using these ligands in metal catalysis is relatively unexplored.[46] The ligand appears to be more useful when synthesizing the metal complexes due to its unique characteristics. The complexes consist of this ligand can show pH dependent redox chemistry associated with protonation or deprotonation of the hydroxyl group attached to the ligand. Deprotonation of the -OH group via PCET enabling easy access of high oxidation state of metal complex.[47] These ligands provide three key functionalities besides charge compensation and strong donation ability. Due to the phosphonate group the complexes shows high water solubility, the potential for PCET allows these complexes to substantially lower the differences between consecutive oxidation potentials, and phosphonate groups can facilitate proton transfer during catalysis.[47]

1.6. Pioneering Work – Ruthenium Catalyzed Alkane Hydroxylation

Ru complexes have played an important role in developing C-H bond hydroxylation. This is due to the combined importance of installing functional groups at unactivated sites in organic synthesis[6,48] and the relevance to the synthesis of liquid fuels from renewable resources.[49] With regards to Ru complexes synthesized for this reaction, a wide variety of ligand scaffolds have been employed, including porphyrins,[50] amines,[51] phosphines[52] and even polyoxometalates.[53] Among these scaffolds, polypyridyl ligands are among the best studied due to their oxidation resistance and synthetic accessibility.[54]

1
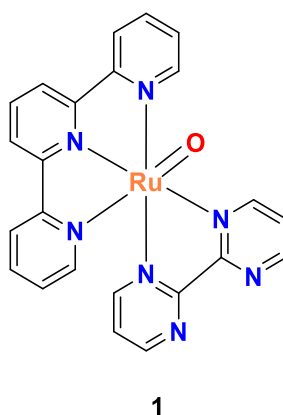
Figure 1.7. Structure diagram of $[Ru^{IV}(tpy)(2,2'\text{-bipyrimidine})(O)]^{2+}$ **1**[55]

A first example is the report by Nam and Shaik in 2015 of alkane hydroxylation complexes using polypyridyl ligands (Fig. 1.7).[55] In this report **1** was found to catalyze the hydroxylation of allylic and aliphatic C-H bonds. The RDS for each of these reactions is H-atom abstraction, however Ru^{III} rather than the Ru^{II} expected from the rebound mechanism (Scheme 1.4) was found as the product during stoichiometric oxidation experiments. Further kinetic experiments revealed that the mechanism involved a "radical non-rebound" mechanism, where the initially formed Ru^{III}-OH species dissociates from the carbon radical. The carbon radical is then further oxidized to the alcohol by a second Ru^{IV}=O molecule (Scheme 1.6). This

mechanism is chemically distinct from the rebound mechanism yet may be indistinguishable

from a slow rebound under catalytic conditions, demonstrating the value of stoichiometric

kinetics studies.

$$Ru^{IV}{:}O \quad Ru^{III}{-}OH \qquad Ru^{IV}{:}O \quad Ru^{III}{-}OH$$

$$R{-}/ \xrightarrow{\hspace{2cm}} R{-}/\cdot \xrightarrow[\;H_2O\;]{\hspace{2cm}} R{-}\!\!\!\diagup\!\!\!\diagdown_{OH}$$
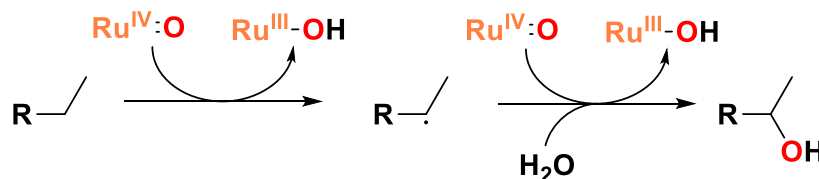
Scheme 1.6. General mechanism of radical non-rebound C-H bond hydroxylation

More recently, the Du Bois and Sigman groups have demonstrated selective C-H bond

oxidation using periodic acid and a Ru complex of 4,4'-di-tert-butyl-2,2'-bipyridine (dtbpy), **2**

(Fig. 1.8).[14] This complex was found to selectively hydroxylate only the most electron rich sites

in a variety of substrates, i.e. the catalysts show a strong preference for benzylic and tertiary

aliphatic sites. Of particular note is the tolerance of **3** for nitrogen-containing functional groups

(Table 1.1), which may be oxidized to N-oxides or coordinate to the metal center of the catalyst,

inhibiting the reaction. Key to this tolerance is the addition of an acid co-catalyst. It is

hypothesized that this acid additive inhibits binding of and oxidation at N-sites by protonating

them, although further investigation into this mechanism is ongoing. Oxidation of chiral

substrates by **3** shows nearly complete retention of stereochemistry, suggesting an oxene

insertion mechanism (Scheme 1.4), although a radical mechanism with rapid rebound cannot be

precluded on this basis alone.

2   **3**
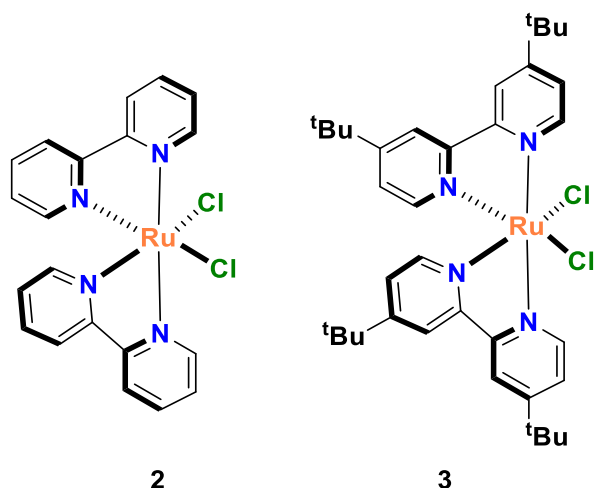
Figure 1.8. Structure diagram of [Ru(bpy)$_2$Cl$_2$] **2** and [Ru(dtbpy)$_2$Cl$_2$] **3**[14]

Table 1.1. Relative turnover frequencies and turnover numbers for C-H bond hydroxylation catalysts discussed in this section

Complex	Substrate	Oxidant	TOF (hr^{-1})	TON[a]	Ref.
2[b]	2-isohexylpyridine	H$_5$IO$_6$	3.5	14	14
3[b]	2-isohexylpyridine	H$_5$IO$_6$	4.1	16.2	14
3[c]	2-isohexylpyridine	H$_5$IO$_6$	4.5	17.8	14
3[c]	4'-isopropylacetophenone	H$_5$IO$_6$	4.6	18.4	14
4[d]	Ethylbenzene	NaIO$_4$	4.2	25	56
5[e]	Ethylbenzene	electrode	133	1600	57
8[f]	4-ethylbenzenesulfonate	CAN[g]	38	38	58
9[f]	4-ethylbenzenesulfonate	CAN[g]	35	35	58
10[f]	4-ethylbenzenesulfonate	CAN[g]	33	33	58

[a]Mols alcohol (ketone/aldehyde)/mols catalyst. [b]Reaction Conditions: 60 mM substrate, 3.0 mM catalyst, 180 mM oxidant, 360 mM triflic acid, 4 hours at RT in 1.67 mL 1:1 acetic acid:water solvent. [c]Reaction Conditions: 60 mM substrate, 3.0 mM catalyst, 120 mM oxidant, 360 mM triflic acid, 4 hours at RT in 1.67 mL 1:1 acetic acid:water solvent. [d]Reaction conditions: 55.6 mM substrate, 560 mM oxidant, 1.7 mM catalyst, in 4.5 mL 2:1 acetonitrile:water solvent for 6 hours at 70 ºC. [e]Reaction conditions: 10 nmol catalyst on a 1 cm^2 nano-ITO electrode, 20.0 mM substrate, 100.0 mM LiClO$_4$ electrolyte, 1.0% water in propylene carbonate solvent, 1.74 V constant potential for 12 hours at 23 ºC. [f]Reaction conditions: 100 mM substrate, 200 mM oxidant, 1 μM catalyst in D$_2$O for 1 hr at 23 ºC. [g]CAN = cerium(IV) ammonium nitrate

In 2017, Gupta and Choudhury reported an NHC-based Ru catalyst, **4**, for oxidation at benzylic C-H bonds (Fig. 1.9).[56] On the basis of ESI-MS and UV-Vis time-course studies, **4** was found to form a cis-di-oxo Ru^{VI} species when oxidized with $NaIO_4$, which then proceeds to abstract a benzylic H-atom in the RDS. This RDS was further supported by an observed H/D KIE of 3.4, indicating involvement of the substrate H-atom in the RDS. Addition of a radical trap to the reaction mixture resulted in a significant reduction in TOF and TON, strongly suggesting a radical rebound mechanism for this catalyst (Scheme 1.4). As is common in C-H bond oxidation, hydroxylation at secondary sites was not observed, with any product alcohols rapidly oxidized to the corresponding ketones.
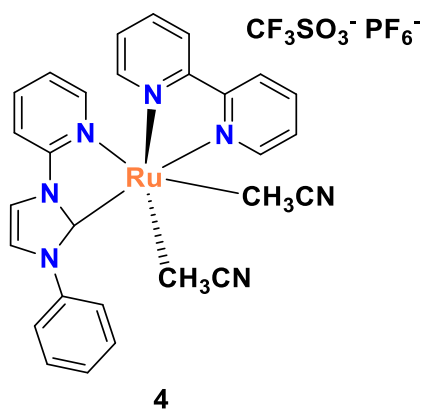
Figure 1.9. Structure diagram of [Ru(NHC)(bpy)(MeCN)$_2$](OTf)(PF$_6$) **4**[56]

A rare example of electrochemical C-H bond oxidation by a well-defined Ru catalyst was reported in 2012 by the Meyer group.[57] In this report, the bpy ligand of a known C-H bond oxidation catalyst, [Ru(Mebimpy)(bpy)(OH$_2$)](PF$_6$)$_2$ (Mebimpy = 2,6-bis(1-methylbenzimidazol-2-yl)pyridine), was modified with phosphonate groups to generate **5** (Fig. 1.10). When attached to a nano-ITO electrode, **5** was found to exhibit significant catalytic activity for the conversion of ethylbenzene to acetophenone (Table 1.1). Remarkably, the catalyst remains stable for hours on the electrode surface, leading to turnover numbers significantly greater than typically seen for

homogeneous catalysts and demonstrating the advantages of heterogenizing known catalysts.

KIE studies showed only a minor H/D KIE of 1.2. In conjunction with a lack of inhibition of the

reaction in the presence of O_2, this result suggests **5** operates via the oxene insertion mechanism

(Scheme 1.4). Unfortunately, during C-H bond oxidation by **5** no alcohol products are observed

to form. This is attributed to rapid oxidation of the alcohol intermediate by **5** at the electrode

surface before diffusion can occur.
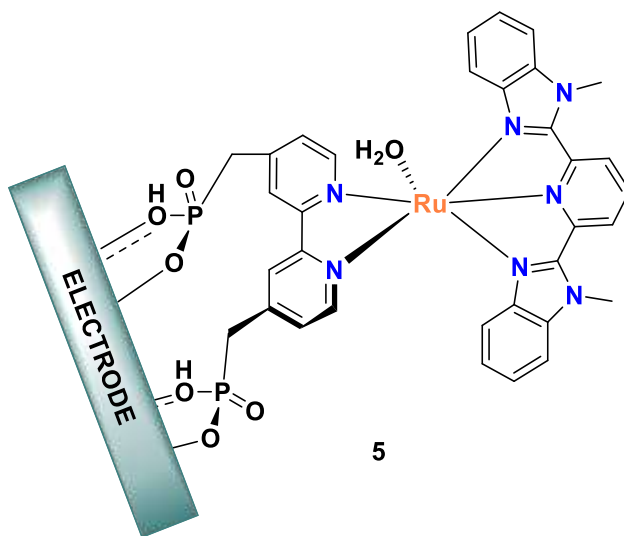
Figure 1.10. Structure diagram of the phosphonate functionalized
[Ru(Mebimpy)(bpy)(OH$_2$)](PF$_6$)$_2$ derivative **5**[57]

Kojima and Fukuzumi reported a particularly well characterized C-H bond hydroxylation

catalyst based on tris(2-pyridylmethyl)amine (tpa), [Ru(tpaH)(bpy)(O)](PF$_6$)$_3$ **6** (Fig. 1.11), in

2011.[24] Kinetic analysis of C-H bond oxidation of cumene by **6** revealed two distinct steps, the

observed rate constant for the first of which exhibited linear dependence on the concentration of

cumene and an H/D KIE of 12, and an observed rate constant for the second of which was

independent of cumene concentration and an H/D KIE of 1. Varying the substrate further

revealed that the observed rate constant for the first step decreased linearly with the substrates'

C-H bond dissociation energy (BDE). Based on these kinetic experiments, **6** was found to follow

the radical rebound mechanism (Scheme 1.4) with H-atom abstraction serving as the RDS in the catalytic cycle. Additionally, the inclusion of radical traps in the catalytic mixture had no effect on the rate or product distribution of **6**, further supporting the rebound over the non-rebound mechanisms. Remarkably, using ESI-MS the authors were able to identify the initial product of the rebound reaction with cumene, i.e. the bound cumyl alcohol species **7** (Fig. 1.11). Further investigation of the products via ESI-MS determined that the second observable step in the C-H bond hydroxylation by **6** is irreversible ligand exchange between the bound, oxidized substrate and the acetonitrile used as solvent.
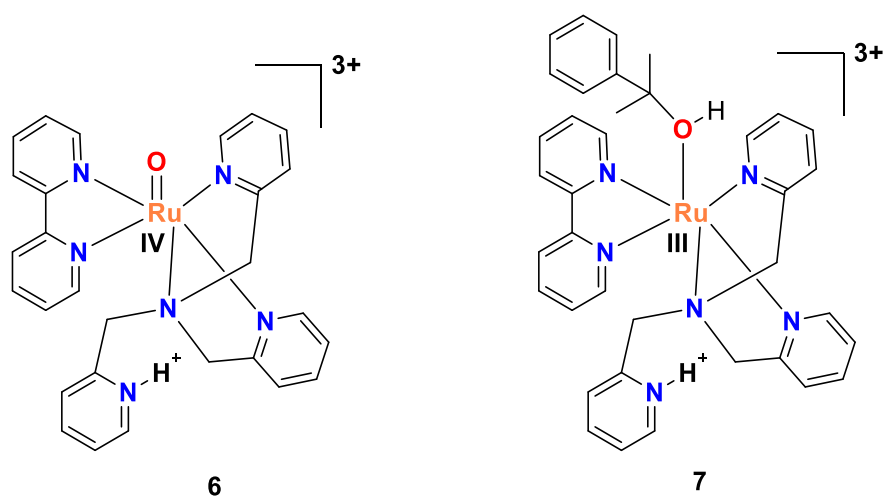
Figure 1.11. Structure diagrams of [Ru(tpaH)(bpy)(O)](PF$_6$)$_3$, **6**, and its rebound product with cumene, **7**[24]

Based on this work, in 2012 Fukuzumi and Kojima reported on the C-H bond oxidation activity of several Ru(tpa)-based complexes (Fig. 1.12).[58] These complexes were found to serve as very active catalysts for the oxidation of alcohol to aldehydes and ketones, and were also capable of oxidizing benzylic C-H bonds to the corresponding ketones (Table 1.1). H/D isotope studies on the oxidation of methanol by the corresponding Ru^{IV} oxo species showed KIEs of 1.7-2.5 depending on the catalyst. These values indicate that the RDS in C-H bond oxidation by these complexes is H-atom abstraction which is followed by radical rebound (Scheme 1.4).
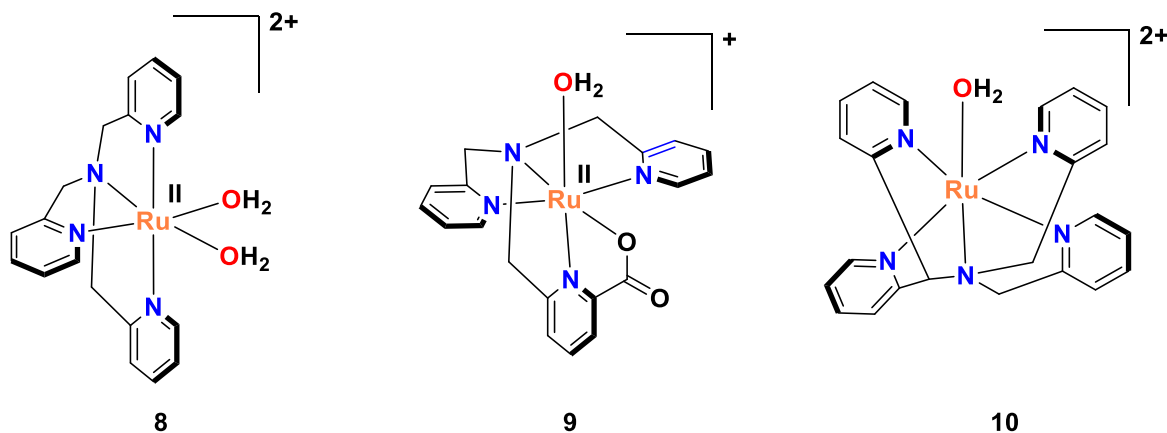
Figure 1.12. Structure diagrams of Ru(tpa)-based C-H bond oxidation catalysts **8-10**[58]

1.7. Research Goal

Selective C-H bond hydroxylation under mild conditions is a significant challenge due to the relative ease of overoxidation and racemization. Reports on converting C-H to C-OH by transition metal complexes are mostly limited and existing catalysts for this conversion are scarce and extremely substrate specific. To design efficient catalysts for C-H bond oxidation, it is often required that metal complexes should be able to reach high oxidation state at a very narrow potential range and be able to survive under harsh oxidation conditions. Our main research goal is to design new ruthenium catalysts, that favor direct two electron oxene insertion pathway over one electron radical pathway, thereby reduce the overoxidation and improve stereoretention during C-H bond hydroxylation. This can be achieved by introducing anionic ligands to the complex and the anionic character of these ligands exert strong donation effect over ruthenium center to achieving the high oxidation state and enable lower oxidation potential of the catalysts. In the current work, we present the work of synthesis, characterization, investigation of electrochemical properties and catalytic performance of new ruthenium complexes towards C-H bond hydroxylation. Designing new ruthenium complexes containing

21

anionic ligands reveals the catalytic properties towards sustainable organic transformations and enable the use of more benign oxidants in these reactions.

1.8. References

1.   Goldman, A. S. & Goldberg, K. I. Organometallic C—H Bond Activation: An Introduction. in *Activation and Functionalization of C—H Bonds* vol. 885 1–43 (American Chemical Society, 2004).

2.   Labinger, J. A. & Bercaw, J. E. Understanding and exploiting C–H bond activation. *Nature* **417**, 507–514 (2002).

3.   Kakiuchi, F. & Chatani, N. Catalytic Methods for C-H Bond Functionalization: Application in Organic Synthesis. *Advanced Synthesis & Catalysis* **345**, 1077–1101 (2003).

4.   Balcells, D., Clot, E. & Eisenstein, O. C—H Bond Activation in Transition Metal Species from a Computational Perspective. *Chem. Rev.* **110**, 749–823 (2010).

5.   Dantignana, V. *et al.* Chemoselective Aliphatic C–H Bond Oxidation Enabled by Polarity Reversal. *ACS Cent. Sci.* **3**, 1350–1358 (2017).

6.   Hartwig, J. F. & Larsen, M. A. Undirected, Homogeneous C–H Bond Functionalization: Challenges and Opportunities. *ACS Cent. Sci.* **2**, 281–292 (2016).

7.   Shilov, A. E. & Shul'pin, G. B. Activation of C−H Bonds by Metal Complexes. *Chem. Rev.* **97**, 2879–2932 (1997).

8.   Borovik, A. S. Role of metal–oxo complexes in the cleavage of C–H bonds. *Chem. Soc. Rev.* **40**, 1870–1874 (2011).

9. Da Silva, J. C. S., Pennifold, R. C. R., Harvey, J. N. & Rocha, W. R. A radical rebound mechanism for the methane oxidation reaction promoted by the dicopper center of a pMMO enzyme: a computational perspective. *Dalton Trans.* **45**, 2492–2504 (2016).

10. Lindhorst, A. C., Haslinger, S. & Kühn, F. E. Molecular iron complexes as catalysts for selective C–H bond oxygenation reactions. *Chem. Commun.* **51**, 17193–17212 (2015).

11. Nanjo, T., de Lucca, E. C. & White, M. C. Remote, Late-Stage Oxidation of Aliphatic C–H Bonds in Amide-Containing Molecules. *J. Am. Chem. Soc.* **139**, 14586–14591 (2017).

12. Kawamata, Y. *et al.* Scalable, Electrochemical Oxidation of Unactivated C–H Bonds. *J. Am. Chem. Soc.* **139**, 7448–7451 (2017).

13. McNeill, E. & Du Bois, J. Ruthenium-Catalyzed Hydroxylation of Unactivated Tertiary C−H Bonds. *J. Am. Chem. Soc.* **132**, 10202–10204 (2010).

14. Mack, J. B. C., Gipson, J. D., Du Bois, J. & Sigman, M. S. Ruthenium-Catalyzed C–H Hydroxylation in Aqueous Acid Enables Selective Functionalization of Amine Derivatives. *J. Am. Chem. Soc.* **139**, 9503–9506 (2017).

15. Crabtree, R. H. Alkane C–H activation and functionalization with homogeneous transition metal catalysts: a century of progress—a new millennium in prospect. *J. Chem. Soc., Dalton Trans.* 2437–2450 (2001) doi:10.1039/B103147N.

16. Nam, W. High-Valent Iron(IV)–Oxo Complexes of Heme and Non-Heme Ligands in Oxygenation Reactions. *Acc. Chem. Res.* **40**, 522–531 (2007).

17. Chen, Z. *et al.* Transition metal-catalyzed C–H bond functionalizations by the use of diverse directing groups. *Org. Chem. Front.* **2**, 1107–1295 (2015).

18. Blakemore, J. D., Crabtree, R. H. & Brudvig, G. W. Molecular Catalysts for Water Oxidation. *Chem. Rev.* **115**, 12974–13005 (2015).

19. Thirunavukkarasu, V. S., Kozhushkov, S. I. & Ackermann, L. C–H nitrogenation and oxygenation by ruthenium catalysis. *Chem. Commun.* **50**, 29–39 (2014).

20. Ishizuka, T., Ohzu, S. & Kojima, T. Oxidation of Organic Substrates with Ru(IV)=O Complexes Formed by Proton- Coupled Electron Transfer. *Synlett* **25**, 1667–1679 (2014).

21. Shimoyama, Y. *et al.* A Ruthenium(III)–Oxyl Complex Bearing Strong Radical Character. *Angewandte Chemie* **128**, 14247–14251 (2016).

22. Gunay, A. & Theopold, K. H. C−H Bond Activations by Metal Oxo Compounds. *Chem. Rev.* **110**, 1060–1081 (2010).

23. Michaelos, T. K. *et al.* A Pyridine Alkoxide Chelate Ligand That Promotes Both Unusually High Oxidation States and Water-Oxidation Catalysis. *Acc. Chem. Res.* **50**, 952–959 (2017).

24. Kojima, T., Nakayama, K., Ikemura, K., Ogura, T. & Fukuzumi, S. Formation of a Ruthenium(IV)-Oxo Complex by Electron-Transfer Oxidation of a Coordinatively Saturated Ruthenium(II) Complex and Detection of Oxygen-Rebound Intermediates in C–H Bond Oxygenation. *J. Am. Chem. Soc.* **133**, 11692–11700 (2011).

25. Hirai, Y. *et al.* Ruthenium-Catalyzed Selective and Efficient Oxygenation of Hydrocarbons with Water as an Oxygen Source. *Angewandte Chemie International Edition* **47**, 5772–5776 (2008).

26. Ishizuka, T., Kotani, H. & Kojima, T. Characteristics and reactivity of ruthenium–oxo complexes. *Dalton Trans.* **45**, 16727–16750 (2016).

27. Weinberg, D. R. *et al.* Proton-Coupled Electron Transfer. *Chem. Rev.* **112**, 4016–4093 (2012).

28.	Michaelos, T. K. *et al.* A Pyridine Alkoxide Chelate Ligand That Promotes Both Unusually High Oxidation States and Water-Oxidation Catalysis. *Acc. Chem. Res.* **50**, 952–959 (2017).

29.	Tong, L. & Thummel, R. P. Mononuclear ruthenium polypyridine complexes that catalyze water oxidation. *Chem. Sci.* **7**, 6591–6603 (2016).

30.	Groves, J. T. & Van der Puy, M. Stereospecific aliphatic hydroxylation by an iron-based oxidant. *J. Am. Chem. Soc.* **96**, 5274–5275 (1974).

31.	Groves, J. T. & McClusky, G. A. Aliphatic hydroxylation via oxygen rebound. Oxygen transfer catalyzed by iron. *J. Am. Chem. Soc.* **98**, 859–861 (1976).

32.	Evans, M. G. & Polanyi, M. Inertia and driving force of chemical reactions. *Trans. Faraday Soc.* **34**, 11–24 (1938).

33.	Fenton, H. J. H. LXXIII.—Oxidation of tartaric acid in presence of iron. *J. Chem. Soc., Trans.* **65**, 899–910 (1894).

34.	Walling, C. Fenton's reagent revisited. *Acc. Chem. Res.* **8**, 125–131 (1975).

35.	Davies, H. M. L. & Beckwith, R. E. J. Catalytic Enantioselective C−H Activation by Means of Metal−Carbenoid-Induced C−H Insertion. *Chem. Rev.* **103**, 2861–2904 (2003).

36.	Ping, L., Chung, D. S., Bouffard, J. & Lee, S. Transition metal-catalyzed site- and regio-divergent C–H bond functionalization. *Chem. Soc. Rev.* **46**, 4299–4328 (2017).

37.	Filatov, M. & Shaik, S. Theoretical Investigation of Two-State-Reactivity Pathways of H−H Activation by FeO+: Addition−Elimination, "Rebound", and Oxene-Insertion Mechanisms. *J. Phys. Chem. A* **102**, 3835–3846 (1998).

38.	Thomsen, J. M., Huang, D. L., Crabtree, R. H. & Brudvig, G. W. Iridium-based complexes for water oxidation. *Dalton Trans.* **44**, 12452–12472 (2015).

39.   Sun, C.-L., Li, B.-J. & Shi, Z.-J. Direct C−H Transformation via Iron Catalysis. *Chem. Rev.* **111**, 1293–1314 (2011).

40.   Crabtree, R. H. Deactivation in Homogeneous Transition Metal Catalysis: Causes, Avoidance, and Cure. *Chem. Rev.* **115**, 127–150 (2015).

41.   Kundu, A., Dey, S. K., Dey, S., Anoop, A. & Mandal, S. Mononuclear Ruthenium-Based Water Oxidation Catalyst Supported by Anionic, Redox-Non-Innocent Ligand: Heterometallic O–O Bond Formation via Radical Coupling Pathway. *Inorg. Chem.* **59**, 1461–1470 (2020).

42.   Dakkach, M. *et al.* New Ru(II) Complexes with Anionic and Neutral N-Donor Ligands as Epoxidation Catalysts: An Evaluation of Geometrical and Electronic Effects. *Inorg. Chem.* **49**, 7072–7079 (2010).

43.   Perrin, L., Clot, E., Eisenstein, O., Loch, J. & Crabtree, R. H. Computed Ligand Electronic Parameters from Quantum Chemistry and Their Relation to Tolman Parameters, Lever Parameters, and Hammett Constants. *Inorg. Chem.* **40**, 5806–5811 (2001).

44.   Lever, A. B. P. Electrochemical Parametrization of Metal Complex Redox Potentials, Using the Ruthenium(III)/Ruthenium(II) Couple To Generate a Ligand Electrochemical Series. *Inorganic Chemistry* **29**, 1271–1285 (1990).

45.   Dovletoglou, A., Adeyemi, S. A. & Meyer, T. J. Coordination and Redox Chemistry of Substituted-Polypyridyl Complexes of Ruthenium. *Inorg. Chem.* **35**, 4120–4127 (1996).

46.   Kamdar, J. M. *et al.* Ruthenium Complexes of 2,2′-Bipyridine-6,6′-diphosphonate Ligands for Water Oxidation. *ChemCatChem* **8**, 3045–3049 (2016).

47. Xie, Y., Shaffer, D. W., Lewandowska-Andralojc, A., Szalda, D. J. & Concepcion, J. J. Water Oxidation by Ruthenium Complexes Incorporating Multifunctional Bipyridyl Diphosphonate Ligands. *Angewandte Chemie International Edition* **55**, 8067–8071 (2016).

48. Newhouse, T. & Baran, P. S. If C□H Bonds Could Talk: Selective C-H Bond Oxidation. *Angewandte Chemie International Edition* **50**, 3362–3374 (2011).

49. Hashiguchi, B. G., Bischof, S. M., Konnick, M. M. & Periana, R. A. Designing Catalysts for Functionalization of Unactivated C–H Bonds Based on the CH Activation Reaction. *Acc. Chem. Res.* **45**, 885–898 (2012).

50. Ito, R., Umezawa, N. & Higuchi, T. Unique Oxidation Reaction of Amides with Pyridine-N-oxide Catalyzed by Ruthenium Porphyrin: Direct Oxidative Conversion of N-Acyl-l-proline to N-Acyl-l-glutamate. *J. Am. Chem. Soc.* **127**, 834–835 (2005).

51. Yip, W.-P., Yu, W.-Y., Zhu, N. & Che, C.-M. Alkene cis-Dihydroxylation by [(Me3tacn)(CF3CO2)RuVIO2]ClO4 (Me3tacn = 1,4,7-Trimethyl-1,4,7-triazacyclononane): Structural Characterization of [3 + 2] Cycloadducts and Kinetic Studies. *J. Am. Chem. Soc.* **127**, 14239–14249 (2005).

52. Marmion, M. E. & Takeuchi, K. J. Preparation and characterization of stable ruthenium(IV)-oxo complexes that contain tertiary phosphine ligands. *J. Am. Chem. Soc.* **108**, 510–511 (1986).

53. Neumann, R. & Dahan, M. Molecular Oxygen Activation by a Ruthenium-Substituted "Sandwich" Type Polyoxometalate. *J. Am. Chem. Soc.* **120**, 11969–11976 (1998).

54. Kojima, T. *et al.* Synthesis and Characterization of Mononuclear Ruthenium(III) Pyridylamine Complexes and Mechanistic Insights into Their Catalytic Alkane

Functionalization with m-Chloroperbenzoic Acid. *Chemistry – A European Journal* **13**, 8212–8222 (2007).

55.   Dhuri, S. N. *et al.* Interplay of Experiment and Theory in Elucidating Mechanisms of Oxidation Reactions by a Nonheme RuIVO Complex. *J. Am. Chem. Soc.* **137**, 8623–8632 (2015).

56.   Gupta, S. K. & Choudhury, J. A Mixed N-Heterocyclic Carbene/2,2′-Bipyridine-Supported Robust Ruthenium(II) Oxidation Precatalyst for Benzylic C−H Oxidation. *ChemCatChem* **9**, 1979–1984 (2017).

57.   Vannucci, A. K., Chen, Z., Concepcion, J. J. & Meyer, T. J. Nonaqueous Electrocatalytic Oxidation of the Alkylaromatic Ethylbenzene by a Surface Bound RuV(O) Catalyst. *ACS Catal.* **2**, 716–719 (2012).

58.   Ohzu, S. *et al.* Mechanistic insight into catalytic oxidations of organic compounds by ruthenium(IV)-oxo complexes with pyridylamine ligands. *Chem. Sci.* **3**, 3421–3431 (2012).

CHAPTER 2. ELECTROCHEMICAL PROPERTIES AND C-H BOND OXIDATION ACTIVITY OF [RU(TPY)(PYALK)CL]$^+$ AND [RU(TPY)(PYALK)(OH)]$^+$

2.1. Introduction

C-H bond activation reactions are one of organic chemistry's most fundamental tools.[1–3] These reactions typically employ a transition metal catalyst to reduce the kinetic barrier for breaking the C-H bond. Due to their importance, a significant amount of effort has been spent increasing the selectivity,[4,5] expanding the substrate scope,[6–8] and improving the sustainability of these C-H bond activation catalysts.[9–12] One key area of C-H bond activation is oxidation of the C-H bonds to form C-OH or C=O bonds.[5,12] Typically, this C-H bond oxidation proceeds via the formation of a high-valent metal oxo or oxyl species generated by reaction of a transition metal catalyst with a sacrificial chemical oxidant. This high-valent oxo species can then participate in two-electron insertion into the C-H bond, or H-atom abstraction followed by radical rebound (Scheme 2.1).[8] The selectivity and substrate scope of the C-H bond oxidation reaction is determined by the pathway followed, which in turn is dependent on the nature of the high-valent oxo species.[13,14]
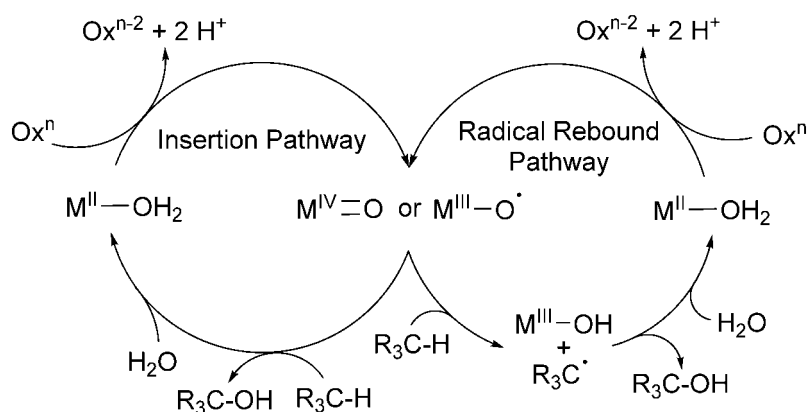
Scheme 2.1. General catalytic cycle for transition metal catalyzed C-H bond hydroxylation. Ox = two-electron sacrificial oxidant, M = transition metal

Among the best characterized C-H bond oxidation catalysts are those based on Ru.[4,15–17] In particular, the redox properties of Ru-based coordination catalysts have been characterized for a wide variety of ligand scaffolds. Despite their well-established redox chemistry,[18–25] relatively few Ru complexes containing inner-sphere anionic ligands have been reported as C-H bond oxidation catalysts. In particular, the authors are aware of only one prior example of a Ru alkoxide complex being used to catalyze C-H bond oxidation.[25]

Our group is interested in developing new C-H bond activation catalysts with lower redox potentials, thereby enabling the use of more sustainable oxidants in these reactions. We hypothesize that anionic ligands can be used to achieve C-H bond oxidation catalysis at these lower potentials. In order to test this hypothesis, we have synthesized [Ru(tpy)(pyalk)Cl]$^+$, **1**, and [Ru(tpy)(pyalk)(OH)]$^+$, **2**, (Fig. 2.1), Ru complexes with a strong-donor alkoxide ligand, and characterized their redox properties and ability to catalyze C-H bond oxidation.

[Ru(tpy)(pyalk)Cl]$^+$ **1**   [Ru(tpy)(pyalk)OH]$^+$ **2**
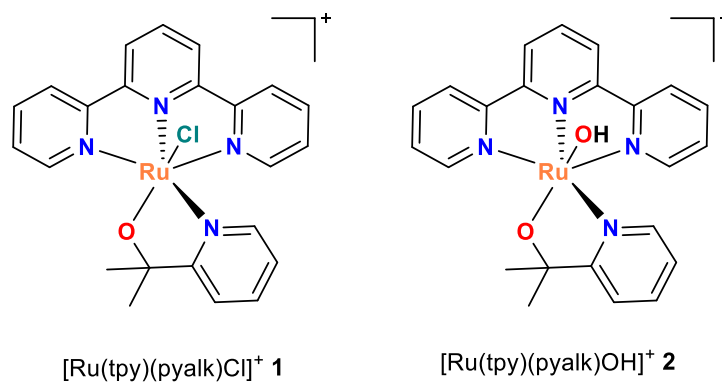
Figure 2.1. Structures of Ru coordination complexes studied in this chapter

2.2. Results

2.2.1. Structural Properties of [Ru(tpy)(pyalk)Cl]$^+$ (1)

Structural parameters for **[1]BPh₄** were determined by X-ray diffraction after exchanging the outer-sphere chloride anion for a tetraphenyl borate anion to promote crystal growth (Fig. 2.2). As visible in the crystal structure, the O-atom of the pyalk ligand binds trans to the inner

sphere Cl ligand, as expected from a comparison of the relative kinetic trans effects of the ligand moieties (RO⁻<py<Cl⁻).[26] The Ru-Cl bond length of 2.383 Å is somewhat shorter than that seen in [Ru(tpy)(phpy)Cl]PF$_6$ (2.443 Å),[27] consistent with a weaker trans influence by the alkoxide moiety in **1** relative to the phenyl group in [Ru(tpy)(phpy)Cl]⁺. Both the Ru-Cl and Ru-O (1.921 Å) bond lengths in **1** are very similar to the Ru-Cl (2.336 and 2.405 Å) and Ru-O (1.929 and 1.949 Å) bond lengths found in the related Ru(III/III) dimer {[RuCl(tpy)]$_2$(μ-Hpbl-κ-N$_2$O$_2$)}(PF$_6$)$_2$·MeOH,[25] supporting the assignment of **1** as a Ru(III) complex containing an anionic alkoxide ligand. Full crystallographic data has been deposited with the CCDC (#1838681).
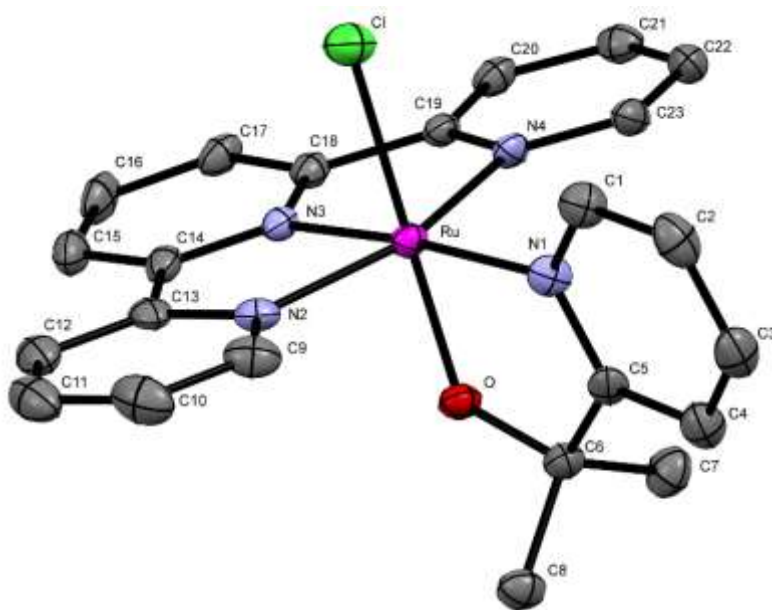
Figure 2.2. Thermal ellipsoid plot of the molecular unit of [1]BPh4·2CH2Cl2 showing 50% probability ellipsoids; hydrogen atoms, counteranions, and lattice solvent molecules omitted for clarity. Color coding: grey, C; blue, N; red, O; green, Cl; magenta, Ru

2.2.2. Redox Properties of [Ru(tpy)(pyalk)Cl]⁺ (1)

The redox properties of **1** were determined via cyclic voltammetry (CV) (Fig. 2.3) by dissolving **[1]Cl** in acetonitrile. Three quasi-reversible redox waves are apparent in the CV, the first at 0.07 V vs. NHE, the second at 1.224 V vs. NHE, and the third at 1.60 V vs. NHE. The

wave at 1.224 V vs. NHE was identified as chloride oxidization at the electrode by collecting a

CV of tetramethylammonium chloride under identical conditions (Fig. 2.4).
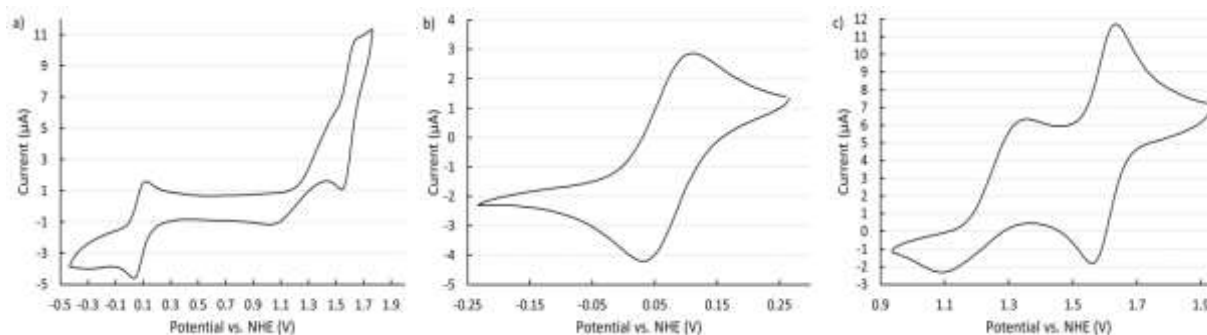
Figure 2.3. Cyclic Voltammograms of 2.5 mM **[1]Cl** 100 mV/s (a) and 50 mV/s (b,c) in acetonitrile containing 100 mM [Bu$_4$N][PF$_6$] as electrolyte. Potentials referenced to Fc/Fc$^+$ and converted to NHE using the standard values Fc/Fc$^+$ = 400 mV vs SCE[33] and SCE = 241 V vs. NHE
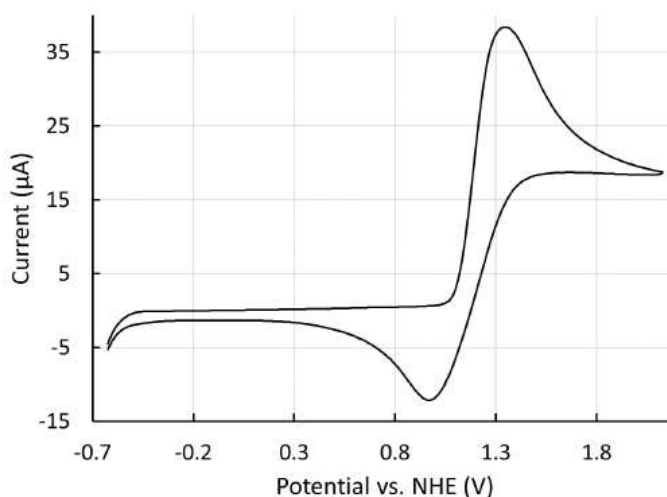
Figure 2.4. Cyclic voltammogram of 9.85 mM tetramethylammonium chloride at 50 mV/s in acetonitrile containing 100 mM tetra-N-butylammonium hexafluorophosphate as electrolyte

In order to assign these redox waves, the UV-visible spectra of **[1]Cl** was recorded at

applied potentials above and below each of the waves (Fig. 2.5). As shown, applying a voltage

below 0.07 V vs. NHE results in a dramatic red-shift of the d-π*(tpy) MLCT band from 446 nm

to 584 nm, as well as the appearance of a second absorption band at ~476 nm, possibly a d-

π*(pyalk) MLCT.[24,29] In addition to these well-defined peaks, a broad absorbance is also

32

observed between ca. 650 and 950 nm upon reduction. Broad absorption of this nature has sometimes been observed in Ru(II) complexes,[29] and have been previously assigned as d–dπ and dπ–π* transitions between mixed ligand–metal orbitals.[30] Application of potentials between 0.07 and 1.224 V vs. NHE results in regeneration of the original spectra. Applying potentials > 1.6 V vs. NHE results in a blue-shift of the MLCT to ~430 nm (Fig. 2.5). As expected for oxidation of Cl⁻, no significant change is observed upon application of potentials between 1.224 and 1.6 V vs. NHE. Based on these results, the wave at 0.07 V can be assigned as the Ru(II/III) redox couple, and the wave at 1.6 V vs. NHE can be assigned as the Ru(III/IV) redox couple.
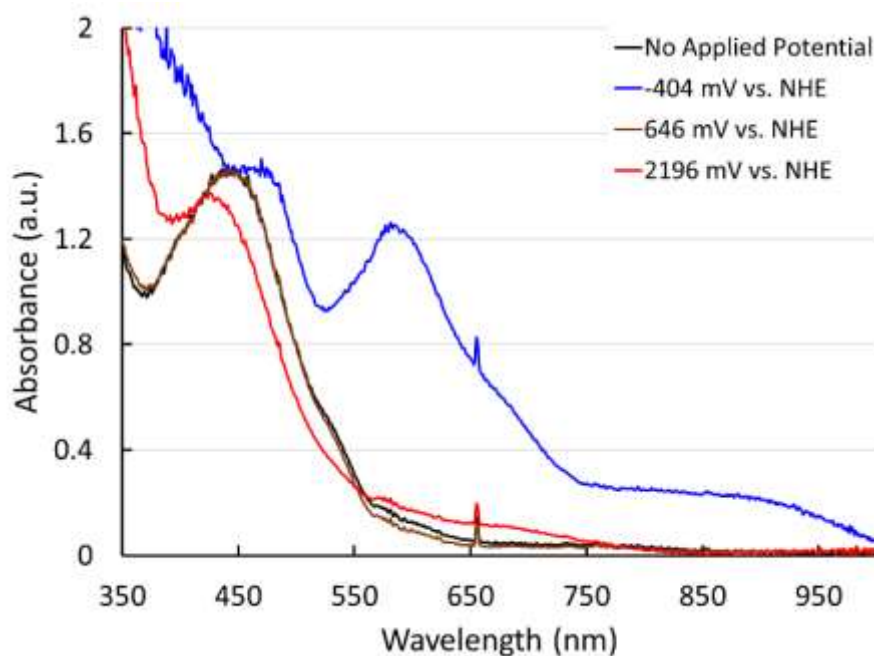
Figure 2.5. UV-visible spectra of 2.5 mM **[1]Cl** in acetonitrile containing 100 mM [Bu$_4$N][PF$_6$] as an electrolyte with constant application of the potentials indicated

2.2.3. Redox Properties of [Ru(tpy)(pyalk)(OH)]⁺ (2) and [Ru(tpy)(phpy)(H₂O)]²⁺ (3)

Relative to its behavior in acetonitrile, in phosphate buffer **1[Cl]** shows much simpler redox chemistry, with only one reversible wave observed (Fig. 2.6). To get further insight of electrochemical stability for various oxidation states of the complex, Pourbaix diagram was

33

constructed by measuring $E_{1/2}$ potentials of the wave at different pHs. The diagonal lines in

Pourbaix diagram represent both redox and acid-base reactions and they are idealized Nernstian

lines (Fig. 2.7). The slope of the line indicates number of electrons and protons transfer, which

is derived from Nernst equation. Slope = -59.2 mV x (m/n) mV/pH; m = number of protons; n =

number of electrons. The pK_a's coincide with the dashed vertical lines and are deduced from

change of slope in Pourbaix diagram (E^0vs pH). This description holds for all Pourbaix diagrams

hereinafter.

The potential of this redox event is pH dependent, showing the characteristic 59 mV/pH

unit shift of a one proton per electron proton-coupled electron transfer (PCET) below pH ~7.5,

and having a constant value of 0.124 V vs. NHE above that pH (Fig. 2.7). The description holds

for all Pourbaix diagrams hereinafter. This pH dependent behavior indicates the presence of a

labile proton with a pK_a of approximately 7.5. This pK_a is significantly more alkaline than

expected for the bound pyalk ligand, and somewhat more acidic than the related

$[Ru(tpy)(Hpbl)(H_2O)]^+$ complex.[24]
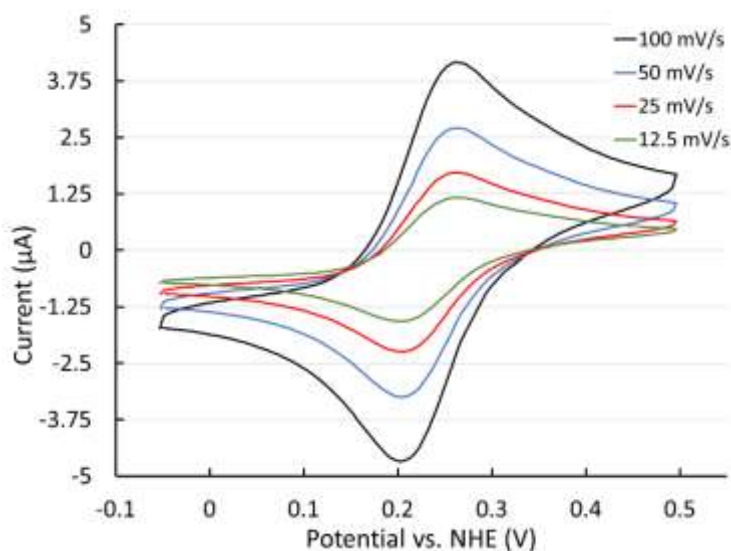
Figure 2.6. Cyclic voltammograms of 1.57 mM **1[Cl]** in 100 mM pH 6.86 P_i buffer at the indicated potentials. Referenced to saturated Ag/AgCl and converted to NHE using the standard value Ag/AgCl = 197 mV vs. NHE[28]

34
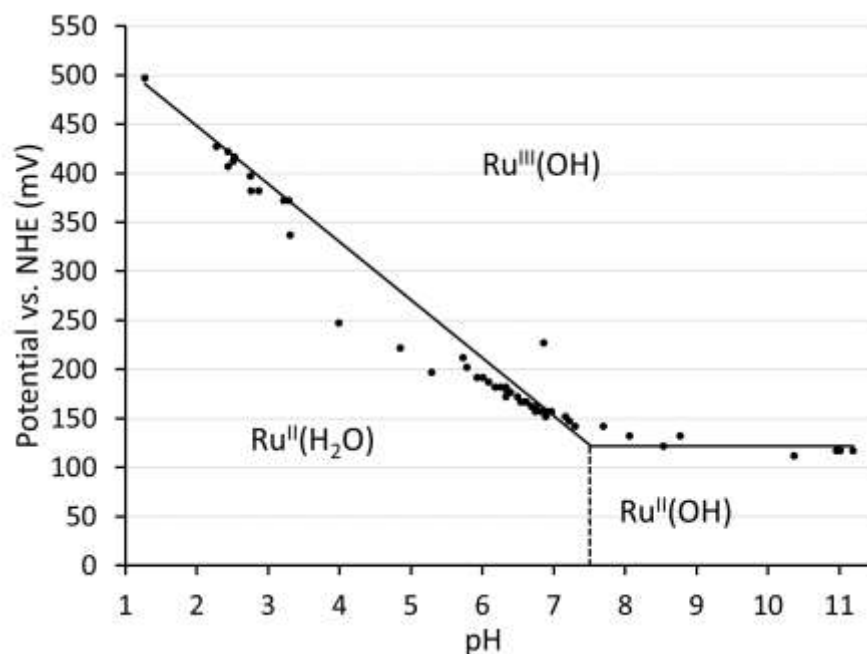
Figure 2.7. Pourbaix diagram of 1.3 mM **2** in 100 mM P_i buffer. Accuracy of measured potential = ±0.05 % range

This pH dependence suggests rapid exchange of the chloride ligand for solvent upon

dissolution, forming $[Ru(tpy)(pyalk)(OH)]^+$, **2**. This solvation in aqueous solution is supported

by the d-π*(tpy) MLCT observed in the UV-visible spectrum of **1[Cl]** in water (Fig. 2.8), which

is blue-shifted relative to that observed for **1[Cl]** in acetonitrile. Upon application of potentials

more reducing that this wave, a distinct red-shift from 450 to 475 nm is observed for the d-

π*(tpy) MLCT. Based on this data we can confidently assign this redox event as a Ru(II/III)

couple.
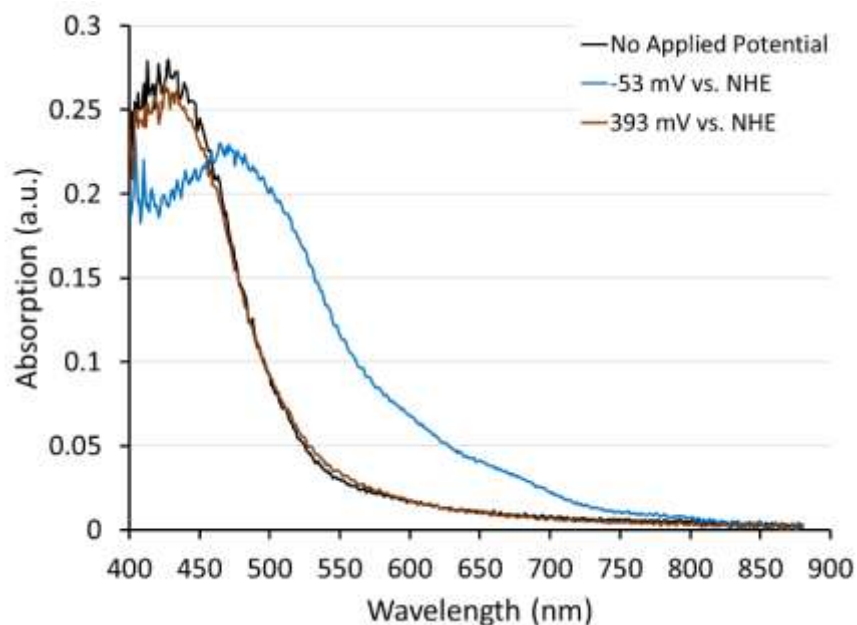
Figure 2.8. UV-visible spectra of 500 μM **[1]Cl** in 100 mM aqueous P$_i$ buffer with constant application of the potentials indicated

In order to compare the effects of the pyalk ligand on the pH dependent redox behavior of

2 to other Ru complexes ligated to tpy and an anionic ligand, we generated a Pourbaix diagram

for [Ru(tpy)(phpy)Cl] (Fig. 2.9, phpy = 2-phenylpyridine). Based on the observed pH

dependence of the Ru(II/III) couple and comparison to the related complex

[Ru(dpp)(bpy)(H$_2$O)]$^{2+}$ (dpp = 1,3-di(pyrid-2-yl)benzene),[29] upon dissolution in Pi buffer

[Ru(tpy)(phpy)Cl] forms a solvento complex similar to that formed by **2**, i.e.

[Ru(tpy)(phpy)(H$_2$O)]+, **3.**

While both **2** and **3** show similar Ru(III/II) potentials at pH 1, the pH dependence of these

potentials differ substantially due to differences in the pK_a values for the complexes.

Specifically the differences in pK_a values cause the Ru(II/III) potential of **3** to remain constant at

~410 mV vs. NHE between pH **1** and ~6.5, while that of **2** decreases dramatically over this pH

region. This results in **2** having lower Ru(III/II) potential than **3** at pH values above ~2.8.
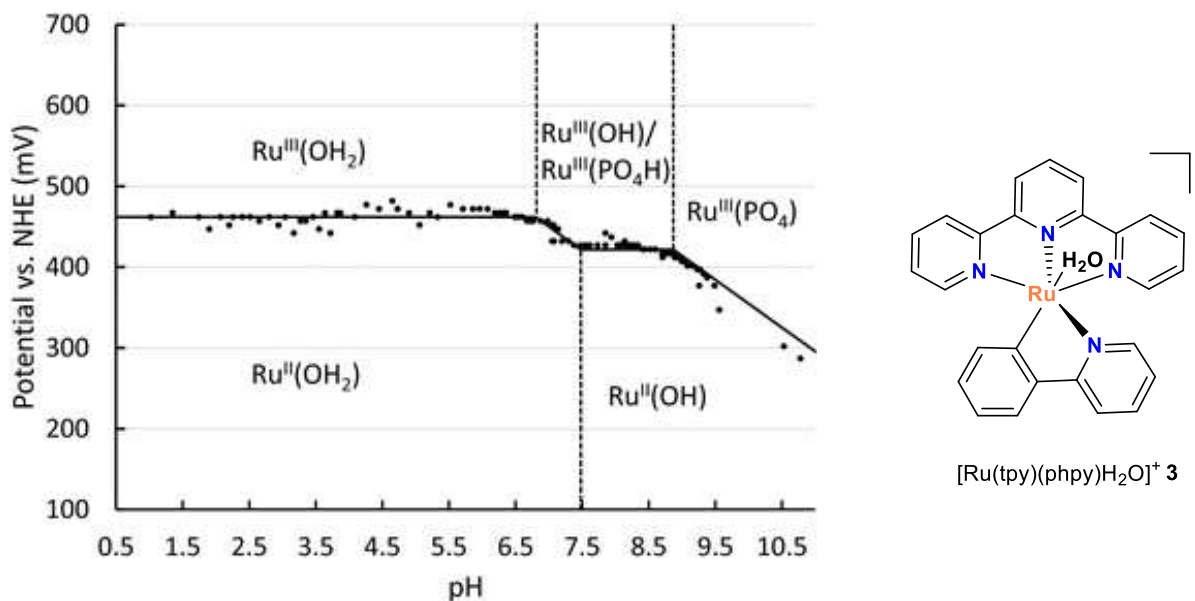
Figure 2.9. Pourbaix diagram for 970 µM **3** in 100 mM Pi buffer. Referenced to saturated Ag/AgCl and converted to NHE using the standard value Ag/AgCl = 197 mV *vs.* NHE[28]. Accuracy of measured potential = ±0.05 % range

2.2.4. C-H Bond Oxidation Activity of [Ru(tpy)(pyalk)(OH)]$^+$ (2)

The ability of **1[Cl]** to catalyze C-H bond oxidation was screened via ^{1}H NMR with a variety of oxidants using THF as a substrate (Table 2.1). Of the oxidants screened, only cerium(IV) ammonium nitrate (CAN) yielded any THF oxidation products. Following this initial screen, we studied the effect of air and light on the oxidation of THF by CAN catalyzed by **1[Cl]**, finding no measurable effect based on either of these factors (Table 2.2). Based on these results, we examined the substrate scope of C-H bond oxidation by **1[Cl]** with CAN *via* initial identification of products *via* GC-MS followed by quantitation using GC. As shown in Table 2.3, **1[Cl]** is capable of catalysing both alkene epoxidation and aliphatic C-H bond hydroxylation. Conversion for these reactions is rather modest, although alkene epoxidation shows significantly greater product yields than alkane oxidation to ketones.

37

Table 2.1. Overall conversion and oxidized product yields for THF oxidation by **1[Cl]** using various chemical oxidants[a]

Oxidants	Yield[b] γ-Butyrolactone	Yield[b] Succinic Acid	Remaining Starting Material[c]
H_2O_2	0%	0%	87%
$NaIO_4$	0%	0%	96%
CAN	25.8%	3.7%	59%
CAN[d]	0%	0%	98%

[a]Reaction conditions: 4.7 μmol **1** (0.95% catalyst loading), 2.4 mmol oxidant, 493 μmol THF in 10 mL D_2O containing 19 μmol 3-(trimethylsilyl)propionic-2,2,3,3-d_4 acid sodium salt as an internal standard at 20° C under air for 1 hr. [b]As determined by ^{1}H NMR, mol product/initial mol THF. [c]As determined by ^{1}H NMR, mol THF/initial mol THF

Table 2.2. Overall conversion and oxidized product yields for THF oxidation by **1[Cl]** under various reaction conditions[a]

Conditions[b]	Yield[c] γ-Butyrolactone	Yield[c] Succinic Acid	Remaining Starting Material[d]
Air and Light	25.8%	3.7%	59%
Air and Dark	20.5%	2.8%	27.3%
N_2 and Light	22%	2.7%	76.5%
N_2 and Dark	22.8%	3.8%	47%

[a]Reaction conditions: 4.7 μmol **1** (0.95% catalyst loading), 2.4 mmol CAN, 493 μmol THF in 10 mL D_2O containing 19 μmol 3-(trimethylsilyl)propionic-2,2,3,3-d_4 acid sodium salt as an internal standard at 20° C for 1 hr. [b]Reaction run sealed using a septum either under air or nitrogen atmosphere, and with or without exclusion of light. [c]As determined by ^{1}H NMR, mol product/initial mol THF. [c]As determined by ^{1}HNMR, mol THF/initial mol THF

Table 2.3. Overall conversion and GC product yields for substrate oxidation by **1** using CAN[a]

Substrate	Major Product (% yield[b])	Remaining Starting Material (%[b])
Cyclooctane	Cyclooctanone (3.8 ± 0.4)	48.9 ± 0.4
Ethylbenzene[c]	Acetophenone (5.4 ± 1.1)	32.6 ± 5.2
Cyclooctene	Cyclooctene Oxide (30.2 ± 0.3)	23.2 ± 1.1

[a]Reaction conditions: 3.1 μmol **1** (~4.1% catalyst loading), 390 μmol CAN, 10 μL substrate (~75 μmol) in 400 μL 1:2 MeCN:H_2O under air for 1 hr. [b]Average of a minimum of 3 runs, error represents 1 standard deviation from the mean, mol product/initial mol starting material. [c]Reaction time of 2 hrs

2.3. Discussion

2.3.1. Redox Properties of [Ru(tpy)(pyalk)Cl]$^+$ (1), [Ru(tpy)(pyalk)(OH)]$^+$ (2), and [Ru(tpy)(phpy)(H$_2$O)]$^{2+}$ (3)

Our goal in synthesizing **1[Cl]** was to lower the potentials of the Ru(II/III) and Ru(III/IV) redox couples. We therefore began our analysis by characterizing **1** electrochemically. In

acetonitrile, **1** is observed to have Ru(II/III) and Ru(III/IV) redox potentials of 0.07 and 1.60 V

vs. NHE, respectively. This Ru(II/III) redox couple is at a significantly lower potential than the

related complexes [Ru(tpy)(phpy)Cl] and [Ru(tpy)(bhq)Cl] (Table 2.4), as well as the dimeric

complex {[RuCl(tpy)]$_2$(μ-Hpbl-κ-N$_2$O$_2$)}, which has a Ru(II,II/III,III) redox potential of 0.54 V

vs. NHE and has the same inner-sphere coordination environment.[25] This extremely low

Ru(II/III) redox potential clearly indicates that **1** has two anionic ligands in the coordination

sphere in acetonitrile solution. Therefore: a) **1** retains its chloride ligand in MeCN and b) the

pyalk ligand is deprotonated.

While inclusion of the strong-donor pyalk ligand successfully lowered the Ru(II/III)

couple relative to other ligand sets, very little change was seen in the Ru(III/IV) potential.

Indeed **1** has potentials quite similar to those of [Ru(bpy)$_2$Cl$_2$], which has Ru(II/III) and

Ru(III/IV) couples at 0.0 and 1.7 V vs. NHE, respectively.[15] This large difference in the

Ru(II/III) and Ru(III/IV) couples is typical of Ru complexes that cannot undergo PCET, as

charge buildup on the complex inhibits further oxidation. One simple method to enable PCET

for Ru chloride complexes is to dissolve them in water, which commonly results in the formation

of an aqua complex capable of deprotonation via hydrolysis.[15]

Table 2.4. Ru(II/III) couples in aprotic solvent for complexes bearing two anionic ligands

Complex[a]	Ru(II/III) Potential (V vs. NHE)[b]	Reference
1	0.07[c]	[d]
[Ru(tpy)(phpy)Cl]	0.46[c]	[27]
[Ru(tpy)(bhq)Cl]	0.48[e]	[30]
cis,cis-[RuCl$_2$(Hbpp)(DMSO)$_2$]	1.081[c]	[31]
[Ru(bpy)$_2$Cl$_2$]	0.0[c]	[15]

[a]Ligand abbreviations used: bhq = benzo[h]quinoline, Hbpp = 3,5-bis(2-pyridyl)pyrazole.
[b]Converted to NHE using the standard value SSCE = 241 mV vs. NHE.[28] [c]Measured in MeCN.
[d]This work. [e]Measured in DMF

Indeed, upon dissolution in water the inner sphere chloride of **[1]Cl** exchanges with solvent to form the Ru(III) hydroxide complex **2** (Scheme 2.2). Unlike **1**, the Ru(II/III) redox couple in **2** is clearly proton-coupled below pH ~7.5, as shown in its Pourbaix diagram (Fig. 2.7). Despite this success in enabling PCET at the Ru center in **2**, no Ru(III/IV) couple is observed for **2** within the solvent window of the phosphate buffer. This indicates that while oxidation of **2** to form the type of Ru(IV) oxo species typically involved in C-H bond oxidation may be possible, it will require oxidants with one-electron redox potentials above 1.23 V vs. RHE (reversible hydrogen electrode).

$$[Ru(tpy)(pyalk)Cl]Cl \xrightarrow{\text{H}_2\text{O}} [Ru(tpy)(pyalk)OH]^+ + \text{H}_3\text{O}^+ + Cl^-$$

$$\text{[1]Cl} \qquad\qquad\qquad\qquad \text{[2]}$$
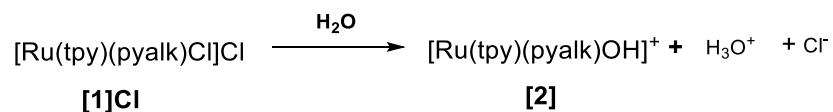
Scheme 2.2. Formation of **2** upon dissolution of **[1]Cl** in water

Comparison between **2** and other Ru complexes bearing tpy and other anionic ligands such as phpy (Fig. 2.9 and Table 2.5) shows little difference in the Ru(II/III) potentials at pH 1. Comparison of proton-coupled redox potentials at a single pH value can be misleading however, as differences in pK_a values can cause dramatic differences in their pH dependence. In order to address this concern, we searched for a Pourbaix diagram of the related organometallic complex **3**, where the alkoxide group has been replaced with a carbanion. Despite the well-characterized redox properties of [Ru(tpy)(phpy)Cl] in MeCN,[27] and DMF,[17,30] the most closely related complex we could find data for in aqueous solution was [Ru(dpp)(bpy)(H$_2$O)]$^{2+}$ (dpp = 1,3-di(pyrid-2-yl)benzene).[323] We were unable to locate any studies where **3** was used in aqueous solution, and are therefore including its Pourbaix diagram in this manuscript (Fig. 2.9).

Table 2.5. Ru(II/III) redox potentials in pH 1 aqueous solution for selected complexes bearing anionic ligands

Complex[a]	Ru(II/III) Potential (V vs. NHE)[b]	Reference
2	0.50	[c]
[Ru(tpy)(phpy)(H$_2$O)]$^{2+}$	0.41	[c]
[Ru(tpy)(Hpbl)(H$_2$O)]$^{2+}$	0.48	[24]
trans-[Ru(tpy)(pic)(H$_2$O)]$^{2+}$	0.73	[33]
cis-[Ru(tpy)(pic)(H$_2$O)]$^{2+}$	0.83	[33]
[Ru(dpp)(bpy)(H$_2$O)]$^{2+}$	0.30	[32]
[Ru(bda)(isoqF)$_2$]$^+$	0.70	[34]
[Ru(bda)(ptzBr)$_2$]$^+$	0.60	[34]

[a]Ligand abbreviations used: phpy = 2-phenylpyridine, Hpbl = 3,5-bis(2-pyridyl)pyrazole, pic = 2-picolinic acid, dpp = 1,3-di(pyrid-2-yl)benzene, bda = 2,2'-bipyridine-6,6'-dicarboxylic acid, isoqF = 6-fluoroisoquinoline, ptzBr = 6-bromophthalazine. [b]At pH 1, potentials converted to NHE using the standard value SCE = 241 mV vs. NHE and Ag/AgCl = 197 mV vs. NHE.[28] [c]This work

Comparison of the Pourbaix diagrams of **2**, **3**, and [Ru(dpp)(bpy)(H$_2$O)]$^{2+}$ reveals that both **3** and [Ru(dpp)(bpy)(H$_2$O)]$^{2+}$ have very similar behavior in water, as expected from two complexes bearing 4 N and 1 C donor ligands. The primary difference in the two complexes is the higher pK_a observed for **3** (~6.5 vs ~4.9 for [Ru(dpp)(bpy)(H$_2$O)]$^{2+}$).[32] In contrast, the aqua ligand on **2** is significantly more acidic than those in **3** and [Ru(dpp)(bpy)(H$_2$O)]$^{2+}$ in both the Ru(II) (pK_a ~7.5) and Ru(III) (pK_a < 1) oxidation states. This dramatic shift occurs despite the fact that the O-donor pyalk ligand is expected to provide more e$^-$ density to the Ru center relative to the organometallic dpp and phpy ligands based on its inability to serve as a π-acceptor and the relative potentials of **2** and **3** in MeCN (Table 2.4). The precise reasons for this pK_a shift are currently under investigation but may be due to the ability of the pyalk ligand to form H-bonds to water in aqueous solution. This competition between the pK_a values and the non-proton coupled Ru(II/III) potentials is responsible for the fact that both **2** and **3** have similar Ru(II/III) potentials under acidic conditions. In contrast, under neutral to alkaline conditions, the Ru(II/III) couple of **2** is significantly lower than that seen for **3**.

41

2.3.2. C-H Bond Oxidation Activity of [Ru(tpy)(pyalk)(OH)]$^+$ (2)

In order to test the ability of **2** to catalyze C-H bond oxidation, we monitored the oxidation of the model substrate THF with various oxidizing agents (Table 2.1). Only CAN was found to be capable of driving oxidation catalysis by **2**. Based on the redox potentials observed for **1** and **2**, this is most likely due to the need for a one-electron oxidation of Ru(III) to Ru(IV) in the catalytic cycle, i.e. none of the two-electron oxidants employed are expected to be thermodynamically capable of oxidizing **2** from Ru(III) to Ru(V).

Two distinct reactions are catalyzed by **2** in water, the oxidation of aliphatic C-H bonds to ketones, as exemplified by THF oxidation to γ-butyrolactone, and alkene epoxidation, as exemplified by the conversion of cyclooctene to cyclooctene oxide. Unfortunately, both of these reactions proceed with only modest turnover, and a significant number of overoxidation products are observed. This is likely due to a similar pathway as observed for [Ru(bpy)$_2$(py)O]$^{2+}$,[35] where two-electron Ru(II/IV) reactions compete with one-electron Ru(III/IV) reactions.

2.4. Conclusions

While we initially hypothesized that the pyalk ligand would reduce the overall potential necessary to form Ru(IV)=O species needed to catalyze C-H bond oxidation, only the Ru(II/III) potential of **1** and **2** was greatly affected by using this ligand, and the potential needed to form a Ru(IV)=O was not lowered significantly in either water or acetonitrile solvents. Indeed, the overall Ru(III/IV) potential of **1** in acetonitrile was found to be almost identical to that of Ru(bpy)$_2$Cl$_2$, despite the inclusion of the O-donor pyalk ligand. In acetonitrile this is likely due to the inability of **1** to participate in PCET due to the quite low pK_a of the bound pyalk ligand. The overall Ru(II/III) potential of **2** in aqueous solution at pH 1 is comparable to that of the

organometallic complex **3**, but this is primarily due to the much lower pK_a values of **2** in both the Ru(II) and Ru(III) oxidation states. Above pH 3, **2** has a lower Ru(II/III) potential than **3**.

Despite its relatively low Ru(II/III) potential, **2** was found to only catalyze C-H bond oxidation using the one-electron oxidant CAN due to the large potential difference between the Ru(II/III) and Ru(III/IV) redox potentials. This need to use CAN to drive catalysis limits the usefulness of **2** relative to other Ru-based C-H bond oxidation catalysts that have been reported,[36–38] as it leads to overoxidation and very low atom economy. In order to overcome this limitation, we are currently investigating strategies for fostering two-electron chemistry at Ru by lowering the Ru(III/IV) potential, e.g. PCET.[15,36]

2.5. Experimental Methods

2.5.1. General Consideration

2,2':6',2''-Terpyridine and cyclooctane were purchased from Alfa Aesar and used without further purification. 2-phenylpyridine, acetophenone, and N-ethylmorpholine were purchased from VWR and used without further purification. Ethylbenzene was purchase from Thermo Fisher Scientific and used without further purification. Anhydrous magnesium sulfate was purchased from AMRESCO, Inc. and used without further purification. Deuterated solvents, methylmagnesium iodide, 2-acetylpyridine, ruthenium(III) chloride hydrate, 3-(trimethylsilyl)propionic-2,2,3,3-d_4 acid sodium salt, potassium chloride, sodium periodate, hydrogen peroxide, cyclooctene oxide, cis-cyclooctene, cyclooctanone, silver chloride, ferrocene, sodium tetraphenylborate and Celite® 545 were purchased from Sigma-Aldrich Co. and were not further purified. Ammonium cerium(IV) nitrate was purchased from Strem Chemicals Inc. and used without further purification. Column chromatography was performed using RediSep® GOLD columns on a CombiFlash RF+ from Teledyne Instruments, Inc.

2.5.2. Synthesis of 2-(2'-Pyridyl)-2-propanol (pyalkH)
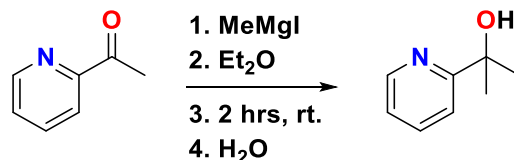
2-(2'-Pyridyl)-2-propanol was synthesized according to the published procedure.[407] In

brief, 14.5 mL of 3.0 M methylmagnesium iodide (43.5 mmol, 1.2 equivalents) was added

dropwise to a solution of 2-acetylpyridine (4 mL, 1.08 g/mL, 35.7 mmol) in diethyl ether (30

mL) in an ice bath. The solution was removed from the ice bath and allowed to warm to room

temperature while being stirred for 2 hours. The reaction was then quenched with 30 mL of

water and acidified with concentrated hydrochloric acid until both phases were clear. The

aqueous layer was separated and extracted with diethyl ether (3 x 50 mL). The organic fractions

were dried with magnesium sulfate, and purified using column chromatography (3:1 ethyl

acetate:hexanes). The product was isolated as a hygroscopic, clear, light yellow oil.

2.5.3. Synthesis of [Ru(tpy)Cl₃]
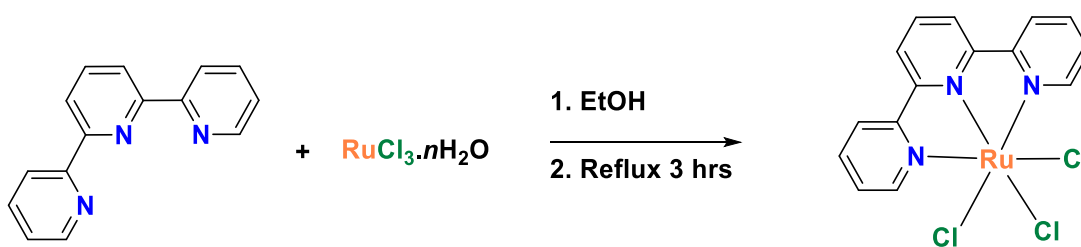
[Ru(tpy)Cl₃] was synthesized according to the literature procedure.[41] In brief, 529 mg

(2.35 mmol) of RuCl₃·nH₂O and 465 mg (1.99 mmol) of tpy was added to 250 mL of ethanol

and refluxed for 3 hours. The solution was then cooled to RT, filtered, and washed with cold

EtOH and Et₂O to yield 527.4 mg (63.0%) of product after drying.

2.5.4. Synthesis of [Ru(tpy)(phpy)Cl] (3)
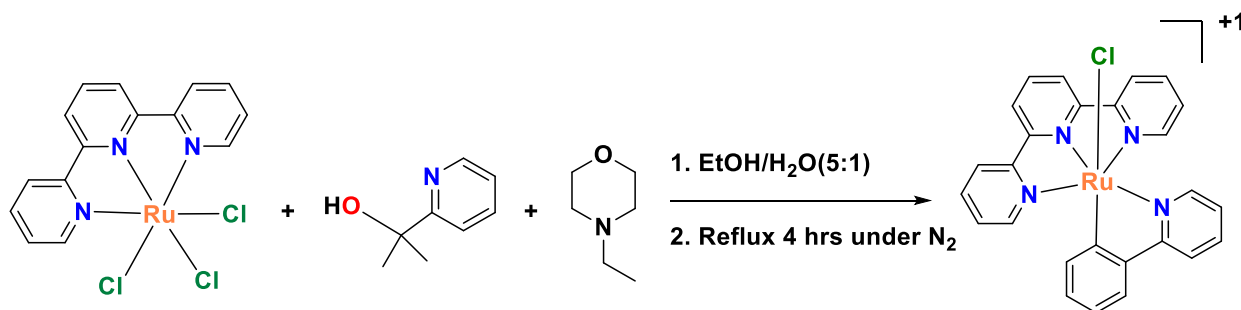
[Ru(tpy)(phpy)Cl] was synthesized according to the literature procedure.[30] In brief, 173 mg (380 µmol) of [Ru(tpy)Cl$_3$] and 70 µL (490 µmol) of phpy were added to 18 mL of a 1:5 H$_2$O:MeOH solution. N-ethylmorpholine (8 drops) was added to the solution, and it was refluxed under N2 for 4 hours. The solution was then cooled to RT, filtered, and the precipitate was washed with 15 mL of Et$_2$O 3 times. The solid was redissolved in MeOH, filtered, and the solvent was removed under reduced pressure to yield 136 mg (68.3%) of product.

2.5.5. Synthesis of [Ru(tpy)(pyalk)(Cl)]Cl·3H$_2$O·MeCN ([1]Cl)
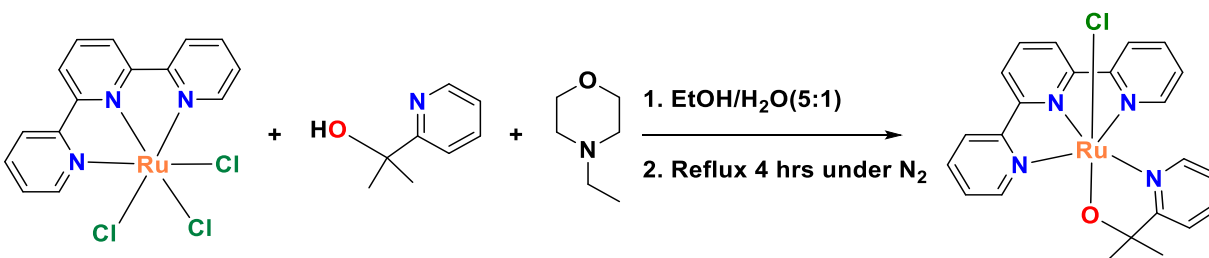
Ru(tpy)Cl$_3$ (299 mg, 678 µmol) and pyalkH (105 mg, 764 µmol, 1.13 equiv) were placed under nitrogen atmosphere. A nitrogen sparged solution of N-ethylmorpholine (86 µL, 78 mg, 680 µmol, 1 equiv) in 36 mL of 5:1 ethanol:water was added to the reaction mixture. The reaction mixture was then heated to 97°C for 4 hours, over which time the reaction mixture turned a dark purple color. The solution was then removed from heat, allowed to cool to room temperature, and filtered through Celite 545. The precipitate was washed with water, and the solvent was removed from the combined filtrates under vacuum. The isolated black solid was

redissolved in a small amount of water and purified via reverse-phase flash chromatography using a mixture of acetonitrile and water as the mobile phase and a 15.5g RediSep C18 GOLD column as the stationary phase. Solvent was removed under vacuum from the product-containing dark purple fractions, which was then dried in a vacuum desiccator yielding 113 mg (31%) of product as a hygroscopic black powder. Calculated: C 47.17, H 4.75, N 11.00; Found: C 47.10, H 5.20, N 11.30.

2.5.6. Crystallization of [Ru(tpy)(pyalk)Cl]BPh₄ ([1]BPh₄)

A solution of saturated NaBPh$_4$ was added dropwise to a solution of **[1]Cl** (20 mg) in water, resulting in immediate formation of a dark grey precipitate. Additional NaBPh$_4$ solution was added until no more precipitate formed. This precipitate was washed with water and dissolved in dichloromethane (DCM). The DCM solution was then dried with anhydrous MgSO$_4$ and filtered. Vapor diffusion of diethyl ether into this solution yielded the solvento-complex, **[1]BPh₄·2CH₂Cl₂**, as dark red crystals suitable for X-ray diffraction studies.

2.5.7. Crystal Structure Determination

Crystals were mounted on MiTeGen's MicroLoops using Immersion oil, type NVH by Cargille and cooled to 110 K in a stream of cold N$_2$ gas. Diffraction data were collected using a Bruker APEX2 Duo CCD area detector diffractometer with the detector positioned at a distance of 4.0 cm from the crystal. The X-ray source was sealed tube Mo-Kα radiation (λ= 0.71073 Å). Data were processed (integrations and multi-scan absorption corrections) by Bruker-AXS software Apex3 v2017.3-0. Using Olex2 software,[42] the structures were solved by Intrinsic Phasing using ShelXT[43] and refined anisotropically on F2 with ShelXL.[441] All hydrogen atoms were refined isotopically.

2.5.8. Procedure for Electrochemical Measurements

Electrochemical measurements were obtained using a Pine WaveDriver potentiostat with platinum working (1.6 mm OD) and counter electrodes. For aqueous measurements an Ag/AgCl electrode in a saturated KCl solution was used as the reference electrode. For measurements in non-aqueous solvents, an Ag/Ag^+ electrode the same electrolyte solution used for measurements was used as a pseudo-reference electrode. Absolute potentials were obtained by referencing to Fc/Fc^+ as both an external and internal standard.[28,452] All measurements were compared with the specified electrolyte solution as a blank measurement under identical electrode conditions.

2.5.9. Procedure for UV-Visible Measurements

UV-visible measurements were collected on a PerkinElmer Lambda 465 spectrophotometer. Solutions for UV-visible measurements were prepared by dissolving solid **[1]Cl** in solvent using volumetric glassware to obtain the indicated concentrations. Standard measurements were taken using a quartz cuvette with a 1 cm path length. Spectroelectrochemical spectra were taken using an optical thin layer (OTL) cell and a Pine gold honeycomb electrode with an effective path length of 1.7 mm. Prior to measuring the UV-visible spectra, a rapid CV was taken using the honeycomb electrode to confirm no change in electrochemical behavior occurred due to the use of the honeycomb electrode. A constant potential was then applied, and UV-visible spectra were recorded once a constant current was obtained, generally within 10 seconds.

2.5.10. Procedure for C-H Bond Oxidant Screening

A 1.00 mg/mL stock solution of **[1]Cl** (3.0 mL, 3.0 mg, 4.7 μmol), 3-(trimethylsilyl)propionic-2,2,3,3-d$_4$ acid sodium salt (3.3 mg, 19 μmol), and 2.4 mmol of the chemical oxidant were dissolved in 7.0 mL of D_2O. The reaction flask was then stoppered, THF

(40 μL, 624 μmol) was added, and the reaction solution stirred for 1 hour at room temperature (20º C). A ^{1}H NMR of the solution was then collected. For reactions under N_2 atmosphere, the solid reactants were placed under vacuum using standard Schlenk techniques, and the D_2O was sparged for a minimum of 30 minutes. For reactions undertaken with exclusion of light, the reaction flask was wrapped in aluminum foil prior to addition of the THF.

2.5.11. Procedure for C-H Bond Substrate Scope Screening

CAN (100 mg, 183 μmol) was dissolved in 150 μL acetonitrile and 250 μL of a 13.5 mM stock solution of **2** prepared by dissolving **[1]Cl** in water. To this solution 12 μL (~100 μmol) of substrate were added, and the reaction was stirred for the specified duration(s). The reaction was then quenched with 100 mg (793 μmol) sodium sulfite, and filtered through glass wool. The reaction vessel was washed with 2 mL of ethyl acetate and 2 mL of water, which was added to the filtered reaction solution. Acetophenone (10 μL, 97 μmol was added to the filtered reaction solution as an internal standard, and the aqueous fraction was extracted ethyl acetate (2 x 2 mL). The combined organic fractions were then extracted with 5 mL of brine to remove any remaining **2** and CAN, dried with $MgSO_4$, filtered, and analyzed via GC.

2.5.12. Procedure for GC Measurements

Product yields determined by GC were obtained using a Thermo Scientific Trace 1300 GC with a flame ionization detector (FID), and a TG-1301MS column. Substrate scope screening results were analyzed by injecting 10 μL of the processed samples onto the column using a split/splitless injection port in a 1:5 split ratio. Concentration-response curves were obtained for each of the products analyzed by injecting 10 μL of a known concentration of each of the identified products using the same GC settings above. The FID response was measured at a minimum of 5 separate concentrations for each product, and the FID response for each

48

concentration was measured 3 times. The effect of the purification process on product yield was determined by measuring the FID response for product samples of known concentration after following the same purification procedure used for the substrate scope screening.

2.6. References

1.   Shilov, A. E. & Shul'pin, G. B. Activation of C−H Bonds by Metal Complexes. *Chem. Rev.* **97**, 2879–2932 (1997).

2.   White, M. C. Adding Aliphatic C–H Bond Oxidations to Synthesis. *Science* **335**, 807–809 (2012).

3.   Crabtree, R. H. Alkane C–H activation and functionalization with homogeneous transition metal catalysts: a century of progress—a new millennium in prospect. *J. Chem. Soc., Dalton Trans.* 2437–2450 (2001) doi:10.1039/B103147N.

4.   Costas, M. Selective C–H oxidation catalyzed by metalloporphyrins. *Coordination Chemistry Reviews* **255**, 2912–2932 (2011).

5.   Nanjo, T., de Lucca, E. C. & White, M. C. Remote, Late-Stage Oxidation of Aliphatic C–H Bonds in Amide-Containing Molecules. *J. Am. Chem. Soc.* **139**, 14586 (2017).

6.   Hashiguchi, B. G., Bischof, S. M., Konnick, M. M. & Periana, R. A. Designing Catalysts for Functionalization of Unactivated C–H Bonds Based on the CH Activation Reaction. *Acc. Chem. Res.* **45**, 885–898 (2012).

7.   Song, G., Wang, F. & Li, X. C–C, C–O and C–N bond formation via rhodium(III)-catalyzed oxidative C–H activation. *Chem. Soc. Rev.* **41**, 3651–3678 (2012).

8.   Hartwig, J. F. Evolution of C–H Bond Functionalization from Methane to Methodology. *J. Am. Chem. Soc.* **138**, 2–24 (2016).

9.   Nam, W. High-Valent Iron(IV)–Oxo Complexes of Heme and Non-Heme Ligands in Oxygenation Reactions. *Acc. Chem. Res.* **40**, 522–531 (2007).

10.   Li, B. & Dixneuf, P. H. sp2 C–H bond activation in water and catalytic cross-coupling reactions. *Chem. Soc. Rev.* **42**, 5744–5767 (2013).

11.   Olivo, G. *et al.* C–H Bond Oxidation Catalyzed by an Imine-Based Iron Complex: A Mechanistic Insight. *Inorg. Chem.* **54**, 10141–10152 (2015).

12.   Kawamata, Y. *et al.* Scalable, Electrochemical Oxidation of Unactivated C–H Bonds. *J. Am. Chem. Soc.* **139**, 7448–7451 (2017).

13.   Zhou, M. & Crabtree, R. H. C–H oxidation by platinum group metal oxo or peroxo species. *Chem. Soc. Rev.* **40**, 1875–1884 (2011).

14.   Chen, Z. & Yin, G. The reactivity of the active metal oxo and hydroxo intermediates and their implications in oxidations. *Chem. Soc. Rev.* **44**, 1083–1100 (2015).

15.   Meyer, T. J. & Huynh, M. H. V. The Remarkable Reactivity of High Oxidation State Ruthenium and Osmium Polypyridyl Complexes. *Inorg. Chem.* **42**, 8140–8160 (2003).

16.   Murahashi, S.-I. & Zhang, D. Ruthenium catalyzed biomimetic oxidation in organic synthesis inspired by cytochrome P-450. *Chem. Soc. Rev.* **37**, 1490–1501 (2008).

17.   Aiki, S. *et al.* Ligand Modification of Cyclometalated Ruthenium Complexes in the Aerobic Oxidative Dehydrogenation of Imidazolines. *ACS Catal.* **3**, 812–816 (2013).

18.   Hirano, T., Ueda, K., Mukaida, M., Nagao, H. & Oi, T. Reactions of [RuCl2(NO)(terpy)]+ (terpy = 2,2′ : 6′,2″-terpyridine) with mono anions such as NO2−, Br− and N3−, and structural studies on terpyridineruthenium having a nitrosyl ligand. *J. Chem. Soc., Dalton Trans.* **0**, 2341–2345 (2001).

19. Gibson, D. H., Andino, J. G. & Mashuta, M. S. Synthesis, Characterization, and Rearrangements of Methoxymethyl Ruthenium(II) Complexes with Polypyridine Ligands. *Organometallics* **24**, 5067–5075 (2005).

20. Johansson, O. & Lomoth, R. Rapid electrochemically induced linkage isomerism in a ruthenium(II) polypyridyl complex. *Chem. Commun.* **0**, 1578–1580 (2005).

21. Nagao, H. *et al.* Synthesis of Nitrosylruthenium Complexes Containing 2,2':6',2' '-Terpyridine by Reactions of Alkoxo Complexes with Acids. *Inorg. Chem.* **46**, 1431–1439 (2007).

22. Taher Deeb, Thibault Michelle E., Di Mondo Domenico, Jennings Michael & Schlaf Marcel. Acid-, Water- and High-Temperature-Stable Ruthenium Complexes for the Total Catalytic Deoxygenation of Glycerol to Propane. *Chemistry – A European Journal* **15**, 10132–10143 (2009).

23. Giglmeier, H., Kerscher, T., Klüfers, P., Schaniel, D. & Woike, T. Nitric-oxide photorelease and photoinduced linkage isomerism on solid [Ru(NO)(terpy)(L)]BPh4 (L = glycolate dianion). *Dalton Trans.* **0**, 9113–9116 (2009).

24. Francàs, L. *et al.* Synthesis, Characterization, and Linkage Isomerism in Mononuclear Ruthenium Complexes Containing the New Pyrazolate-Based Ligand Hpbl. *Inorg. Chem.* **53**, 8025–8035 (2014).

25. Francàs, L. *et al.* Dinuclear Ruthenium Complexes Containing the Hpbl Ligand: Synthesis, Characterization, Linkage Isomerism, and Epoxidation Catalysis. *Inorg. Chem.* **53**, 10394–10402 (2014).

26. Coe, B. J. & Glenwright, S. J. Trans-effects in octahedral transition metal complexes. *Coordination Chemistry Reviews* **203**, 5–80 (2000).

27. Hadadzadeh, H., DeRosa, M. C., Yap, G. P. A., Rezvani, A. R. & Crutchley, R. J. Cyclometalated Ruthenium Chloro and Nitrosyl Complexes. *Inorg. Chem.* **41**, 6521–6526 (2002).

28. Bard, A. J. & Faulkner, L. R. *Electrochemical Methods: Fundamentals and Applications*. (Wiley, 2000).

29. Wada, T., Hiraide, T. & Miyazato, Y. Water Oxidation Catalyzed by a Ruthenium Complex with an Ru–C Bond. *ChemistrySelect* **1**, 3045–3048 (2016).

30. Bomben, P. G., Robson, K. C. D., Sedach, P. A. & Berlinguette, C. P. On the Viability of Cyclometalated Ru(II) Complexes for Light-Harvesting Applications. *Inorg. Chem.* **48**, 9631–9643 (2009).

31. Sens, C. *et al.* Synthesis, Structure, and Spectroscopic, Photochemical, Redox, and Catalytic Properties of Ruthenium(II) Isomeric Complexes Containing Dimethyl Sulfoxide, Chloro, and the Dinucleating Bis(2-pyridyl)pyrazole Ligands. *Inorg. Chem.* **42**, 2040–2048 (2003).

32. Wada, T., Hiraide, T. & Miyazato, Y. Water Oxidation Catalyzed by a Ruthenium Complex with an Ru–C Bond. *ChemistrySelect* **1**, 3045–3048 (2016).

33. Llobet, A., Doppelt, P. & Meyer, T. J. Redox properties of aqua complexes of ruthenium(II) containing the tridentate ligands 2,2':6',2"-terpyridine and tris(1-pyrazolyl)methane. *Inorg. Chem.* **27**, 514–520 (1988).

34. Wang, L., Duan, L., Wang, Y., Ahlquist, M. S. G. & Sun, L. Highly efficient and robust molecular water oxidation catalysts based on ruthenium complexes. *Chem. Commun.* **50**, 12947–12950 (2014).

35. Stultz, L. K., Binstead, R. A., Reynolds, M. S. & Meyer, T. J. Epoxidation of Olefins by [RuIV(bpy)2(py)(O)]2+ in Acetonitrile Solution. A Global Kinetic Analysis of the Epoxidation of trans-Stilbene. *J. Am. Chem. Soc.* **117**, 2520–2532 (1995).

36. Shilov, A. E. & Shul'pin, G. B. Activation of C−H Bonds by Metal Complexes. *Chem. Rev.* **97**, 2879–2932 (1997).

37. Crabtree, R. H. Alkane C–H activation and functionalization with homogeneous transition metal catalysts: a century of progress—a new millennium in prospect. *J. Chem. Soc., Dalton Trans.* **0**, 2437–2450 (2001).

38. White, M. C. Adding Aliphatic C–H Bond Oxidations to Synthesis. *Science* **335**, 807–809 (2012).

39. Weinberg, D. R. *et al.* Proton-Coupled Electron Transfer. *Chem. Rev.* **112**, 4016–4093 (2012).

40. Wong, Y.-L. *et al.* Synthesis, structure and oxo-transfer properties of dioxotungsten(VI) complexes with pyridine-based NO- and NS-bidentate ligands. *New J. Chem.* **25**, 353–357 (2001).

41. Sullivan, B. P., Calvert, J. M. & Meyer, T. J. Cis-trans isomerism in (trpy)(PPh3)RuC12. Comparisons between the chemical and physical properties of a cis-trans isomeric pair. *Inorg. Chem.* **19**, 1404–1407 (1980).

42. Dolomanov, O. V., Bourhis, L. J., Gildea, R. J., Howard, J. a. K. & Puschmann, H. OLEX2: a complete structure solution, refinement and analysis program. *J Appl Cryst, J Appl Crystallogr* **42**, 339–341 (2009).

43. Sheldrick, G. M. SHELXT – Integrated space-group and crystal-structure determination. *Acta Cryst A, Acta Cryst Sect A, Acta Crystallogr A, Acta Crystallogr Sect A, Acta*

Crystallogr A Cryst Phys Diffr Theor Gen Crystallogr, Acta Crystallogr Sect A Cryst Phys Diffr Theor Gen Crystallogr **71**, 3–8 (2015).

44.   Sheldrick, G. M. A short history of SHELX. *Acta Cryst A, Acta Cryst Sect A, Acta Crystallogr A, Acta Crystallogr Sect A, Acta Crystallogr A Found Crystallogr, Acta Crystallogr Sect A Found Crystallogr* **64**, 112–122 (2008).

45.   Connelly, N. G. & Geiger, W. E. Chemical Redox Agents for Organometallic Chemistry. *Chem. Rev.* **96**, 877–910 (1996).

CHAPTER 3. PYRIDYLPHOSPHONATE LIGANDS FOR PROTON-COUPLED ELECTRON TRANSFER (PCET)

3.1. Introduction

Proton-coupled electron transfer (PCET) is a powerful tool in the inorganic chemists' toolbox for reducing the thermodynamic redox potentials of high-valent transition metal complexes.[1–5] For this reason, a number of groups have investigated PCET capable ligands for enhancing the activity of C-H bond[6,7] and water oxidation[8–14] catalysts. In order for a ligand to be capable of PCET, it must contain a protonatable site that does not coordinate directly to metal center and whose acidity varies as a function of the oxidation state of the metal it is ligated to. A wide variety of acidic and basic moieties have been employed for this purpose, for example: carboxylic acids,[8] N-heterocycles,[9] and hydroxyl groups.[12] One potentially PCET enabling moiety that has not been well investigated is the phosphonate group, RPO_3H_2. To the best of our knowledge, there are only three reports of complexes using phosphonates to enable PCET, with two of these reports focusing on water oxidation by the Ru complex of 2,2'-bipyridine-6,6'-diphosphonate (H_4dPa),[15,16] and the third describing water oxidation by the Ru complex of 2,2':3',2''-terpyridine-6,6''-diphosphonate (H_4tPa).[17] We are unaware of any studies of the C-H bond oxidation capabilities of Ru phosphonate complexes, or of any electrochemical data reported for Ru phosphonates in the absence of a second phosphonate group.

As part of our group's interest in C-H bond oxidation, we hypothesized that pyridylphosphonate ligands could be used to generate Ru complexes with redox potentials appropriate for C-H bond activation. In order to test this hypothesis, we synthesized several Ru complexes using the ligands (pyridin-2-ylmethyl)phosphonic acid ($MepyPO_3H_2$) and (6,6'-bipyridin-2-yl)phosphonic acid ($bpyPO_3H_2$): [Ru(MepyPO_3H)(tpy)Cl], **1**,

[Ru(bpyPO$_3$H$_2$)(bpy)Cl]Cl, **2**, and [Ru(bpyPO$_3$H$_2$)(bpy)(OH$_2$)] (NO$_3$)$_2$ **3** (Figure 3.1). We then characterized the redox properties of these compounds and assessed their ability to serve as catalysts for C-H bond oxidation.

[Ru(tpy)(MepyPO$_3$H)Cl] **1**   [Ru(bpyPO$_3$H)(bpy)Cl]$^+$ **2**   [Ru(bpyPO$_3$H)(bpy)OH$_2$]$^{2+}$ **3**
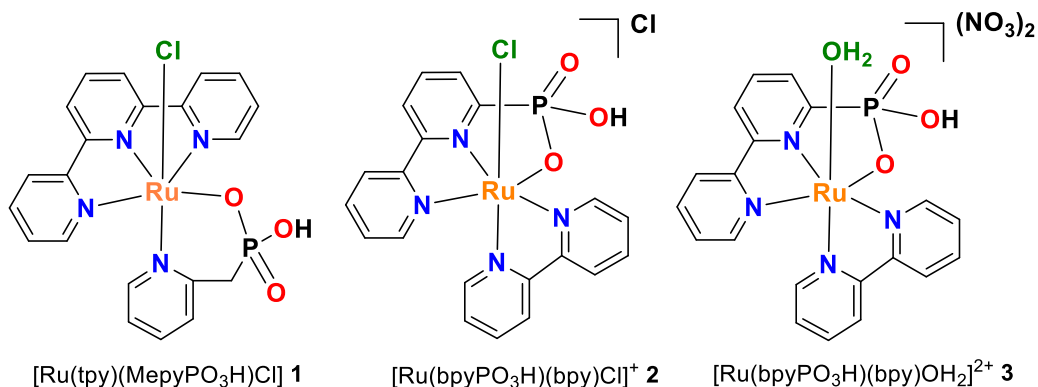
Figure 3.1. Structures of Ru coordination complexes studied in this chapter

3.2. Results

3.2.1. Structural Properties of [Ru(tpy)(MepyPO₃H))Cl] (1)

The ESI-MS spectrum of **1** (Figure 3.2) shows 4 strong peaks at 284.06, 507.02, 541.99, and 564.98 m/z corresponding to [Ru(tpy)(MepyPO$_3$H)(OH)(MeOH)]$^{2+}$, [Ru(tpy)(MepyPO$_3$H)]$^+$, [Ru(tpy)(MepyPO$_3$H)Cl]$^+$, and [Ru(tpy)(MepyPO$_3$HNa)Cl]$^+$, respectively, consistent with the proposed formula for **1**. In addition to these peaks, a smaller peak is observed at 369.96 m/z consistent with the formulation [Ru(tpy)Cl]$^+$ suggesting partial loss of the MepyPO$_3$H ligand upon ionization. ^{1}H NMR of **1** in D$_2$O (Fig 3.3) presents 15 proton resonances with the correct integrated values in the aromatic region, suggesting the formation of Ru(II) oxidation state during the preparation of **1**.
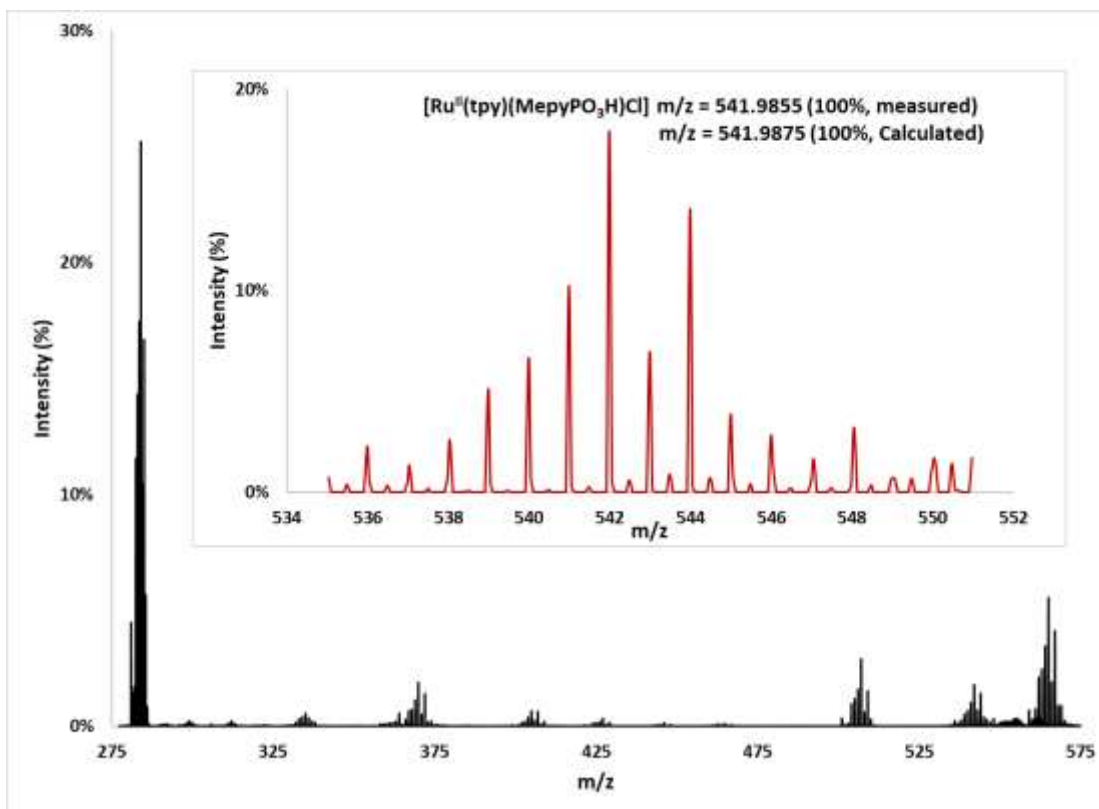
Figure 3.2. Positive-mode ESI-MS spectrum showing different ionization peaks of **1** in MeOH; (insert) observed and calculated peak cluster at 541.98 m/z assigned to **1**
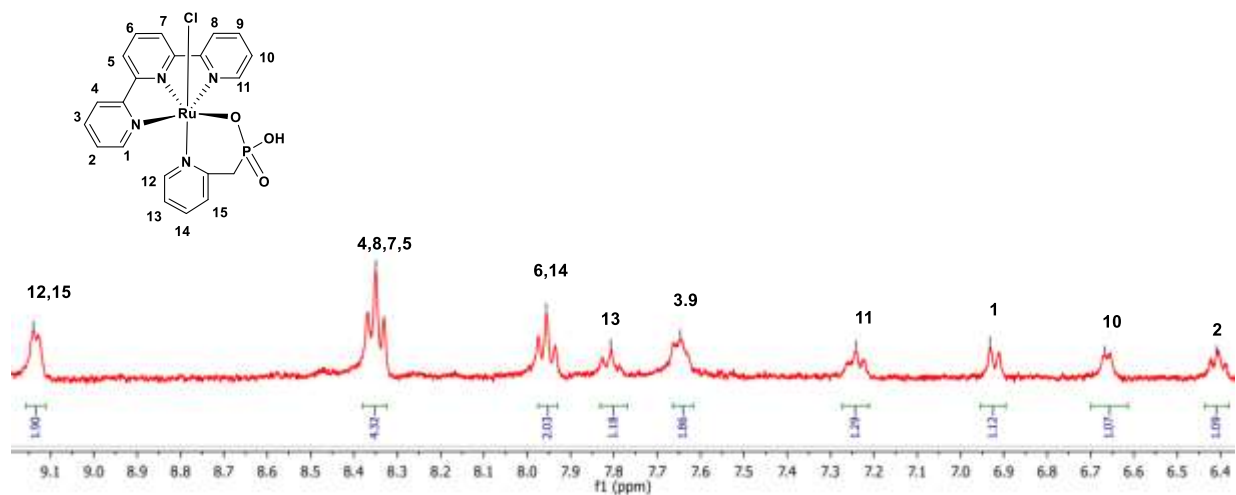
Figure 3.3. ^{1}HNMR spectrum (aromatic region) of **1** in D_2O

3.2.2. Structural Properties of [Ru(bpyPO₃H)(bpy)Cl]Cl (2)

3.2.2. Structural Properties of [Ru(bpyPO$_3$H)(bpy)Cl]Cl (2)

Crystallization of **2** was readily achieved upon vapor diffusion of diethyl ether into a concentrated solution of **2** in methanol. As can be seen in Figure 3.1, **2** is monomeric in the solid state. X-ray crystal structure of **2** is presented in Figure 3.2. Comparison with the structural parameters determined for [Ru(tpy)(bpy)Cl]Cl shows comparable bond lengths for all Ru-N bonds, as well as a slightly shorter Ru-Cl bond in **2** (2.37 vs. 2.41 Å), consistent with a Ru(II) oxidation state for **2**.[18] Comparison of **2** with the previously reported Ru(II) complex {[Ru(H$_3$tPa-κ-N^{3}O)(py)$_2$](H$_2$O)$_3$}$^+$ shows **2** has a significantly shorter Ru-O (phosphonate) bond length (2.06 vs. 2.19 Å) as well as a significantly wider N-Ru-O(phosphonate) bond angle (84.9 vs. 83.7°). This indicates the tridentate bpyPO$_3$H$_2$ ligand adopts a less strained conformation than the previously reported tetradentate H$_3$tPa ligand.[17] Selected bond lengths and angles are provided in Table 1.
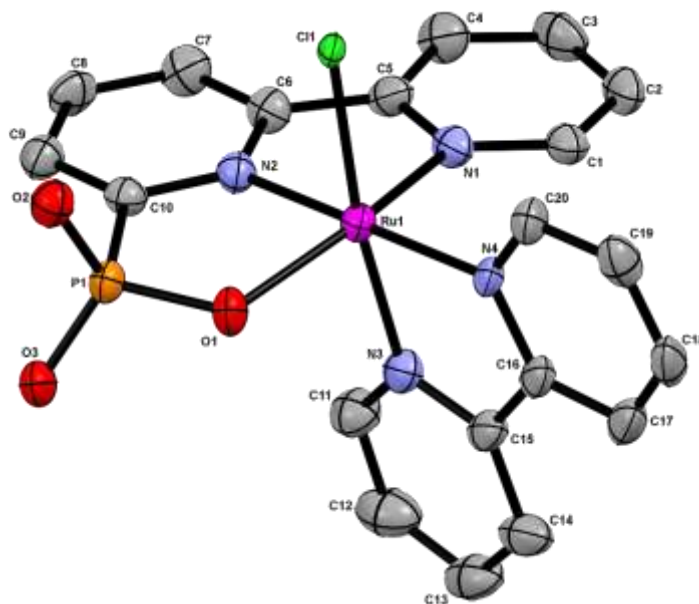
Figure 3.4. X-ray crystal structure of **2** showing ellipsoids at 50% probability; hydrogen atoms, counter anions, and lattice solvent molecules omitted for clarity; color code; ruthenium (blue), nitrogen (purple), oxygen (red), carbon (grey), phosphorous (yellow) and chloride (green)

Table 3.1. Selected bond distances (Angstrom) and bond angles (degrees) for **2**

2	Bond distances	2	Bond angles
Ru-N1	2.037	N3-Ru-N4	79.30
Ru-N2	2.008	N1-Ru-N2	79.02
Ru-N3	2.042	N1-Ru-O	161.12
Ru-N4	2.082	N2-Ru-O	84.92
Ru-O1	2.061	N1-Ru-N2-O	7.53
Ru-Cl	2.371	O-P-C	103.93

The oxidation state of **2** in solution was probed using the Evans method,[19] which showed no paramagnetic shift of the residual solvent peak in water, further confirming this assignment. The sharp NMR peaks observed for the aromatic protons in **2** also preclude the presence of a monomer/dimer equilibrium in solution for this species.

3.2.3. Spectroscopic Properties of [Ru(tpy)(MepyPO₃H)Cl] (1)

UV-visible spectra were obtained for **1** between pH 2.6 and 11.6 (Figure 3.5). Two isosbestic points are visible in these spectra, one at approximately 421 nm under mildly acidic conditions (Fig. 3.6a), and the second at approximately 450 nm under alkaline conditions (Fig. 3.6b), consistent with two pK_a values of 4.7 and 11.2. Interpretation of the second pK_a is complicated by an increasing absorbance at longer wavelengths under very alkaline conditions.
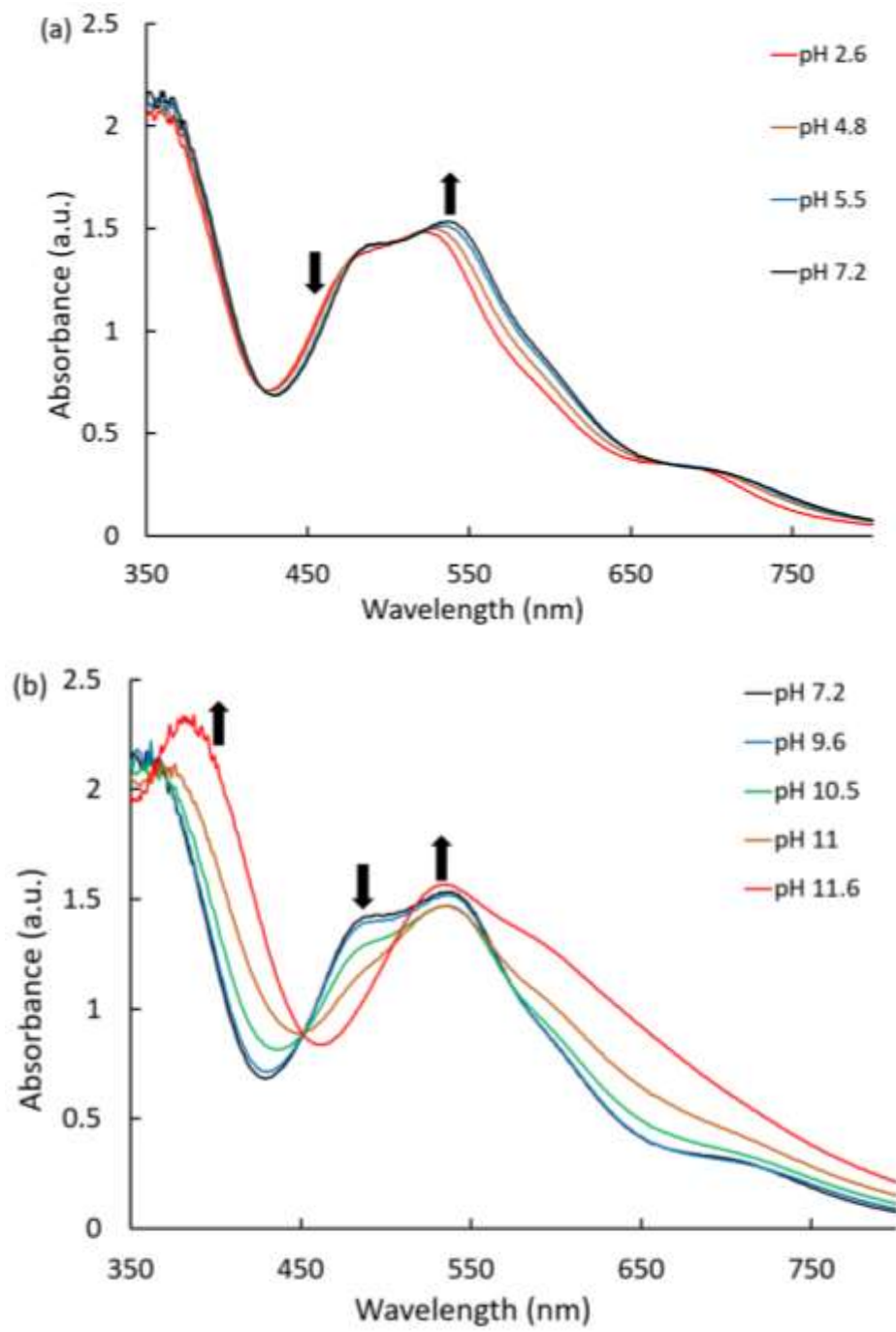
Figure 3.5. UV-Visible spectra of 1.92 mM **1** between (a) pH 2.6 and 7.2 and (b) 7.2 and 11.6. Bold arrows indicate the direction of the change in absorbance as a function of increasing pH
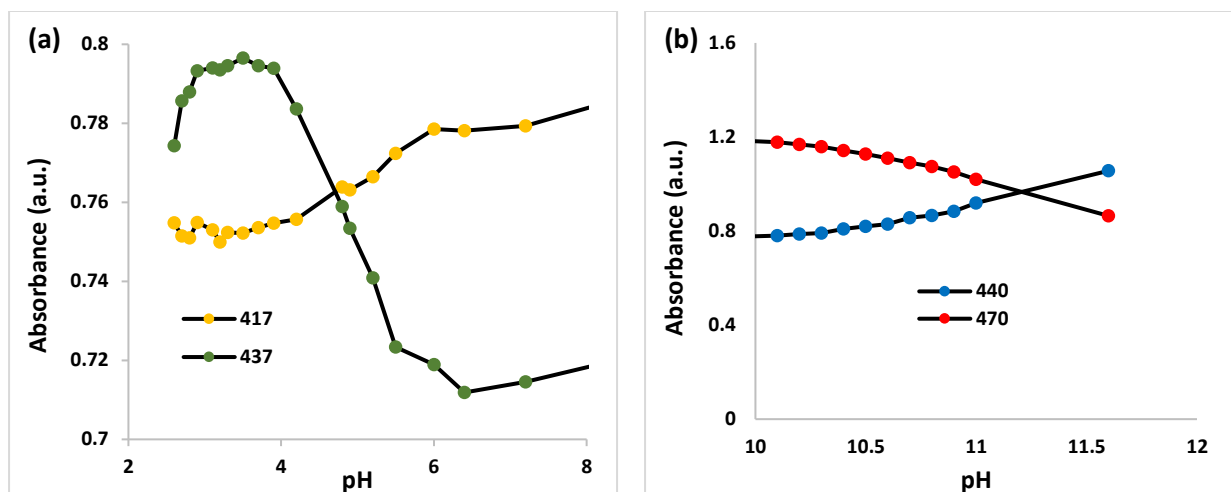
Figure 3.6. Absorption spectral changes at different wavelengths of **1** as a function of pH (a) The point of inflection shows the acidic pK_a 4.7 at 421nm (b) The point of inflection shows the alkaline pK_a 11.2 at 451nm

3.2.4. Spectroscopic Properties of [Ru(bpyPO₃H₂)(bpy)Cl]Cl (2) and [Ru(bpyPO₃H₂)(bpy)(OH₂)](NO₃)₂ (3)

(Section heading as printed: 3.2.4. Spectroscopic Properties of [Ru(bpyPO$_3$H$_2$)(bpy)Cl]Cl (2) and [Ru(bpyPO$_3$H$_2$)(bpy)(OH$_2$)](NO$_3$)$_2$ (3))
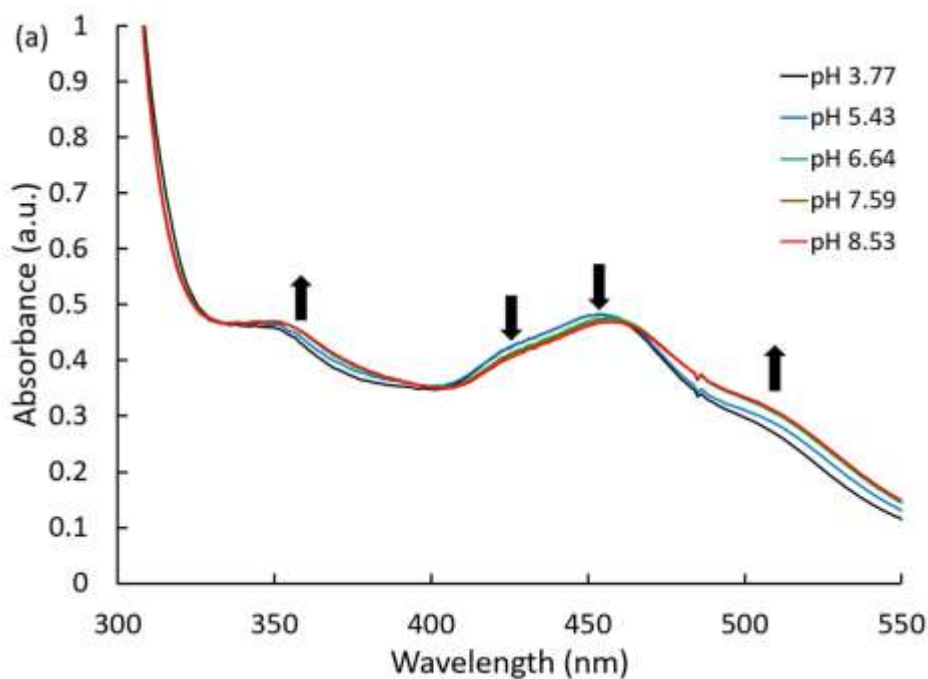
Figure 3.7. (a) Absorption spectral changes of (a) **2** (0.1 mM) and (b) **3** (0.1 mM) between pH 2.6 and 9. Bold arrows indicate the direction of the change in absorbance as a function of increasing pH
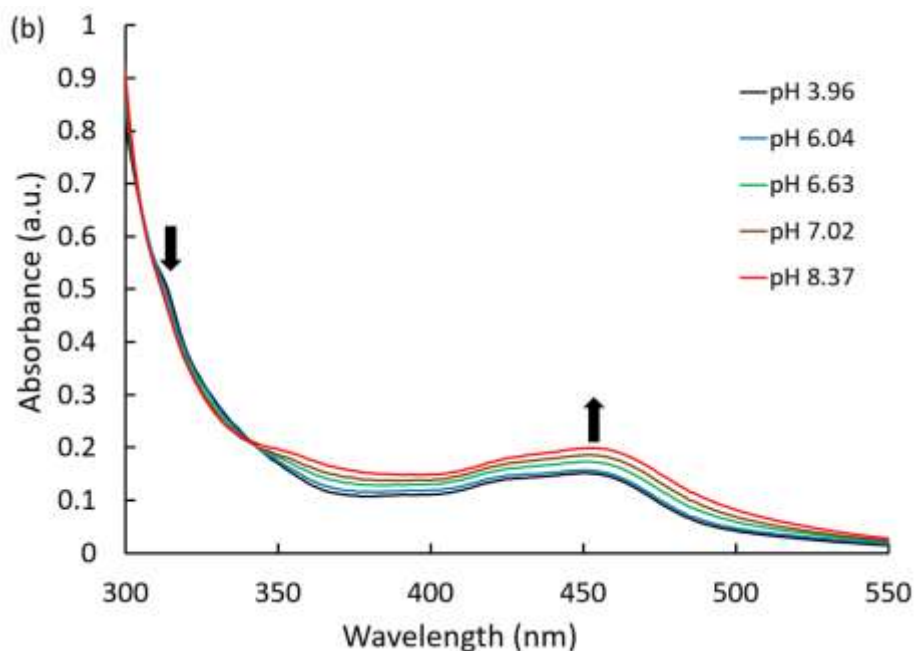
Figure 3.7. (a) Absorption spectral changes of (a) **2** (0.1 mM) and (b) **3** (0.1 mM) between pH 2.6 and 9 (continued). Bold arrows indicate the direction of the change in absorbance as a function of increasing pH

UV-visible spectra of **2** and **3** were collected as a function of pH in order to determine whether solution chloride would affect the electronic properties of these compounds (Figures 3.7a-b). As shown, the UV-visible spectra of **2** show an additional peak at 350 nm that is not visible in **3**, suggesting that chloride may be binding to the Ru center under these measurement conditions. In order to avoid complications from potential chloride binding equilibria, all further UV-visible spectra were collected on **3**. In contrast to **1**, the UV-visible spectra of **3** displays only one pK_a with a value of 6.7 and isosbestic points at 304 and 344 nm, and no additional pK_a is observed between pH 7 and 12.
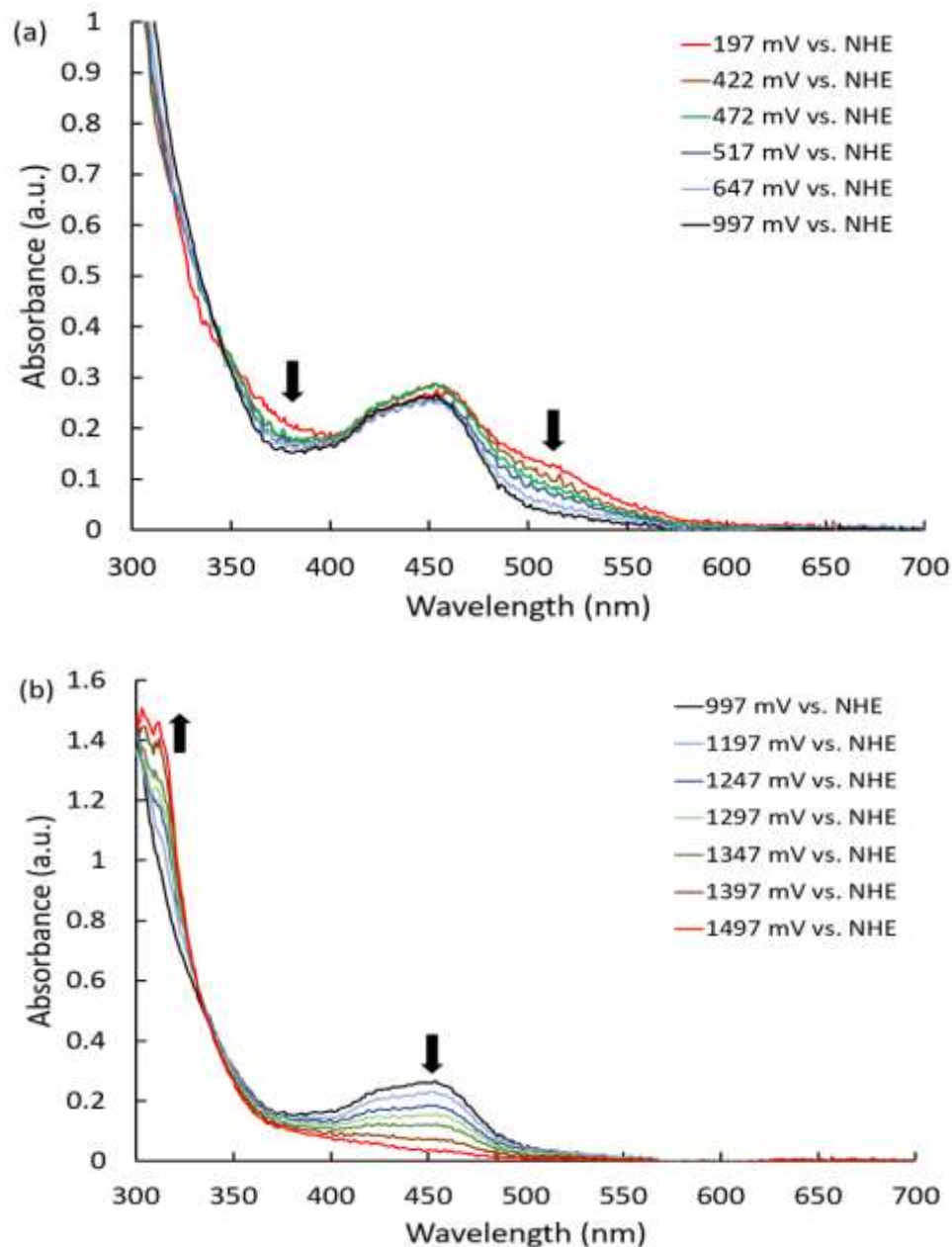
Figure 3.8. UV-Visible spectra of 250 µM **3** in pH 4.17 water under constant application of (a) 197 to 997 and (b) 997 to 1497 mV vs NHE potentials. Bold arrows indicate the direction of the change in absorbance as a function of increasing applied potential. Referenced to saturated Ag/AgCl and converted to NHE using the standard value Ag/AgCl = 197 mV vs. NHE[28]

UV-visible spectra of **3** were also collected as a function of applied potential at a constant

pH of 4.17 (Figure 3.8a-b). Three distinct species are observed as the applied potential is

increased from 0.197 to 1.50 V vs. NHE, the first is present at applied potentials below

approximately 0.5 V vs. NHE, the second at applied potentials between approximately 0.5 and

1.3 V vs. NHE, and the third at applied potentials above 1.3 V vs. NHE. The species present at

potentials below approximately 500 mV vs. NHE has a peak centered around 453 nm, with a

broad tail extending to about 590 nm. The molar absorptivities for this species are comparable to

those observed in the absence of an electrode, and this species can be safely assigned as **3** in the

Ru(II) oxidation state. Distinct isosbestic points are observed at 350 nm for the first oxidation

and at 335 nm for the second oxidation (Figure 3.9), indicating clean conversion between

oxidation states. These spectra allow us to estimate and assign the thermodynamic potentials of

these two oxidations as 0.52 V vs. NHE for the Ru(II/IV) couple and 1.3 V vs. NHE for the

Ru(IV/V) couple, respectively, in good agreement with the potentials measured

electrochemically (vide infra).
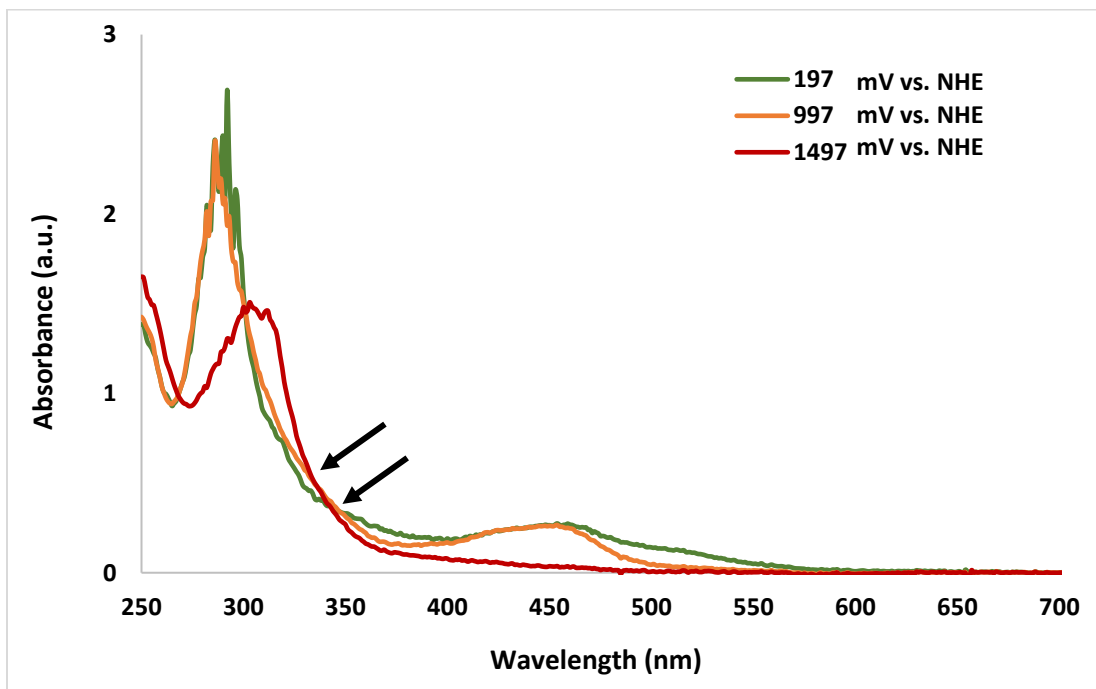
Figure 3.9. UV-Visible spectra of 0.25 mM of **3** in water with constant application of the
potentials indicated. Solid arrows indicate the two isosbestic points at 335 and 350 nm.
Referenced to saturated Ag/AgCl and converted to NHE using the standard value Ag/AgCl = 197
mV vs. NHE[28]

3.2.5. Redox Properties of [Ru(tpy)(MepyPO₃H)Cl] (1)

Cyclic voltammetry (CV) was used to measure the thermodynamic redox potentials of **1** in aqueous phosphate buffer as a function of pH (figure 3.10). As shown in the Pourbaix diagram (Figure 3.11), only one redox couple is observed for **1** between pH 1 and 10. This redox couple has a potential of 765 mV at a pH of 2, and exhibits a strong pH dependence. Between pH 1.7 and 4.7 the slope of this pH dependence is 59 mV/pH unit. This slope decreases to 29.5 mV/pH unit between pH 4.7 and pH 6.5, then increases back to 59 mV/pH unit above pH 6.5. This pH dependence indicates a 2 e⁻, 2 H⁺ PCET process at pH values below 4.7 and above 6.5, and a 2 e⁻, 1 H⁺ PCET process between pH 4.7 and 6.5. Taken together, this data indicates the redox couple observed for **1** corresponds to a concerted two-electron oxidation of Ru(II) to Ru(IV).
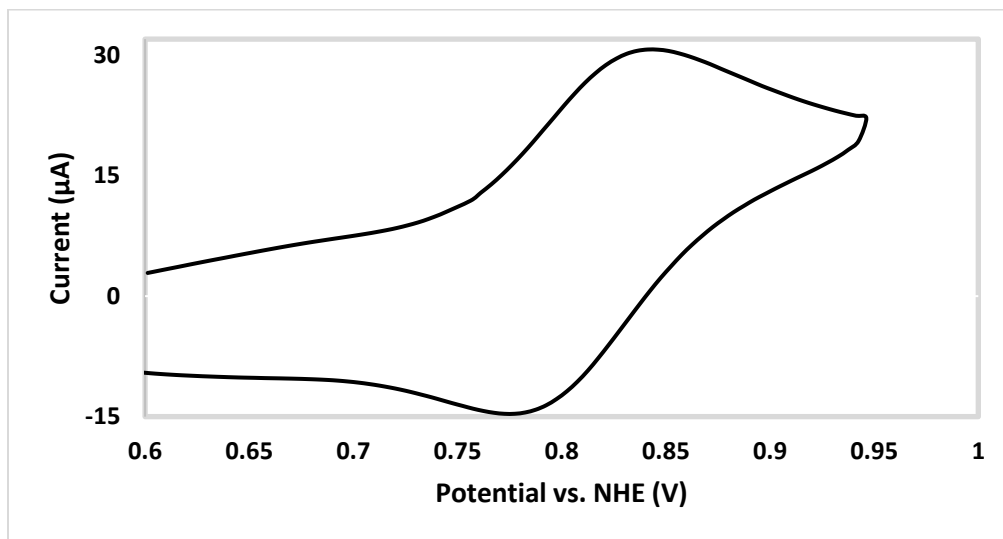
Figure 3.10. Cyclic voltammogram for **1** in pH 2.00 P$_i$ buffer; scan rate 100 mVs^{-1}. Referenced to saturated Ag/AgCl and converted to NHE using the standard value Ag/AgCl = 197 mV *vs.* NHE[28]
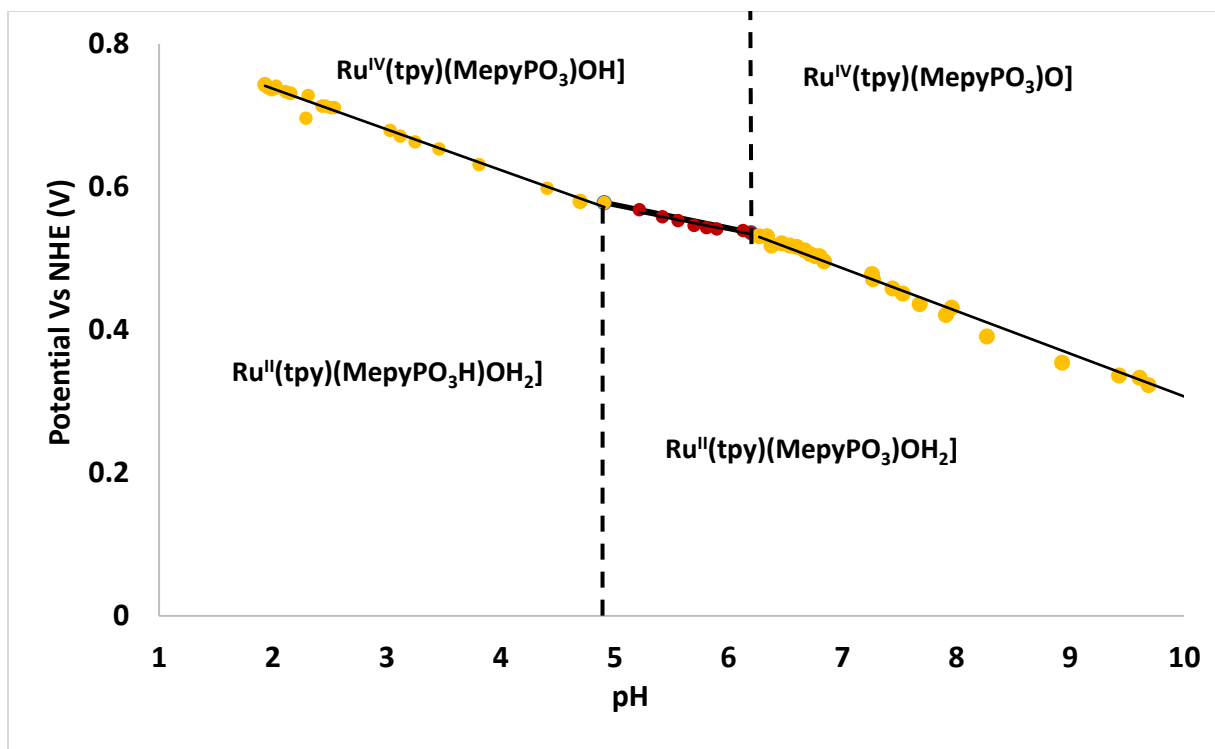
Figure 3.11. Pourbaix diagram of 10mM **1** in 100 mM 6.86 aqueous P_i buffer. Referenced to saturated Ag/AgCl and converted to NHE using standard value Ag/AgCl = 197 mV vs. NHE[28]. Accuracy of measured potential = ±0.05 % range[29]

3.2.6. Redox Properties of [Ru(bpyPO₃H₂)(bpy)Cl]Cl (2) and [Ru(bpyPO₃H₂)(bpy)(OH₂)](NO₃)₂ (3)

The redox potentials of **2** were investigated using CV. As shown in Fig. 3.12a, in pH 7.1 phosphate buffer **2** exhibits three redox couples with half-potentials of approximately 460, 980, and 1270 mV vs. NHE. As suggested by the UV-visible experiments, it is not clear whether the observed redox potentials correspond to **2** with or without a bound chloride ion. In order to resolve the potential ambiguities introduced by the presence of chloride ions in solution, the redox properties of the nitrate salt **3** were also examined. As shown in Fig. 3.12b, three distinct redox events centered near 514, 1050 and 1300 mV vs. NHE are present in the cyclic voltammogram of **3** in pH 6.17 phosphate buffer. This suggests that, in contrast to the conditions

used for UV-visible measurements, chloride does not bind strongly to the Ru center under the

conditions used for electrochemical measurements.
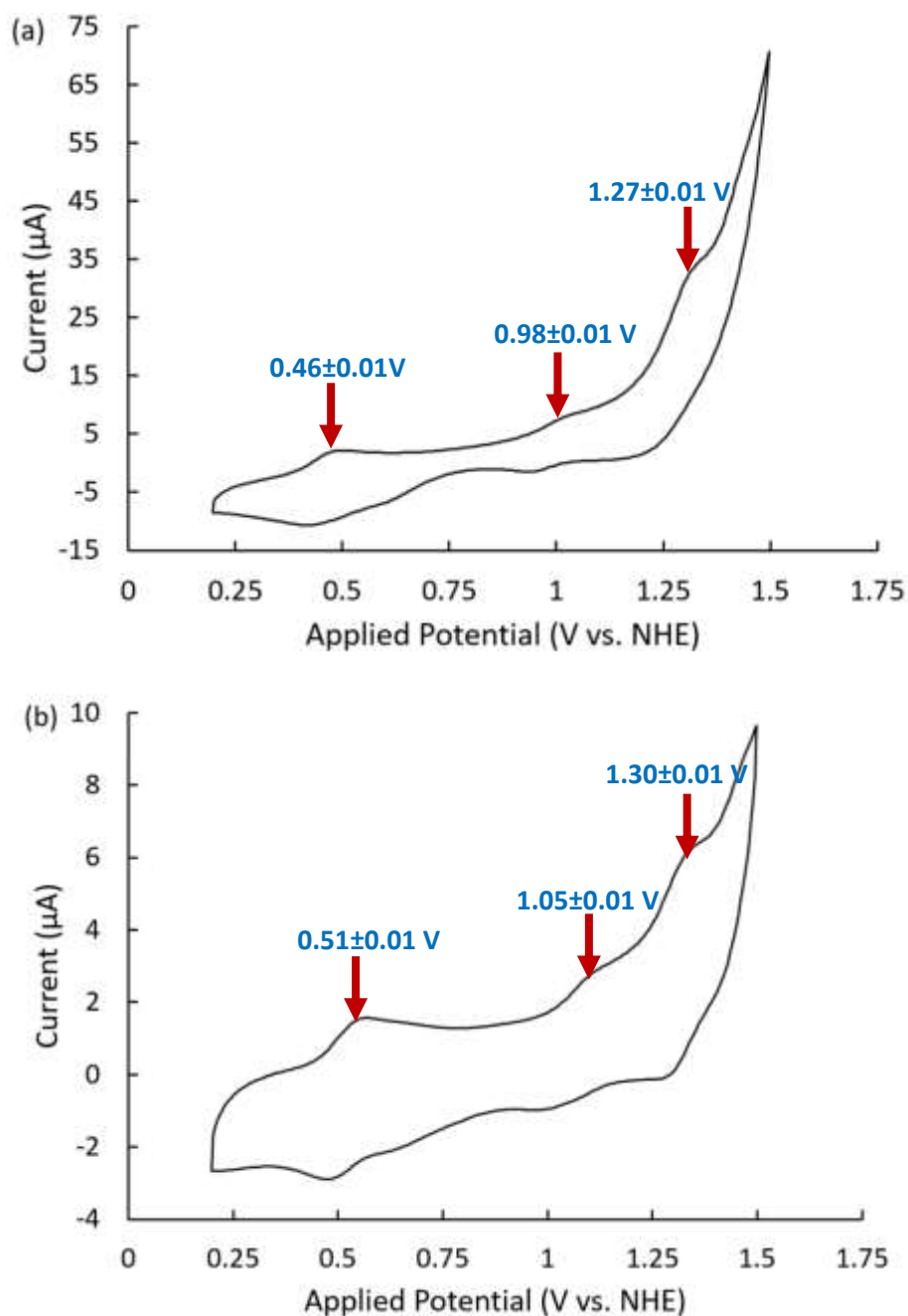
Figure 3.12. Cyclic voltammogram of (a) 1.0 mM **2** in 100 mM pH 7.1 aqueous P_i buffer and (b) 1.0 mM **3** in 100mM pH 6.17 aqueous buffer; scan rate 100 mV/s. Referenced to saturated Ag/AgCl and converted to NHE using the standard value Ag/AgCl = 197 mV *vs.* NHE[28]

In order to assign the three redox events observed for **3**, their peak currents and half-potentials were measured as a function of electrode scan rate (Fig. 3.13). As shown in Fig. 3.13a, the potentials for both the oxidative and reductive waves of redox event centered at 650 mV vs. NHE do not change with the scan rate, indicating a reversible process. In contrast, the potentials for the redox events centered at 1200 and 1325 mV vs. NHE do vary as a function of scan rate, indicating these events correspond to quasi-reversible or irreversible processes (Figs. 3.13b-c).
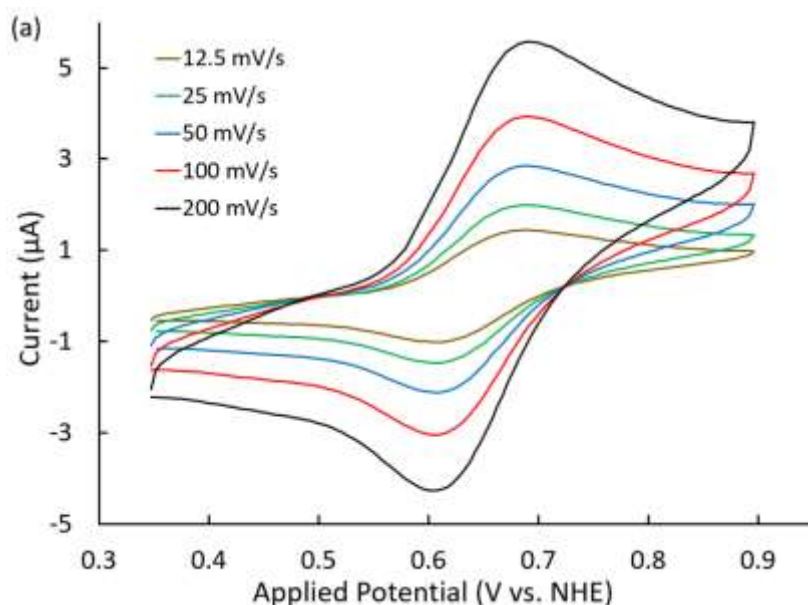
Figure 3.13. Cyclic voltammograms of 1.0 mM **3** in 100 mM pH 4.5 aqueous P_i buffer at multiple scan rates collect with applied potentials between: (a) 300-900, (b) 1047-1267, and (c) 1197-1447 mV vs. NHE. Referenced to saturated Ag/AgCl and converted to NHE using the standard value Ag/AgCl = 197 mV vs. NHE[28]
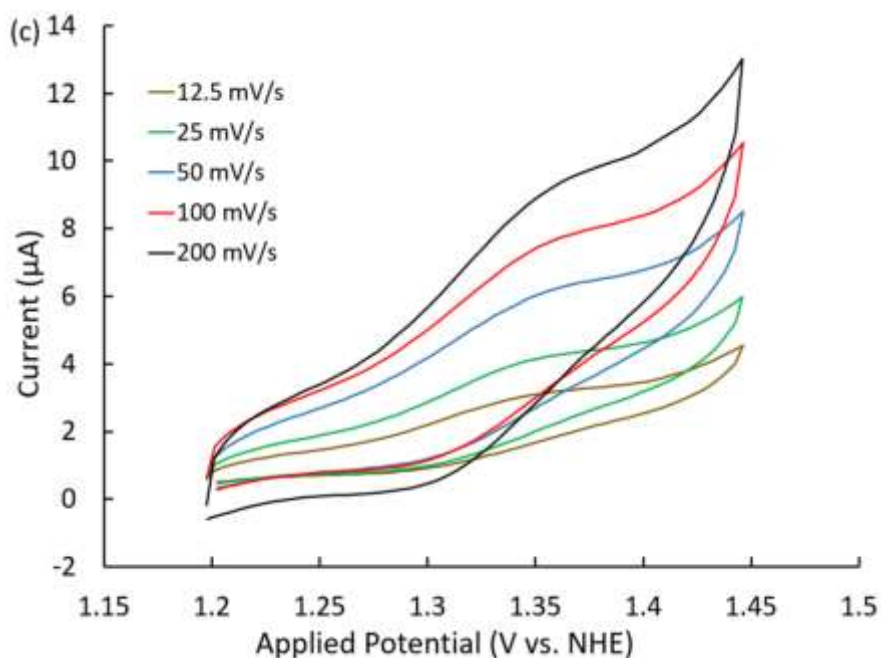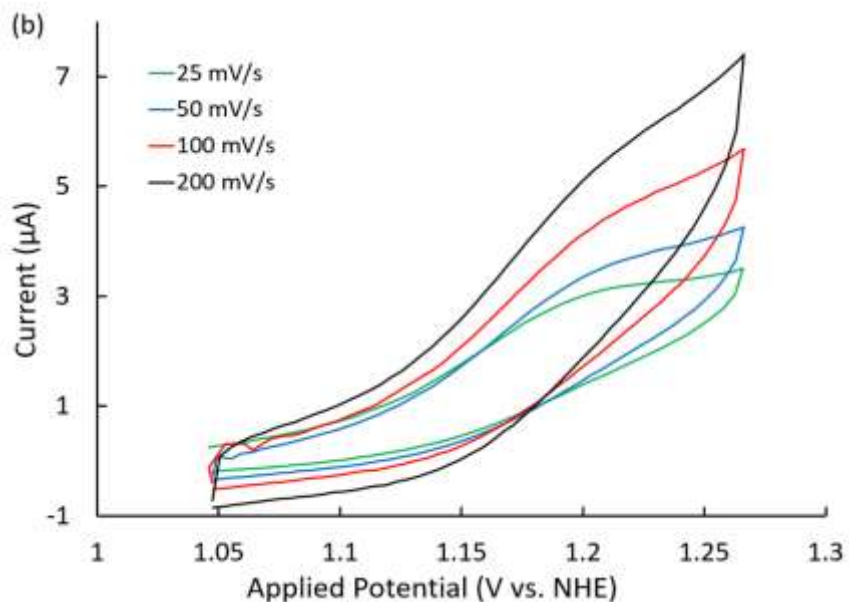
Figure 3.13. Cyclic voltammograms of 1.0 mM **3** in 100 mM pH 4.5 aqueous P_i buffer at multiple scan rates collect with applied potentials between: (a) 300-900, (b) 1047-1267, and (c) 1197-1447 mV vs. NHE (continued). Referenced to saturated Ag/AgCl and converted to NHE using the standard value Ag/AgCl = 197 mV vs. NHE[28]

As a first step toward generating a Pourbaix diagram for **3**, the behavior of these three

redox events with respect to pH was measured in borate buffer (Fig 3.14). As shown in Fig. 3.13,

the lowest potential redox couple shows a pH dependence with a slope of 29.5 mV/pH unit

between pH 3 and pH 5.5, indicating a 2 e⁻, 1 H⁺ PCET process. Above pH 5.5 and below pH 3

this redox couple exhibits a pH dependence with a slope of 59 mV/pH unit, consistent with a 2 e⁻

, 2 H⁺ PCET process. In contrast with this behavior, the potential of the redox couple centered at

1325 mV vs. NHE shows no dependence on pH, indicating this redox event is not proton-

coupled. Finally, the redox couple centered at 1200 mV vs NHE at pH 4.5 shows no pH

dependence at pH values below 6 and above 7.5 indicating no proton involvement in this redox

couple, but shows a pH dependence of 120 mV/pH unit between pH 6 and 7.5, suggesting a 1 e⁻,

2 H⁺ PCET process through this pH range.
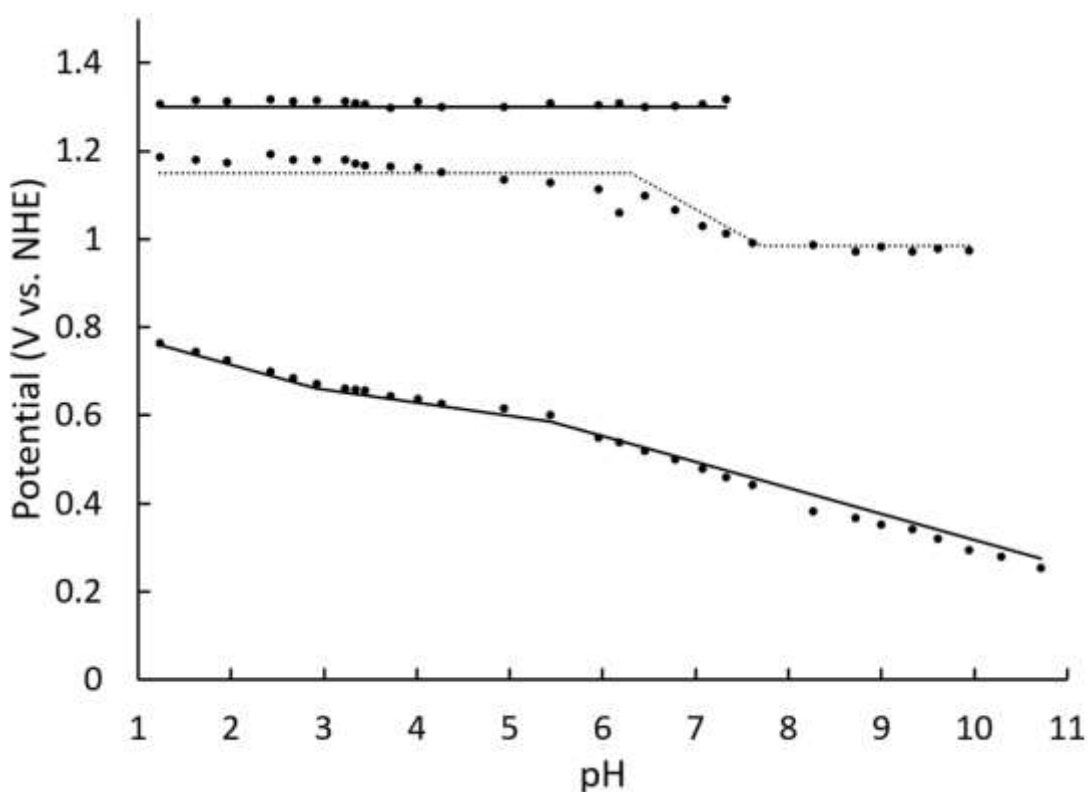
Figure 3.14. Midpoint potentials as a function of pH for a 1.0 mM solution of **3** in 100 mM aqueous borate buffer. Referenced to saturated Ag/AgCl and converted to NHE using the standard value Ag/AgCl = 197 mV vs. NHE[28]. Accuracy of measured potential = ±0.05 % range[29]

In order to determine if any of the observed redox couples resulted from the formation of dimeric or higher order species forming in solution, the peak current of each redox couple was measured as a function of concentration. As shown in Figure 3.15, the current for each of the redox couples obeys a linear dependence on the concentration of **3**, precluding the possibility that these redox couples result from an equilibrium between monomeric and dimeric (or higher order) species in solution.
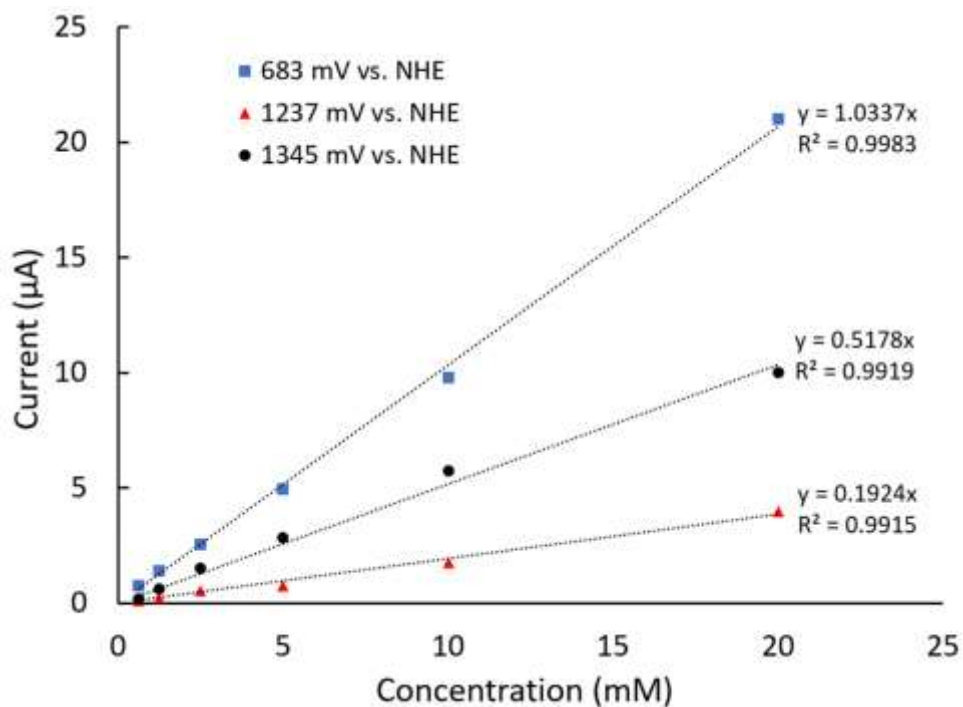
Figure 3.15. Peak current at indicated applied potentials as a function of concentration for **3** in 100 mM pH 7.61 aqueous P_i buffer. Dotted lines indicate the best fit linear regression with a fixed intercept at the origin. Fitting parameters and quality of fit is shown next to each regression. Scan rate 100 mV/s. Referenced to saturated Ag/AgCl and converted to NHE using the standard value Ag/AgCl = 197 mV vs. NHE[28]. Accuracy of measured current = ±0.05% range[29]

Based on a combination of the electrochemical and spectroscopic data collected for **3**, we can now generate a Pourbaix diagram for this complex (Fig. 3.16). As demonstrated by the linear relationship between peak current and concentration (Fig. 3.15), we only monomeric species can be included in the Pourbaix diagram. The first redox couple observed for **3** has a region with a

71

pH dependence of 29.5 mV/pH, indicating a 2 e⁻, 1 H⁺ PCET process. Given the spectroscopic

evidence that this redox couple corresponds to oxidation of the Ru(II) oxidation state, we can

assign this redox event as a two electron concerted Ru(II/IV) couple. The pK_a of 6.7 observed

spectroscopically for **3** in the Ru(II) oxidation state does not appear in the electrochemical data.

This likely indicates that the Ru(IV) oxidation state also possesses a pK_a close to this value, a

situation not unusual for coordination complexes possessing ligands with multiple potential

protonation states, as a PCET at the metal center does not always have a great effect on the pK_a

values of the ligands.[20]

Assignment of the second redox couple observed for **3** is more difficult. The midpoint

potential of the second, irreversible, redox couple exhibits no pH dependence except for a region

between 6.3 and 7.6 where a 1 e⁻, 2 H⁺ PCET is observed. These pH values do not correspond to

any of those found for the Ru(II/IV) redox couple (Fig. 3.13). In addition, the potentials applied

above and below this couple does not result in a distinct change in the any change in the visible

spectrum of **3** (Fig. 3.14). These data are consistent with two hypotheses: a) that this redox

couple is due to oxidation followed by irreversible decomposition of the complex or b) this redox

couple results from a reaction of **3** with the electrode surface. To distinguish between these two

possibilities, we measured the potential of this redox couple using both Pt and glassy carbon

electrodes. The observed difference in potential with different electrode materials supports the

hypothesis that this couple is due to an interaction of **3** with the electrode surface.
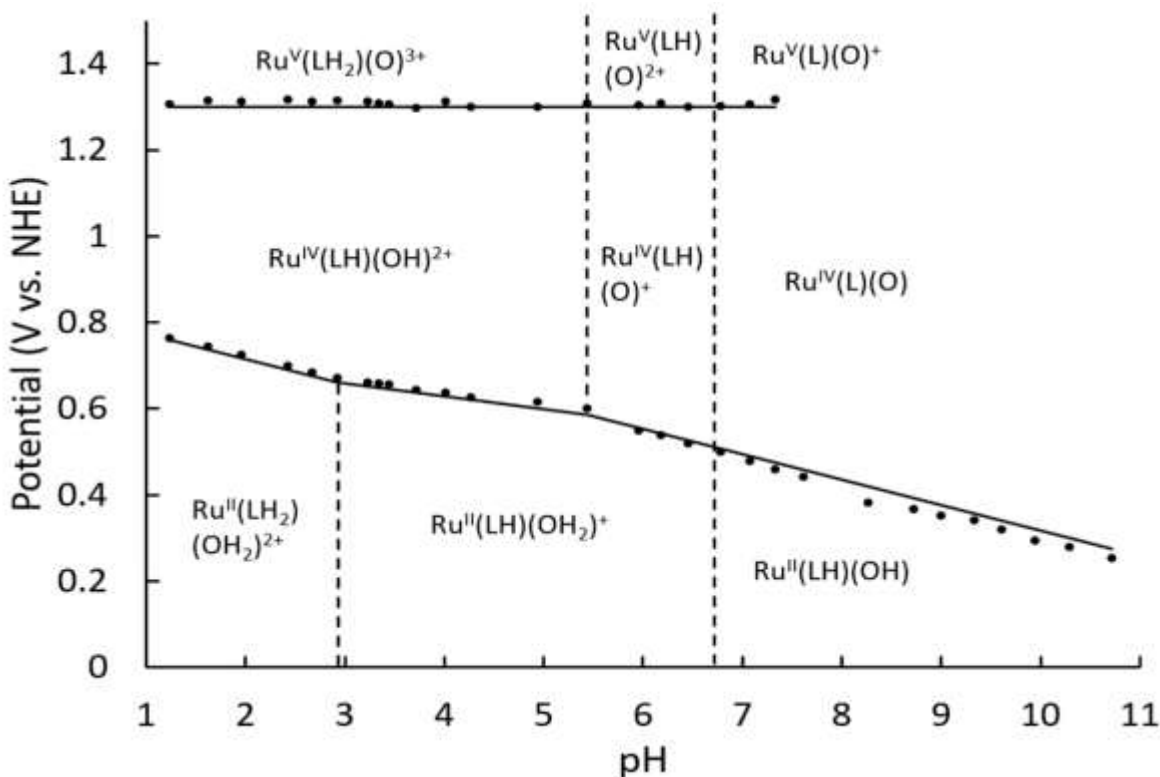
Figure 3.16. Pourbaix diagram of 1mM **3** in 100 mM borate buffer. Species labeling excludes bpy ligand for clarity. $L = bpyPO_3^{2-}$, $LH = bpyPO_3H^-$, $LH_2 = bpyPO_3H_2$. Referenced to saturated Ag/AgCl and converted to NHE using standard value Ag/AgCl = 197 mV vs. NHE[28]. Accuracy of measured potential = ± 0.05 % range[29]

The potential of the final redox couple observed for **3** shows no pH dependence, and so passes above the solvent window at pH values greater than 7. The simplest assignment of this redox couple is as the Ru(IV/V) couple, which is consistent with the spectroelectrochemical results (Fig. 3.8b) and 1:2 ratio of the peak currents for this couple and that of the first peak (Fig. 3.15). As with the second redox couple, the pH values observed for the Ru(II/IV) couple have no corresponding effect on the pH dependence of this couple. This again likely results from the presence of ligand pK_as not strongly affected by a proton-coupled oxidation at the metal center.

3.2.7. C-H Bond Oxidation Activity of [Ru(tpy)(MepyPO₃H)Cl] (1) and [Ru(bpyPO₃H₂)(bpy)Cl]Cl (2)

In order to assess the ability of **1** and **2** to serve as C-H bond oxidation catalysts, we first measured their ability to oxidize THF in aqueous solution using cerium(IV) ammonium nitrate (CAN), sodium periodate (NaIO₄), and hydrogen peroxide (H₂O₂). As shown in Table 3.2, **1** shows only a small amount of THF oxidation after 2 hours when using CAN as the oxidant and shows no product formation with sodium periodate or hydrogen peroxide. In contrast, **2** shows moderate to good yields of oxidation products when CAN is used as the oxidant and shows some activity when sodium periodate is used.

Table 3.2. Overall conversion and oxidized product yields for THF oxidation by **1** and **3** using various chemical oxidants.[a]

Catalyst	Oxidants	Yield[b] γ-Butyrolactone	Yield[b] Succinic Acid	Remaining Starting Material[c]
1	CAN	5%	6%	64%
	NaIO₄	0%	0%	86%
2	CAN	40%	14%	11%
	NaIO₄	1.4%	0%	78%
	H₂O₂	0%	0%	57%
None	NaIO₄	0%	0%	98%

[a]Reaction conditions: 4.9 µmol Ru complex (1% catalyst loading), 2.4 mmol oxidant, 490 µmol THF in 10 mL D₂O containing 19 µmol 3-(trimethylsilyl)propionic-2,2,3,3-d₄ acid sodium salt as an internal standard at 20° C under air for 1 hr. [b]As determined by ^{1}H NMR, mol product/initial mol THF. [c]Remaining starting material as determined by ^{1}H NMR, mol THF/initial mol THF

The substrate scope of C-H bond oxidation by **2** was then examined using CAN and sodium periodate with cyclooctane and cyclooctene as model alkane and alkene substrates. As shown in Table 3.3, **2** shows modest alkene epoxidation activity when CAN is used as the oxidant but does not oxidize cyclooctane to desirable products. In contrast, when sodium periodate is used as the oxidant 2 oxidized both cyclooctene and cyclooctane, albeit also modest yields.

Table 3.3. Overall conversion and GC product yields for substrate oxidation by **2** using CAN and NaIO$_4$.[a]

Reactant	Oxidant	Cyclooctanone (% Yield)[b]	Cyclooctene oxide (% yield)[b]	Remaining Starting Material (%)[c]
Cyclooctane	CAN	0 ± 0.2	-	37.0 ± 1.9
	CAN[d]	1.0 ± 0.2	-	83.7 ± 5.5
	NaIO$_4$	30.6 ± 0.3	-	37.0 ± 6.0
	NaIO$_4$[d]	1.8 ± 0.1	-	101 ± 21.8
Cyclooctane[d]	CAN[e]	1.2 ± 0.9	15.9 ± 0.1	46.1 ± 4.9
	NaIO$_4$[d]	-	11.2 ± 0.7	75.4 ± 17.8
	NaIO$_{4f}$	-	21.6 ± 0.5	24.5 ± 5.3

[a]Reaction conditions: 4.2 µmol **2** (~5.7% catalyst loading), 10 oxidizing equivalents (1500 µmol CAN, 740 µmol NaIO$_4$), 10 µL substrate (~74 µmol) in 400 µL 1:2 MeCN:H$_2$O under air for 24 hrs. [b]Average of a minimum of 3 runs; error represents 1 standard deviation from the mean; mol product/initial mol reactant; standardized to acetophenone. [c]Remaining starting material; average of a minimum of 3 runs; error represents 1 standard deviation from the mean; final mol reactant/initial mol reactant. [d]Reaction conditions: 1 hr, 1 oxidizing equivalent. [e]Reaction conditions: 1 hr, 3 oxidizing equivalents. [f]Reaction Conditions: 2 hr, 7 oxidizing equivalents

3.3. Discussion

3.3.1. Redox Properties of [Ru(tpy)(MepyPO₃H)Cl] (1), and [Ru(bpyPO₃H₂)(bpy)(OH₂)](NO₃)₂ (3)

As shown in their respective Pourbaix diagrams (Figs. 3.10 and 3.15), both **1** and **3** clearly possess proton-coupled two-electron concerted Ru(II/IV) redox couples, consistent with our initial hypothesis that pyridylphosphonate ligands could reduce energy difference between Ru(II/III) and Ru(III/IV) couples by enabling PCET. Closer examination of the values of the redox potentials reveals a complication with this interpretation, however, as two-electron Ru(II/IV) have been observed in aqueous solution when PCET is enabled by a bound aqua or hydroxo ligand even in the absence of other PCET enabling ligands. Indeed, a method for predicting complexes with concerted Ru(II/IV) redox couples based on Lever parameters (E$_L$)[21] was proposed by Dovletogou, Ademi and Meyer in 1996.[22] Using this method, Ru complexes possessing an aqua ligand can be expected to have a concerted Ru(II/IV) redox couple when the sum of the Lever parameters of the other ligands (ΣE$_L$) lies between ~950 mV and 1150 mV vs.

NHE. Experimental support for this prediction was provided by Dakkach *et al.* using Ru NHC complexes to generate Ru complexes with ΣE_L values of 1090 and 1440 mV vs. NHE.[23]

Based on their measured Ru(II/IV) potentials, we can estimate ΣE_L values of 1025 and 1000 mV vs. NHE for **1** and **3** respectively. Serendipitously, these values are well withing the region predicted to show concerted Ru(II/IV) couples even in the absence of additional PCET enabling ligands, and thus the fact that we observe this behavior for **1** and **3** cannot, unfortunately, be taken as either supporting or refuting our initial hypothesis.

Lever parameters for bpy and tpy are well established,[24] and we can thus use our measured ΣE_L values to estimate E_L values for the MepyPO$_3$H and bpyPO$_3$H$_2$ ligands as 138 and 160.7 mV vs. NHE, respectively, giving an approximate E_L value of 4 mV vs. NHE for a bound phosphonate group. E_L values close to 0 indicate a ligand that is neither a strong σ-donor nor a strong π-acceptor, e.g. water, and thus 4 mV is a reasonable value for a bound phosphonate group.

However, there are few possible sources of errors within the electrochemical measurement. One source of error is that the peak at 1325 mV looks distorted and determination of accurate peak position is difficult. The reproducibility tests can be carried out by obtaining the few measurements of the peak with independent background noise under typical reaction conditions to minimization of errors. Another source of error associated with this peak is that peak separation is >59 mV, indicates electrochemical irreversibility. The irreversibility (quasi-reversible or non-reversible) of the peaks mainly arises due to the slow reaction kinetics between analyte and the electrode surface. In such cases, the thermodynamic potential $\Delta E_{1/2}$ is often deduced by simulation. The magnitude of this error can be determined by measuring the $\Delta E_{1/2}$ potentials of a known reversible standard compound (ferrocene) under the same experimental conditions, that being used in the characterization of the unknown sample. In practice, the

theoretical value of 59 mV for peak-to-peak separation (ΔEp) is seldom observed. The most common error associated with electrochemical irreversibility is the deviation of a ratio of peak currents from 1, indicates the product is not very stable under scale of experiment.   The peak current measurement of the third peak (Fig 3.12) is complicated without proper baseline assignments. However, the current ratio can be calculated using different empirical methods, that is differentiate peak currents of forward and reverse peaks from the baseline measurement.

3.3.2. C-H Bond Oxidation by [Ru(bpyPO$_3$H$_2$)(bpy)Cl]Cl (2)

While only modest yields result from the oxidation of organic substrates by **2**, its ability to catalyze C-H Bond oxidation using sodium periodate as the primary oxidant is promising for further development in this area, as sodium periodate can be readily used to incorporate labeled O atoms from isotopically enriched water.[25] We believe the greater stability of **2** relative to **1** under oxidizing conditions results from a combination of: a) the lack of an oxidizable methylene linker in bpyPO$_3$H$_2$ and b) the more rigid structure of **2** inhibiting the formation of dimeric and higher order structures in higher Ru valence states. Studies to test these hypotheses and determine the mechanism of C-H bond oxidation by this family of catalysts is ongoing.

3.4. Conclusions

Two Ru coordination complexes containing pyridylphosphonate ligands were synthesized in order to test the ability of bound phosphonate groups to participate in proton-coupled electron transfer (PCET). While both complexes were found to exhibit two-electron, two-proton Ru(II/IV) couples in aqueous media, the redox potentials observed for both **1** and **3** fall a region predicted to exhibit this behavior due solely to PCET enabled by a bound aqua ligand. Thus, further characterization of phosphonate ligands is required to determine the extent to which bound phosphonate ligands can effect PCET. Both complexes were found to be capable of

alkene epoxidation, and **3** is also capable of oxidizing aliphatic C-H bonds using either CAN or NaIO$_4$ as the primary oxidant. While turnover numbers for this C-H bond oxidation are modest, to the best of our knowledge, this is the first demonstrated example of aliphatic alkane oxidation by a Ru complex using sodium periodate as the oxidant. Development of catalysts with improved stability is currently ongoing.

3.5. Experimental Methods

3.5.1. General Consideration

6-bromo-2,2'-bipyridyl and (pyridin-2-ylmethyl)phosphonic acid were purchased from TCI Chemicals and used without further purification. Triethylamine, 2,2':6',2"-terpyridine (tpy), and cyclooctane were purchased from Alfar Aesar and used without purification. Acetophenone was purchased from VMR and used without purification. Ethylbenzene was purchased from Thermo Fisher Scientific and used without further purification. Anhydrous magnesium sulfate was purchased from AMRESCO, Inc. and used without further purification. Deuterated solvents, ruthenium(III) chloride hydrate, sodium periodate, hydrogen peroxide, *cis*-cyclooctene, cyclooctane, Celite® 545, diethyl phosphite, 2,2'-bipyridine, bromotrimethylsilane, and tetrakis(triphenylphosphine)palladium(0) were purchased from Sigma-Aldrich Co. and were not further purified. Ammonium cerium(IV) nitrate and silver nitrate were purchased from Strem Chemicals, Inc. and used without further purification. Tetrahydrofuran DriSol was purchased from EMD Millipore and used without further purification. Column chromatography was performed using RediSep® GOLD columns on a CombiFlash RF+ from Teledyne Instruments, Inc. All procedures were performed under nitrogen atmosphere unless otherwise specified.

3.5.2. Synthesis of [Ru(tpy)Cl₃]
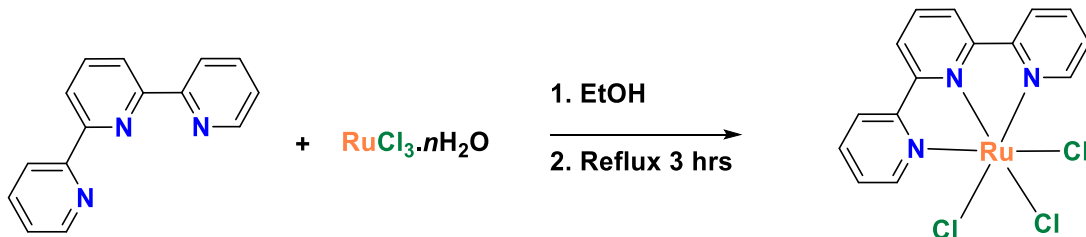
[[Ru(tpy)Cl₃] was prepared according to the published procedure.[26] In brief, a solution of 447.4 mg (2.16 mmol) of RuCl₃•nH₂O, 500 mg (2.14 mmol) of tpy and EtOH (250 mL) was refluxed for 3 hours. After being allowed to cool room temperature, the resulting dark brown solid was collected by filtration, washed with cold EtOH and Et₂O to yield 549 mg (58.1%) of product after vacuum drying.

3.5.3. Synthesis of [Ru(tpy)(MepyPO₃H)Cl] (1)
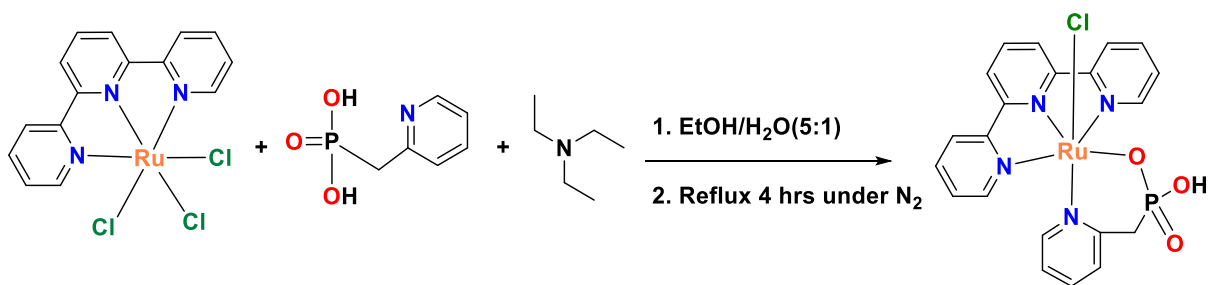
Ru(tpy)Cl₃ (200 mg, 0.454 mmol) and (pyridin-2-ylmethyl)phosphonic acid (MepyPO₃H₂) were placed under nitrogen atmosphere. A nitrogen sparged solution of triethylamine (54 µL, 0.44 mmol) in 36 mL EtOH/H₂O (5:1) was transferred to solid mixture and kept under refluxed at 85 ⁰C for 4 hours, over which time the reaction mixture turned to a dark purple/pink color. The solution was removed from the heat, allowed cool to room temperature, filtered through a frit containing Celite® 545 and washed with EtOH (15 mL x 3) to yield a purple filtrate. Solvent was removed from the filtrate using a rotary evaporator and the resultant precipitate was further dried in a vacuum desiccator. The precipitate was then re-dissolved in

MeOH (~2 mL) and re-precipitated by addition of EtOAc (~20 mL). The precipitate was collected by filtration and washed with dichloromethane (10 mL x 1) and Et$_2$O (5 mL x 3) to yield a dark purple/pink solid which was further dried under vacuum, yielding 183 mg (74.4%) of product. ^{1}H NMR (400 MHz, D$_2$O) δ 9.14 (d, 2H), 8.35 (t, 4H), 7.96 (t, 2H), 7.81 (t, 1H), 7.65 (d, 2H), 7.24 (t, 1H), 6.93 (d, 1H), 6.41 (t, 1H). Anal. Calcd. for [Ru(IV)(MepyPO$_3$H$_2$)(tpy)Cl]Cl$_3$•2H$_2$O: C, 36.81; H, 3.38; N, 8.18, Found: C, 36.77; H, 3.33; N, 8.00.

3.5.4. Synthesis of 2,2'-bipyridine-6-diethylphosphonate (bpyPO$_3$Et$_2$)
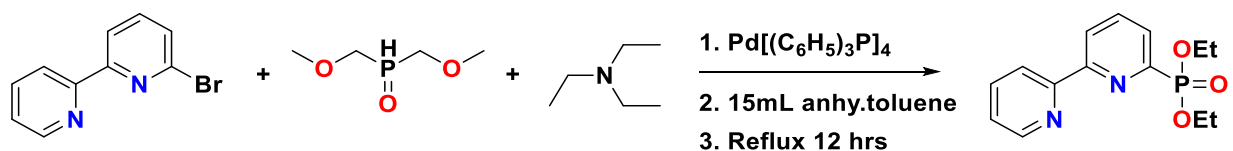
2,2'-bipyridine-6-diethylphosphonate was synthesized as described in the literature procedure with slight modification.[16] First, diethyl phosphite (1.178 g, 8.530 mmol) and triethylamine (1.2 mL, 8.525 mmol) were mixed with dry toluene (30 mL) under nitrogen. Tetrakis(triphenylphosphine)palladium(0) (985 mg, 852 μmol) and 6-bromo-2,2'-bipyridine (2.0 g, 8.525 mmol) and were added to a separate 100 mL Schlenk flask. The toluene solution was transferred to the solid mixture via cannula and refluxed at 95 ºC overnight under the protection of nitrogen. After cooling to room temperature, the reaction mixture was filtered to remove NEt$_3$HBr. The filtrate was collected and concentrated under vacuum. The crude product was further purified by HPLC over silica using a variable gradient of EtOAc/hexane as eluent. Upon removal of solvent, the desired product was attained as light-yellow needles (1.995 g, yield = 80%). ^{1}H NMR (400 MHz, D$_2$O) δ 8.70 (td, 1H), 8.59 (td, 1H), 8.52 (m, 1H), 7.95 (m, 2H), 7.85 (td, 1H), 7.37 (m, 1H), 4.34 (m, 4H), 1.41 (t, 6H).

3.5.5. Synthesis of 2,2'-bipyridine-6-diethylphosphonic acid (bpyPO₃H₂)
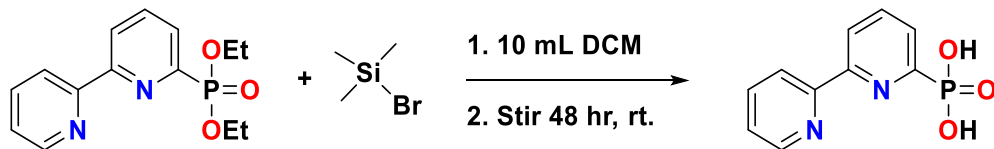
2,2'-bipyridine-6-diethylphosphonic acid (bpyPO₃H₂) was prepared according to the procedure described in literature with slight modification.[16] 2,2'-bipyridine-6-diethylphosphonate (1.198 g, 4.099 mmol) was dissolved in anhydrous DCM (25 mL). Bromotrimethylsilane (2.13 mL, 16.40 mmol) was slowly added via syringe, and the reaction mixture was stirred at room temperature for 48 hours. EtOH (2.5 mL) was then added and the reaction mixture was stirred for ~30 min until a white precipitate formed. The white solid was collected through filtration, washed with dichloromethane (5 mL x 2) and dried in a vacuum desiccator to yield 904 mg (93%) of desired product. ^{1}H NMR (400 MHz, D₂O) δ 8.79 (d, 1H), 8.63 (m, 2H), 8.29 (d, 1H), 8.13 (m, 1H), 8.02 (td, 1H), 7.97 (td, 1H).

3.5.6. Synthesis of [Ru^{III}(bpyPO₃H)Cl₃]/[Ru^{III}(bpyPO₃H)Cl₃](Et₃NH)
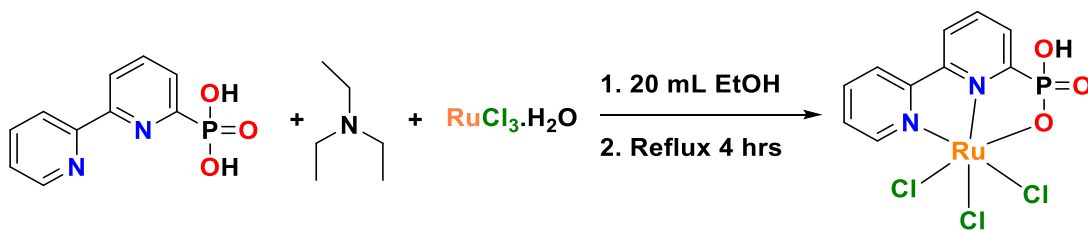
A solution of triethylamine (0.18 mL, 1.31 mmol) in anhydrous MeOH (25 mL) was added to a Schlenk flask containing RuCl₃•nH₂O (362 mg, 1.61 mmol) and bpyPO₃H₂ (310 mg, 1.31 mmol). The reaction solution was heated to reflux for 4 hours with vigorous stirring. After cooling to room temperature, the reaction mixture was filtered through a frit containing Celite® 545. The filtrate volume was reduced using a rotary evaporator and EtOAc (~20 mL) was added to precipitate the desired product. The precipitate was collected, washed with Et₂O (5 mL x 3)

and dried in a vacuum desiccator. A roughly 1:1 mixture of [Ru(III)(bpyPO$_3$H$_2$)Cl$_3$] and

[Ru(III)(bpyPO$_3$H)Cl$_3$](Et$_3$NH) was obtained attained as a dark orange solid (599 mg, 75.3% Ru

basis). Attempts to remove the remaining Et$_3$NH$^+$ led to substantial loss of product without

improving purity, and the mixture was used as isolated in future steps. Crystals of

[Ru(III)(bpyPO$_3$H)Cl$_3$](HNEt$_3$)(CH$_2$Cl$_2$) suitable for X-ray diffraction were obtained by slow

evaporation of a solution of [Ru(III)(bpyPO$_3$H)Cl$_3$](HNEt$_3$) in DCM. Anal. Calcd. for a 1:1

mixture of [Ru(III)(bpyPO$_3$H$_2$)Cl$_3$] and [Ru(III)(bpyPO$_3$H)Cl$_3$](HNEt$_3$): C, 31.60; H, 3.37; N,

7.09, Found: C, 31.02; H, 3.45; N, 7.25.

3.5.7. Synthesis of [Ru^{II}(bpyPO$_3$H)(bpy)Cl]Cl (2)
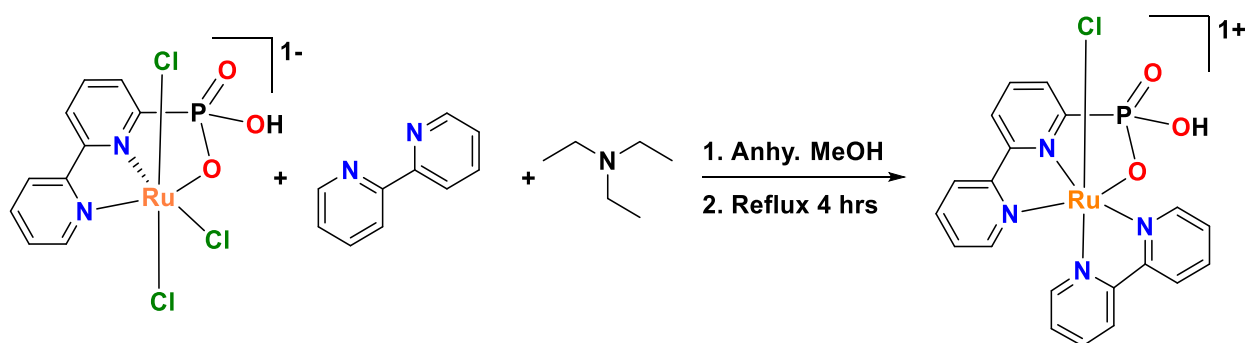
[Ru(III)(bpyPO$_3$H)Cl$_3$]/[Ru(III)(bpyPO$_3$H)Cl$_3$](Et$_3$NH) (251 mg, 0.508 mmol) and 2,2-

bipyridyl (bpy) (87 mg, 0.560 mmol) were added to 100 mL Schlenk flask. A solution of

triethylamine (64 µL, 0.46 mmol) in MeOH (45 mL) was added to the solids and refluxed at 80

ºC for 5 hours. The reaction mixture was cooled to room temperature and filtered through Celite$^®$

545. The filtrate was concentrated on a rotary evaporator, and EtOAc was added to precipitate

the product. Precipitate was collected by filtration, washed with Et$_2$O (5 mL x 3) and kept in

vacuum desiccator for further drying to yield 163 mg (50.7%) of desired product as a dark

orange powder. Crystals suitable for X-ray crystallography were obtained by allowing vapors of

diethyl ether to slowly diffuse into a solution of **2** in MeOH. Anal. Calcd. for

[Ru(II)(bpyPO$_3$H$_2$)(bpy)Cl]Cl•2H$_2$O•MeOH: C, 39.88; H, 3.98; N, 8.86, Found: C, 40.08; H, 3.86; N, 8.27.

3.5.8. Synthesis of [Ru^{II}(bpyPO$_3$H)(bpy)(OH$_2$)](NO$_3$)$_2$ (3)
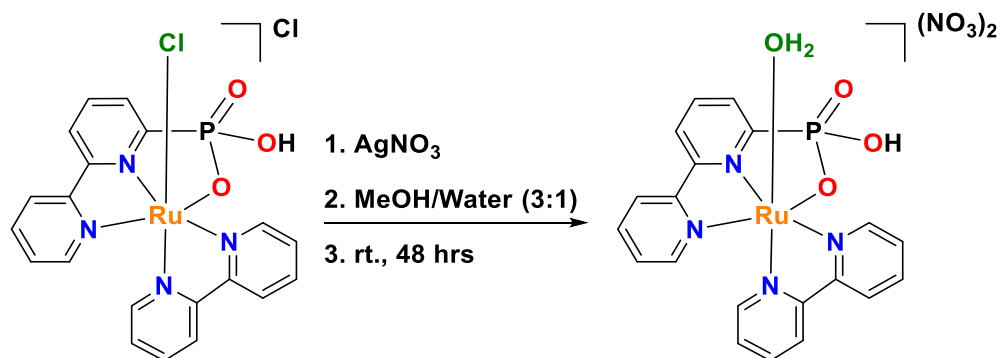
AgNO$_3$ (120.7 mg, 0.71 mmol) was added to a solution of **2** (200.2 mg, 0.36 mmol) in MeOH/water (3:1). The reaction mixture was stirred at room temperature for 48 hours and filtered through Celite® 545. The filtrate was reduced to dryness using a rotary evaporator and dried under vacuum yielding a very hygroscopic dark orange solid (78 mg, 40%). Two separate samples were submitted for elemental analysis as the first sample returned had anomalously low N values. The second sample had acceptable N, but very high H, possibly due to the hygroscopic nature of **3**. Anal. Calcd. for [Ru(II)(bpyPO$_3$H$_2$)(bpy)(OH$_2$)](NO$_3$)$_2$•MeOH: C, 37.79; H, 3.47; N, 12.59. Found (1): C, 37.59; H, 3.29; N, 11.07. Found (2): C, 37.97; H, 5.47; N, 12.52.

3.5.9. Crystallization of [Ru^{III}(bpyPO$_3$H)Cl$_3$]$^-$ and [Ru^{II}(bpyPO$_3$H)(bpy)Cl]Cl (2)

X-ray-quality single crystals of [Ru^{III}(bpyPO$_3$H)Cl$_3$]$^-$ was obtained from slow evaporation of their dichloromethane solution at room temperature. Crystals of **(2)** was obtained from vapor diffusion method by diffusing diethyl into Methanol at room temperature.

3.5.10. Crystal Structure Determination

The crystal mounted on MiTeGen's Micro Loops using Immersion oil, type NVH by Cargille and cooled to 110 K in a stream of cold N$_2$ gas. Diffraction data were collected using a

Bruker APEX2 Duo CCD area detector diffractometer with the detector positioned at a distance of 4.0 cm from the crystal. The X-ray source was sealed tube Mo-Kα radiation ($\lambda = 0.71073$ Å). Data were processed (integrations and multi-scan absorption corrections) by Bruker-AXS software Apex3 v2017.3–0. Using Olex2 software,[3] the structures were solved by Intrinsic Phasing using ShelXT[4] and refined anisotropically on F^2 with ShelXL.[5] All hydrogen atoms were refined isotopically.

3.5.11. Procedure for Electrochemical Measurements

Electrochemical measurements were obtained using a Pine WaveDriver potentiostat with platinum working (1.6 mm OD) and counter electrodes. For aqueous measurements an Ag/AgCl electrode in a saturated KCl solution was used as the reference electrode. For measurements in non-aqueous solvents, an Ag/Ag$^+$ electrode the same electrolyte solution used for measurements was used as a pseudo-reference electrode. Absolute potentials were obtained by referencing to Fc/Fc$^+$ as both an external and internal standard.[27,28] All measurements were compared with the specified electrolyte solution as a blank measurement under identical electrode conditions.

3.5.12. Procedure for UV-Visible Measurements

UV-visible measurements were collected on a PerkinElmer Lambda 465 spectrophotometer. Solutions for UV-visible measurements were prepared by dissolving the solid complex in solvent using volumetric glassware to obtain the indicated concentrations. Standard measurements were taken using a quartz cuvette with a 1 cm path length. Spectroelectrochemical spectra were taken using an optical thin layer (OTL) cell and a Pine gold honeycomb electrode with an effective path length of 1.7 mm. Prior to measuring the UV-visible spectra, a rapid CV was taken using the honeycomb electrode to confirm no change in electrochemical behavior occurred due to the use of the honeycomb electrode. A constant

potential was then applied, and UV-visible spectra were recorded once a constant current was obtained, generally within 2 minutes.

3.5.13. Procedure for C-H Bond Oxidant Screening

A 1.00 mg/mL stock solution of **1** (3.0 mL, 3.0 mg, 5.2 μmol) or **2** (3.0 mL, 3.0 mg, 5.5 μmol), 3-(trimethylsilyl)propionic-2,2,3,3-d_4 acid sodium salt (3.3 mg, 19 μmol), and 2.4 mmol of the chemical oxidant were dissolved in 7.0 mL of D_2O. The reaction flask was then stoppered, THF (40 μL, 624 μmol) was added, and the reaction solution stirred for 1 hour at room temperature (20⁰ C). A ^1H NMR of the solution was then collected.

3.5.14. Procedure for C-H bond Substrate Scope Screening

Solid oxidant was dissolved in a solution containing 150 μL acetonitrile, 250 μL of water, and the indicated amount of ruthenium complex. To this solution 10 μL (~83 μmol) of substrate were added, and the reaction was stirred for the specified duration(s). The reaction was then quenched with 100 mg (793 μmol) sodium sulfite, and filtered through glass wool. The reaction vessel was washed with 2 mL of ethyl acetate and 2 mL of water, which was added to the filtered reaction solution. Acetophenone (10 μL, 97 μmol) was added to the filtered reaction solution as an internal standard, and the aqueous fraction was extracted ethyl acetate (2 x 2 mL). The combined organic fractions were then extracted with 5 mL of brine to remove any remaining inorganic compounds, dried with $MgSO_4$, filtered, and analyzed via GC.

3.5.15. Procedure for GC Measurements

Product yields determined by GC were obtained using a Thermo Scientific Trace 1300 GC with a flame ionization detector (FID), and a TG-1301MS column. Substrate scope screening results were analyzed by injecting 10 μL of the processed samples onto the column using a split/splitless injection port in a 1:5 split ratio. Concentration-response curves were obtained for

each of the products analyzed by injecting 10 μL of a known concentration of each of the identified products using the same GC settings above. The FID response was measured at a minimum of 5 separate concentrations for each product, and the FID response for each concentration was measured 3 times. The effect of the purification process on product yield was determined by measuring the FID response for product samples of known concentration after following the same purification procedure used for the substrate scope screening.

3.6. References

1.   Mayer, J. M. Understanding Hydrogen Atom Transfer: From Bond Strengths to Marcus Theory. *Acc. Chem. Res.* **44**, 36–46 (2011).

2.   Weinberg, D. R. *et al.* Proton-Coupled Electron Transfer. *Chem. Rev.* **112**, 4016–4093 (2012).

3.   Fukuzumi, S. Electron-transfer properties of high-valent metal-oxo complexes. *Coordination Chemistry Reviews* **257**, 1564–1575 (2013).

4.   Solis, B. H. & Hammes-Schiffer, S. Proton-Coupled Electron Transfer in Molecular Electrocatalysis: Theoretical Methods and Design Principles. *Inorg. Chem.* **53**, 6427–6443 (2014).

5.   Kotani, H. *et al.* Fundamental electron-transfer and proton-coupled electron-transfer properties of Ru(iv)-oxo complexes. *Dalton Trans.* **48**, 13154–13161 (2019).

6.   Kojima, T., Nakayama, K., Ikemura, K., Ogura, T. & Fukuzumi, S. Formation of a Ruthenium(IV)-Oxo Complex by Electron-Transfer Oxidation of a Coordinatively Saturated Ruthenium(II) Complex and Detection of Oxygen-Rebound Intermediates in C–H Bond Oxygenation. *J. Am. Chem. Soc.* **133**, 11692–11700 (2011).

7.   Hashiguchi, B. G., Bischof, S. M., Konnick, M. M. & Periana, R. A. Designing Catalysts for Functionalization of Unactivated C–H Bonds Based on the CH Activation Reaction. *Acc. Chem. Res.* **45**, 885–898 (2012).

8.   Dogutan, D. K., McGuire, R. & Nocera, D. G. Electocatalytic Water Oxidation by Cobalt(III) Hangman β-Octafluoro Corroles. *J. Am. Chem. Soc.* **133**, 9178–9180 (2011).

9.   Okamura, M. *et al.* A mononuclear ruthenium complex showing multiple proton-coupled electron transfer toward multi-electron transfer reactions. *Dalton Trans.* **41**, 13081–13089 (2012).

10.   Padhi, S. K., Fukuda, R., Ehara, M. & Tanaka, K. Photoisomerization and Proton-Coupled Electron Transfer (PCET) Promoted Water Oxidation by Mononuclear Cyclometalated Ruthenium Catalysts. *Inorg. Chem.* **51**, 5386–5392 (2012).

11.   Badiei, Y. M. *et al.* Water Oxidation with Mononuclear Ruthenium(II) Polypyridine Complexes Involving a Direct RuIV═O Pathway in Neutral and Alkaline Media. *Inorg. Chem.* **52**, 8845–8850 (2013).

12.   DePasquale, J. *et al.* Iridium Dihydroxybipyridine Complexes Show That Ligand Deprotonation Dramatically Speeds Rates of Catalytic Water Oxidation. *Inorg. Chem.* **52**, 9175–9183 (2013).

13.   Gerlach, D. L. *et al.* Studies of the Pathways Open to Copper Water Oxidation Catalysts Containing Proximal Hydroxy Groups During Basic Electrocatalysis. *Inorg. Chem.* **53**, 12689–12698 (2014).

14.   Marelius, D. C. *et al.* How Do Proximal Hydroxy or Methoxy Groups on the Bidentate Ligand Affect [(2,2′;6′,2″-Terpyridine)Ru(N,N)X] Water-Oxidation Catalysts? Synthesis,

Characterization, and Reactivity at Acidic and Near-Neutral pH. *Eur. J. Inorg. Chem.* **2014**, 676–689 (2014).

15. Kamdar, J. M. *et al.* Ruthenium Complexes of 2,2′-Bipyridine-6,6′-diphosphonate Ligands for Water Oxidation. *ChemCatChem* **8**, 3045–3049 (2016).

16. Xie, Y., Shaffer, D. W., Lewandowska-Andralojc, A., Szalda, D. J. & Concepcion, J. J. Water Oxidation by Ruthenium Complexes Incorporating Multifunctional Bipyridyl Diphosphonate Ligands. *Angew. Chem. Int. Ed.* **55**, 8067–8071 (2016).

17. Vereshchuk, N. *et al.* Second Coordination Sphere Effects in an Evolved Ru Complex Based on Highly Adaptable Ligand Results in Rapid Water Oxidation Catalysis. *J. Am. Chem. Soc.* **142**, 5068–5077 (2020).

18. Chrzanowska, M. *et al.* Structure and reactivity of [RuII(terpy)(N^N)Cl]Cl complexes: consequences for biological applications. *Dalton Trans.* **46**, 10264–10280 (2017).

19. Evans, D. F. 400. The determination of the paramagnetic susceptibility of substances in solution by nuclear magnetic resonance. *J. Chem. Soc.* 2003–2005 (1959) doi:10.1039/JR9590002003.

20. Weinberg, D. R. *et al.* Proton-Coupled Electron Transfer. *Chem. Rev.* **112**, 4016–4093 (2012).

21. Lever, A. B. P. Electrochemical Parametrization of Metal Complex Redox Potentials, Using the Ruthenium(III)/Ruthenium(II) Couple To Generate a Ligand Electrochemical Series. *Inorganic Chemistry* **29**, 1271–1285 (1990).

22. Dovletoglou, A., Adeyemi, S. A. & Meyer, T. J. Coordination and Redox Chemistry of Substituted-Polypyridyl Complexes of Ruthenium. *Inorg. Chem.* **35**, 4120–4127 (1996).

23. Dakkach, M. *et al.* New Aqua N-Heterocyclic Carbene Ru(II) Complexes with Two-Electron Process as Selective Epoxidation Catalysts: An Evaluation of Geometrical and Electronic Effects. *Inorg. Chem.* **52**, 5077–5087 (2013).

24. Lever, A. B. P. Electrochemical parametrization of metal complex redox potentials, using the ruthenium(III)/ruthenium(II) couple to generate a ligand electrochemical series. *Inorg. Chem.* **29**, 1271–1285 (1990).

25. Zhou, M. *et al.* Cp* Iridium Precatalysts for Selective C–H Oxidation with Sodium Periodate As the Terminal Oxidant. *Organometallics* **32**, 957–965 (2013).

26. Sullivan, B. P., Calvert, J. M. & Meyer, T. J. Cis-trans isomerism in (trpy)(PPh3)RuC12. Comparisons between the chemical and physical properties of a cis-trans isomeric pair. *Inorg. Chem.* **19**, 1404–1407 (1980).

27. Connelly, N. G. & Geiger, W. E. Chemical Redox Agents for Organometallic Chemistry. *Chem. Rev.* **96**, 877–910 (1996).

28. Bard, A. J. & Faulkner, L. R. *Electrochemical Methods: Fundamentals and Applications*. (Wiley, 2000).

29. WaveDriver 200 Bipotentiostat/Galvanostat with EIS User Guide*: This user guide describes the WaveDriver 200 Bipotentiostat/Galvanostat with EIS system,* Pine Research Instrumentation, Inc. 2741 Campus Walk Avenue, Building 100, Durham, NC 27705, USA. Accessed on: Nov. 3, 2020. [Online]. Available: https://pineresearch.com/shop/wp-content/uploads/sites/2/2018/09/DRU10162-WaveDriver-200-User-Guide-REV-003.pdf

CHAPTER 4. SUMMARY AND CONCLUSIONS

Designing the catalysts for selective C-H bond hydroxylation reaction is one of the greatest challenges, as it suffers from major drawbacks, overoxidation and racemization. The limitations often correlate with electronic structure of the catalysts and each result from one-electron HAT step over two-electron O-atom insertion. Ligands play a crucial role when determining the electrochemical properties of a complex. My research studies show that incorporation of anionic ligands promotes high oxidation states of metal complexes. Much of the work devoted in the present research is to develop catalysts to overcome above limitations which favoring concerted two electron O-atom insertion. The synthesis, characterization, electrochemical properties and catalytic behavior on C-H bond oxidation were addressed in this dissertation.

With the consideration of designed principles above, $[Ru(tpy)(pyalk)Cl]^+$ was developed by introducing anionic ligand 2-(2'-pyridyl)-2-propanol (pyalk) since it is one of the best robust ligands for achieving high oxidation activity, due to its strong donor ability and oxidative resistance. Electrochemical studies of the complex revealed that the anionic ligand actively participates in lowering the reduction potential of the Ru(III)/(II) couple as expected; however, no decrease in potential was observed for the Ru(III)/(IV) couple. Based on the published relationship between Lever parameters ($\sum E_L$) and the $\Delta E_{1/2}$ value by Adamai and Meyer, small $\sum E_L$ values favor one-electron over two-electron processes. To address this issue, phosphonate ligands have been explored and introduced.

Understanding the ligand participation on pH dependent redox chemistry of metal complexes will lead to develop more effective catalysts. Phosphonate ligands are expected to promote PCET thereby stabilizing high oxidation states of the metal. We have successfully

synthesized two complexes, [Ru(tpy)(MepyPO$_3$H)Cl] and [Ru(bpyPO$_3$H)(bpy)Cl] with ligands containing phosphonate groups. These phosphonate groups were shown to regulate the pH dependent redox chemistry associated with protonation or deprotonation of the ligand.   Based on the electrochemical studies, [Ru(tpy)(MepyPO$_3$H)Cl] complex was clearly undergone the two-electron process, indicating direct Ru(IV)/(II) couple, i.e. $\Delta E_{1/2}$ value is <0.   Unfortunately, deactivation of the catalyst was observed in the presence of chemical oxidant, mainly due to the oxidation of methylene group.   Therefore, the existing ligand (MepyPO$_3$H) was replaced with a new phosphonate containing ligand (bpyPO$_3$H) which lacks weak link of methylene group. The new catalyst, [Ru(bpyPO$_3$H)(bpy)Cl] contained all positive structural and electrochemical features as the [Ru(tpy)(MepyPO$_3$H)Cl] including two electron chemistry, however, it exhibits only moderate catalytic activity towards C-H bond oxidation.

Recent years have witnessed of developing many ruthenium catalysts for selective C-H bond oxidation reactions. However, most reported catalytic systems suffered from catalyst deactivation and low selectivity for C-H bond hydroxylation. An advantageous aspect of currently available ruthenium complexes is that use as a toolbox for easy access of innovative applications in terms of mechanisms, electrochemical and structural properties to design more reasonable catalysts. For instance, some of the strategies highlighted in this dissertation include introduction of negatively charged anionic ligands, ligand participation on remote PCET to reduce $\Delta E_{1/2}$, and establishment of Lever parameter for unknown ligands.   Further research on, ruthenium catalyze C-H activation based on the study of other factors influence on catalytic activity, computational methods to study the mechanisms and structure will have major impact in developing efficient catalysts.